Bioengineering Human Full Thickness Skin Equivalents to Investigate the Effects of Skin Ageing on Pigmentation

Sara Sherif Hassan Shaanoun

Bioengineering Human Full Thickness Skin Equivalents to Investigate the Effects of Skin Ageing on Pigmentation

Author
Sara Sherif Hassan Shaanoun

A report submitted to fulfil the requirements for the degree of:
Master of Science by Research in Cell Technology
Year of Submission: 2025

Supervisor
Professor Stefan Przyborski

Department of Biosciences
Durham University
United Kingdom

Abstract

The skin is the largest organ in the human body, serving critical functions in water homeostasis, thermoregulation, and protection against environmental stressors. However, as we age, both the structure and function of skin become compromised due to complex and multifactorial underlying processes. Among the many visible signs of skin aging, pigmentary changes are common, yet the mechanisms driving these alterations remain poorly understood. Moreover, as the global population of elderly individuals increases and ethnic diversity in skin research remains underrepresented, there is a pressing need to explore more advanced models that more accurately reflect the complexities of skin ageing and pigmentation across different demographics. While melanocytes have been included in 3D *in vitro* skin models using intrinsically aged cells, the existing models are limited in scope and require optimisation for greater complexity.

The objective of this project was to construct novel bioengineered ageing pigmented 3D *in vitro* full thickness human skin equivalents, developed using Alvetex® technology, to investigate the effects of ageing on pigmentation. It was hypothesised that melanocytes would be successfully integrated into the ageing skin equivalents to produce pigmented models of aged skin. Moreover, it was hypothesised that there would be phenotypic effects on pigmentation in the ageing skin models, including an overall reduction in pigmentation and the appearance of age spots. Melanocytes were incorporated into these models, which were constructed using age-matched, intrinsically aged fibroblasts and keratinocytes. Phenotypic changes in pigmentation, including a decrease in gross pigmentation and the development of hyperpigmented lesions, were observed and quantitatively validated, with findings comparable to those seen in native human skin. This innovative model offers a promising platform for advancing our understanding of skin ageing and pigmentation and holds potential for industrial applications in dermatological research.

Acknowledgements

Firstly, I would like to thank Professor Stefan Przyborski for giving me the opportunity to undertake this exciting research and for his investment in my project throughout.

I am extremely grateful to Dr. Lucy Smith for being an excellent mentor, providing continuous motivation and support, offering guidance and patience when things inevitably went wrong in the laboratory, and serving as an inspiring scientist. I would also like to thank Dr. Paola De Los Santos Gomez for her training and expertise in the construction of pigmented human skin equivalents, and for her uplifting spirit.

I extend my gratitude to the members of the Przyborski laboratory group for their willingness to share their skills, expertise and advice, all of which contributed to the progress of this research.

Lastly, I would like to express my gratitude towards my incredible support network. Thank you to my loving family, especially my mother, for providing me with the endless love and motivation that I needed to help me through this challenging time. To my amazing boyfriend for your unwavering encouragement and continuous support through the ups and downs of my research and thesis writing period. Finally, I would like to thank my friends for bringing a source of laughter and joy throughout this journey.

Declaration

This work described herein was carried out in the Department of Biosciences, Durham University between October 2023 and September 2024. All of the work is my own, except otherwise stated. No part has previously been submitted for a degree at this or any other university.

Statement of Copyright

Table of Contents

List of Figures

List of Tables

1 Introduction

The global population is experiencing an unprecedented increase in its ageing demographic, with both the number and proportion of older individuals rising exponentially (WHO, 2023; **Figure 1**). This demographic shift underscores the growing importance of research focused on the processes of ageing and age-related health conditions, particularly in relation to the ageing population. Alongside this, there is a noticeable gap in research on skin of colour, despite individuals of colour constituting the majority of the global population (Rawlings, 2006). The term “global majority” has been introduced to reflect the reality that those historically categorized as “ethnic minorities” actually represent 85 % of the world’s population (NCVO, 2023). Consequently, it is crucial to refocus scientific research to include a more diverse range of ethnicities and skin pigmentation levels, ensuring that studies are inclusive and truly representative of the global population.

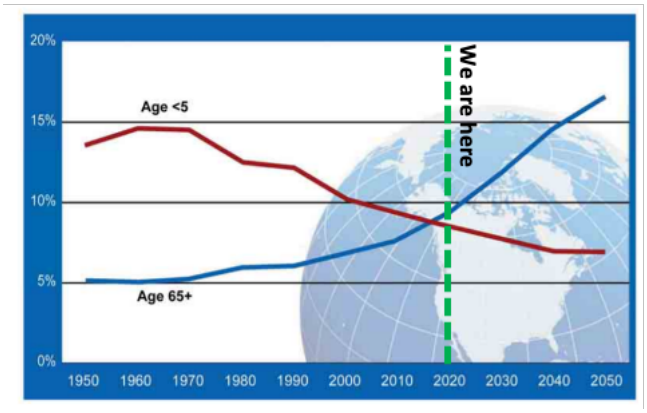

Figure 1: The ageing population.

A graphical representation of the proportion of the population aged 5 and under decreasing with those aged 65+ increasing over the course of a century (1950-2050). The ageing population aged 65+ is predicted to continue to increase to the point where it will have more than tripled by 2050 compared with in 1950. Image sourced from United Nations, 2010.

The processes of skin ageing and pigmentation are highly intricate and involve a series of cellular and molecular mechanisms that are interconnected with one another. While it is known that ageing impacts skin pigmentation, the exact biological mechanisms behind these changes remain poorly understood. This lack of comprehensive research has created a pressing need for studies that explore the interplay between skin ageing and pigmentation.

This review will discuss the current understanding of the mechanisms of skin ageing and pigmentation, as outlined in the existing literature. It will also highlight the importance of developing novel skin models that enable more in-depth investigation into how ageing

influences pigmentation, thus contributing to a more comprehensive understanding of these complex processes.

1.1 The Anatomy and Physiology of Healthy Human Skin

1.1.1 Skin Structure and Function

Skin is the largest organ in the body, accounting for over 15 % of the body weight of an adult (McLafferty *et al.,* 2012). It is an important component of the integumentary system that functions as a protective barrier against external stresses and pathogens, as well as playing a role in thermoregulation and water homeostasis (Rittié & Fisher, 2015). Skin is composed of approximately 20 different cell types forming three distinct layers: the epidermis, dermis, and hypodermis (Kolarsick *et al.,* 2011). Skin also contains appendages including hair follicles, sweat glands, sebaceous glands, nerves, and muscle, which are located in the dermis (Ho & Dreesen, 2021; **Figure 2**). The composition of human skin differs across parts of the body depending on the specific functional needs, as well as differing between males and females (Arda *et al.*, 2014).

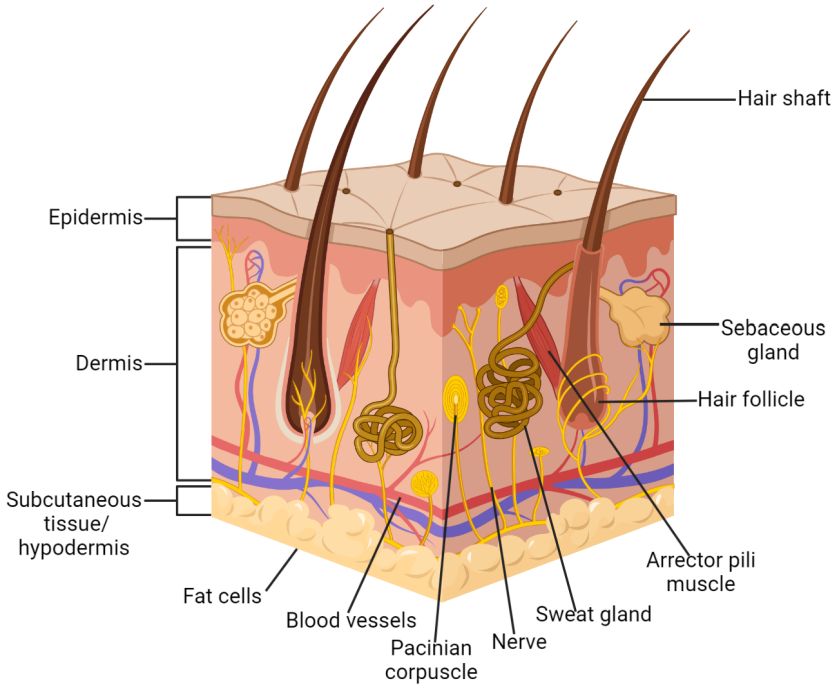

Figure 2: The anatomy of human skin.

A schematic depiction of a cuboidal cross-section of human skin, showing the epidermis, dermis, hypodermis, and the appendages of skin. The appendages depicted in the dermis include blood vessels, arrector pili muscles, and hair follicles with sweat glands and sebaceous glands. Created with BioRender.com.

The epidermal component of skin is made up of 5 sublayers: the stratum-basale, -spinosum, -granulosum, -lucidum, and -corneum (Ho & Dreesen, 2021; **Figure 3**). These layers are formed by keratinocytes that produce keratin and differentiate upwards from the basal layer to become increasingly cornified, eventually forming a layer of anucleated, horny cells at the surface of the skin (Kolarsick *et al.,* 2011). This layer of dead cells is responsible for providing the waterproof barrier function of skin (Ho & Dreesen, 2021). In addition to keratinocytes, the epidermis also contains other cell types including melanocytes for melanin production, Langerhans cells of the immune system, and sensory Merkel cells (Kolarsick *et al.,* 2011; **Figure 3**). The thickness of the epidermis differs across various locations on the body; the thick skin found on the soles of the feet and palms of the hands have a thicker epidermis and a stratum lucidum can be visualised. However, this additional layer of the epidermis is not present in the skin of the face and the rest of the body, which has a thinner epidermis (Arda *et al.*, 2014).

The dermal component is made up of fibroblasts, which synthesise the components of the extracellular matrix (ECM) (Ho & Dreesen, 2021; **Figure 3**). These components include collagens (mostly type I collagen), elastin, glycosaminoglycans (GAGs) including hyaluronic acid, and proteoglycans (Reilly & Lozano, 2021). The dermis is subdivided into two layers, the highly vascular papillary dermis and dense reticular dermis (Brown & Krishnamurthy, 2023). The papillary (upper) dermis contains thin collagen fibres, whereas the reticular (deep) dermis comprises dense collagen fibres, and lies directly over the hypodermis (Watt & Fujiwara, 2011).

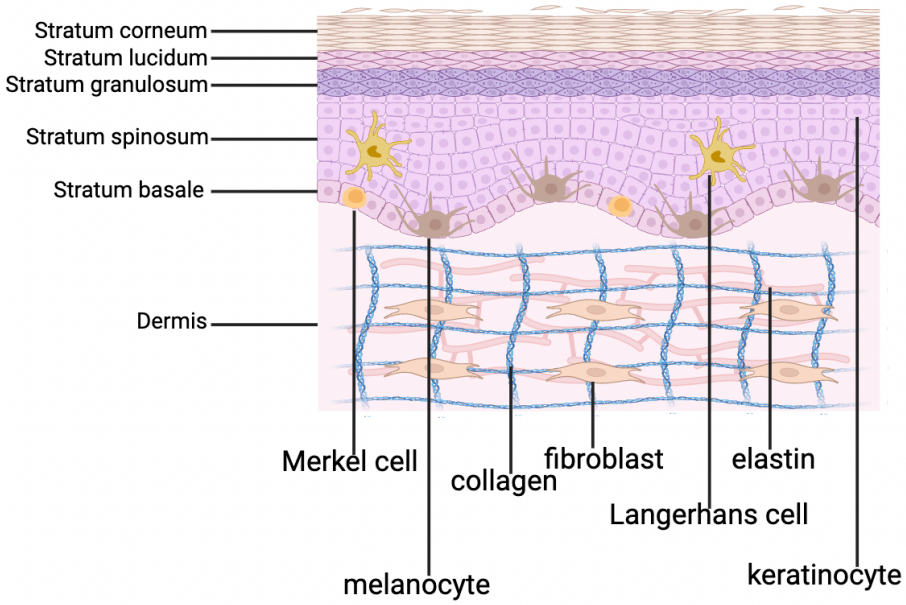

Figure 3: The microanatomy of human skin.

A schematic diagram of a cross-section of human skin showing the epidermal and dermal compartments. The epidermal layers shown are the stratum-corneum, -lucidum, -granulosum, -spinosum and -basale. The epidermis is mostly composed of keratinocytes, with the depiction of some melanocytes, Langerhans cells, and Merkel cells. Although it has been included in this schematic, the stratum lucidum is only present in thick skin, not on the skin of the face or most of the body. The dermal layer shows fibroblasts in the extracellular matrix constructed of collagen and elastin fibres. Created with BioRender.com.

The hypodermis is a vascular layer of subcutaneous tissue made up of lipocytes (fat cells), which store energy and produce leptin, a hormone that plays a role in regulating body weight (Kolarsick *et al.,* 2011; **Figure 2**). Additionally, the subcutaneous layer (hypodermis) provides mechanical support and cushioning to the skin to help with absorption of shock, as well as playing an essential role in thermoregulation (Mohaned & Hargest, 2022).

1.1.2 The Epidermis

The epidermis is separated from the dermis by the basal lamina, upon which the mitotically active stem cells of the stratum basale are attached by hemidesmosomes. These cells are cuboidal to columnar and are responsible for the constant production of keratinocytes (Yousef *et al.*, 2023). The keratinocytes of all layers are bound to adjacent keratinocytes via desmosomes, and melanocytes are scattered among the cells of the stratum basale (Arda *et al.*, 2014).

The nuclear protein Ki67 is expressed in proliferative cells in the G1, S, G2, and M-phases of the cell cycle, and not expressed in non-proliferative cells in the G0-phase (Rousselle *et al.*, 2017). A study by Knaggs *et. al* (1994) found that approximately 11 % of the nuclei in the basal layer of normal cells were Ki67 positive. Ki67 is also expressed in the first three suprabasal

layers (Rousselle *et al.*, 2017). P63 is a gene belonging to the p53 tumour suppressor family. This gene also plays a role in epidermal proliferation, and its expression is localised in the nuclei. According to Tsujita-Kyutoku *et al.* (2003), p63 is expressed in the nuclei of almost all cells in the basal and suprabasal layers, whereas Ki67 is expressed in fewer cells and confined to the basal cells in normal human skin.

Cytokeratins are a large group of proteins that form intermediate filaments and are therefore involved in the formation of the cytoskeleton of epithelial cells including keratinocytes and their appendages (Mykhaliuk *et al.*, 2022). Cytokeratins K14 and K5 are expressed in non-differentiated stem cells of the basal layer. When keratinocytes differentiate from the basal layer to the suprabasal layer, the expression of cytokeratins K5 and K14 are switched off, and expression of epidermal differentiation markers K1 and K10 are switched on (Rousselle *et al.*, 2017). A 2019 study by Zhou *et. al* found that K10 was detected in the stratum spinosum and stratum granulosum, and that the molecular weight of cytokeratins gradually increases as the keratinocytes differentiate into the upper layers.

Additional markers of epidermal differentiation include the cornified envelope precursors loricrin and involucrin; involucrin is a marker of intermediate differentiation, whereas loricrin is a marker of terminal differentiation (Rousselle *et al.*, 2017). Loricrin is the main component of the cornified envelope, making up over 80 % of its protein mass (Rinnerthaler *et al.*, 2013). According to Tharakan *et al.* (2009), involucrin expression is localised in the keratinocytes of the stratum granulosum and stratum corneum in normal human skin, and in the suprabasal layers of sweat gland- and keratinocytes-derived epidermal substitutes. They also found that loricrin is mainly expressed in the upper stratum granulosum of normal human skin, with slight staining in the stratum corneum. The same staining was visualised in the epidermal substitutes, with a lower fluorescence intensity than in normal skin (Tharakan *et al.,* 2009).

Periplakin is a further example of a cornified cell envelope precursor, as it is involved in the formation of a scaffold upon which the cornified cell envelope is assembled (Groot *et al.*, 2004). This protein is a cytolinker belonging to the plakin family, a group of giant proteins that play a role in the cross-linking of the cytoskeleton (Bouamer *et al.*, 2014). This marker is abundantly expressed in the stratum granulosum, particularly in the desmosomes and interdesmosomal plasma membrane (Groot *et al.*, 2004).

As desquamation occurs and keratinocytes differentiate and move up layers of the epidermis, the morphology of cells becomes increasingly flattened (Milstone, 2004; **Figure 4**). The stratum corneum is made up of horny scales that are comprised of keratin and flat anucleate

squamous cells, or dead keratinocytes, attached to each other via corneodesmosomes (Yousef *et al.*, 2023).

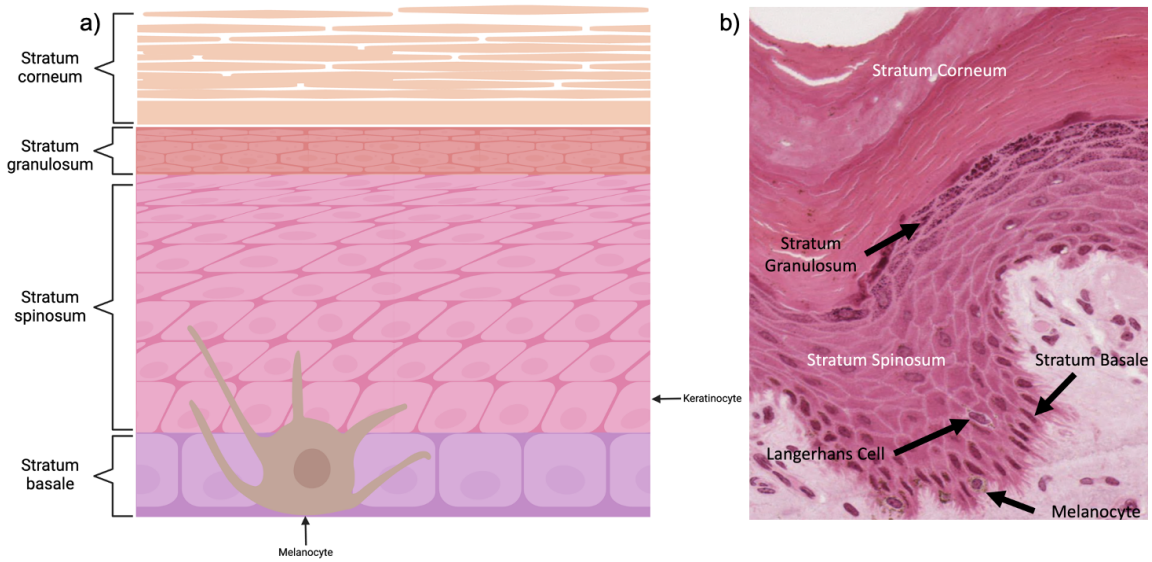

Figure 4: The structure of the epidermis.

a) schematic representation of the layers of the epidermis with a melanocyte. The layers of the epidermis depicted are the stratum-corneum, -granulosum, -spinosum and -basale, the layers present in 'thin' skin, such as facial skin. Created with *BioRender.com*. b) a representative H&E micrograph of a cross-section of the epidermis of healthy, normal human skin with the same visible layers as the schematic and visible melanocytes. Image sourced from https://ubwp.buffalo.edu/histology/integument-histology-notes/.

The corneocytes suspended within the lipid matrix of the stratum corneum can be described as a 'brick and mortar system', a term originally used in 1975 by Michaels *et al*. The composition of the lipid matrix consists of a complex mixture of ceramides, cholesterols, and free fatty acids (Menon *et al.*, 2012). These lipids provide a permeability barrier, which is vital to the normal function of healthy human skin; alterations in the lipid composition and impairment of the barrier function are associated with skin conditions such as atopic dermatitis (Uche *et al.*, 2019). Larger structural proteins such as filaggrin are also integral to the robust mechanics of the skin barrier (Yousef *et al.*, 2023). In fact, loss-of-function mutations in the filaggrin gene are associated with skin conditions such as ichthyosis vulgaris (Sandilands *et al.*, 2009).

1.1.3 The Dermis

The dermis is a layer of connective tissue that provides a framework for the protection of deeper anatomical structures, as well as a supportive foundation for the epidermis (Brown & Krishnamurthy, 2023). Additionally, the dermis is a scaffold that provides the skin with elasticity

and strength (Ganier *et al.,* 2022). This can be attributed to the composition of the extracellular matrix, consisting of mostly type I and type III collagens, elastin, and other structural proteins (Watt & Fujiwara, 2011). Type 1 collagen is the most abundant collagen found in the skin, making up to 90 % of total collagen composition (Reilly & Lozano, 2021). A 2013 study by Ren *et al.* found that in normal Sirius Red stained rat skin tissue, collagen I fibres are thick and have a dense arrangement, making up 83.31 % ± 15.80 % of the total collagen content, whereas collagen III made up 13.93 % ± 5.60 % of the extracellular collagen composition.

Between these fibrous components, an amorphous extracellular substance is made from GAGs such as hyaluronic acid, proteoglycans, and glycoproteins (Brown & Krishnamurthy, 2023). One of the predominate glycoproteins is fibronectin, which is found amongst the highly organised ECM structures in abundance. Fibronectin is one of the first fibrils assembled during tissue development and wound healing, since it is an adhesive molecule involved in the assembly of the ECM during these processes (Dalton & Lemmon, 2021). Fibronectin also plays a role in the regulation of cell proliferation and re-epithelialisation (Lenselink, 2015).

Fibroblasts are the primary cell type of the dermis; they are responsible for the synthesis of the components of the ECM, including fibrillar collagens (Watt & Fujiwara, 2011; **Figure 5**). Fibroblasts also orchestrate the construction of a healthy skin barrier, and they are vital in the process of epidermal differentiation (Jevtić *et al.,* 2020*)*. The support provided by fibroblasts is also implicated in skin pigmentation, as they are important in the correct localisation of melanin and formation of supranuclear caps (Goncalves *et al*., 2023).

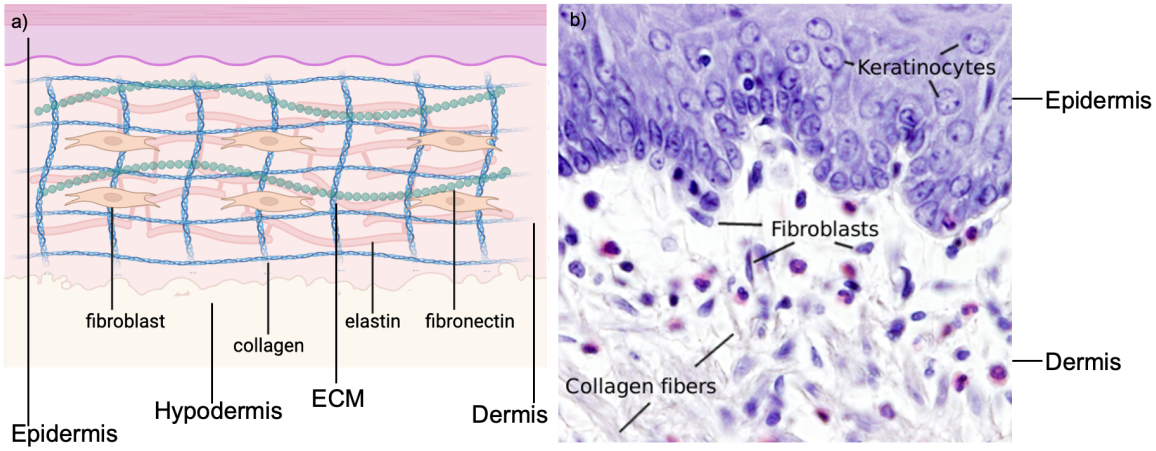

Figure 5: The structure of the dermis.

a) schematic representation of human dermis with fibroblasts and the extracellular matrix with collagen, elastin, and fibronectin fibres. Created with BioRender.com. b) a representative H&E micrograph of a cross-section of the dermis with visible collagen fibres and fibroblasts. Part of the epidermis and keratinocytes can also be visualised in the photograph. Image sourced from https://mmegias.webs.uvigo.es/02-english/8-tipos-celulares/fibroblasto.php.

1.1.4 Communication between layers

In healthy human skin, epidermal keratinocytes and dermal fibroblasts engage in crosstalk to maintain homeostasis (Russo *et al.,* 2020). These interactions occur predominantly via growth factors and cytokines (Amiri *et al.,* 2021; **Figure 9**). According to a 2020 study by Jevtić *et al.*, this dermal-epidermal crosstalk is critical for the adequate differentiation of the skin.

The dermis is anchored to the epidermis via hemidesmosomes and other adhesive components of the basement membrane (Brown & Krishnamurthy, 2023). The basal lamina is secreted by basal keratinocytes themselves and is a specialised layer of ECM composed of networks of type IV collagen, laminins, nidogens, and heparan sulphate proteoglycans such as perlecan (Breitkreutz *et al*., 2013). These structures form the dermal-epidermal junction (DEJ), the interface between the dermis and the epidermis. The DEJ is involved in the regulation of the cellular microenvironment, ultimately playing a key role in maintaining normal homeostasis and skin integrity (Aleemardani *et al.,* 2021).

In addition to normal skin maintenance, communication between keratinocytes and fibroblasts is fundamental in tissue repair and reepithelialisation. For instance, during the process of wound healing, keratinocytes utilise IL-1 and TGF-β signalling pathways to modulate fibroblasts, which differentiate into myofibroblasts to upregulate the production of the ECM at the wound site (Amiri *et al.,* 2021). Furthermore, a study by Egles *et al.* (2008) found that the ECM directly interacts with fibroblasts to mediate cellular modifications in the context of wound repair and reepithelialisation. This study emphasises the importance of the regulation of communication between fibroblasts and the ECM.

Additionally, the DEJ and the signalling between the ECM, fibroblasts, and keratinocytes play a role in skin pigmentation (Bastonini *et al.*, 2016). In fact, the communication between melanocytes, keratinocytes, and fibroblasts is required for several processes involved in determining skin pigmentation, including melanogenesis, melanin transfer, and normal melanin distribution (De Los Santos Gomez *et al.*, 2024). When dysregulation of the signalling between these cell types occurs, it can lead to pigmentary disorders (Bastonini *et al.*, 2016; **Figure 9**). Several *in vitro* skin platforms lack this crosstalk, which can affect several vital cellular processes (De Los Santos Gomez *et al.*, 2024).

1.2 Skin Ageing

Ageing is a complex, multifaceted process which occurs at the molecular, cellular, and whole organ level, and refers to the functional decline of an organism with the passage of time. Although the exact mechanisms of ageing are unknown, there are various theories behind the phenomenon of ageing (Schumacher *et al.,* 2021). A 2023 paper by López-Otín *et al.* proposes 12 hallmarks of ageing: “genomic instability, telomere attrition, epigenetic alterations, loss of proteostasis, disabled macroautophagy, deregulated nutrient-sensing, mitochondrial dysfunction, cellular senescence, stem cell exhaustion, altered intercellular communication, chronic inflammation, and dysbiosis”. These hallmarks are grouped into 3 categories: primary, integrative, and antagonistic (**Figure 6**). These hallmarks of ageing are interconnected, rather than being separate factors independent of one another (López-Otín *et al.*, 2023).

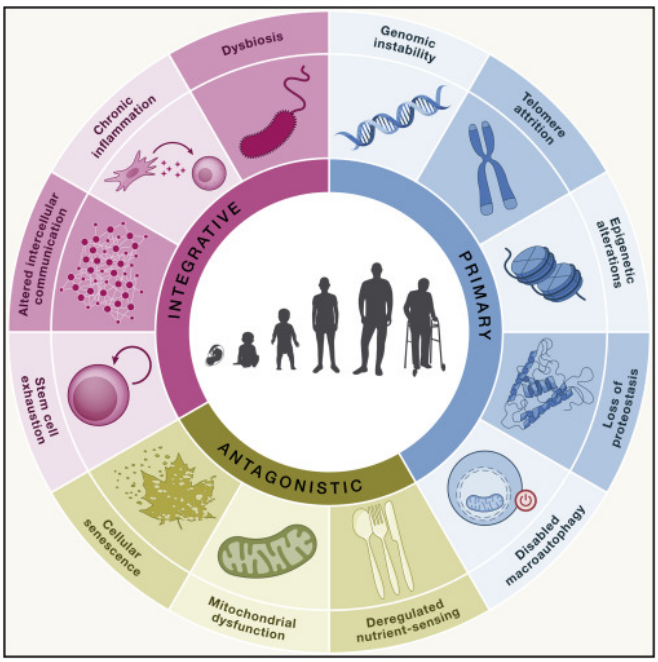

Figure 6: The 12 hallmarks of ageing.

The hallmarks of ageing categorised into primary hallmarks (genomic instability, telomere attrition, epigenetic alterations, loss of proteostasis, disabled macroautophagy), integrative hallmarks (stem cell exhaustion, altered intercellular communication, chronic inflammation, dysbiosis), and antagonistic hallmarks (cellular senescence, mitochondrial dysfunction, deregulated nutrient-sensing). Image sourced from López-Otín et al, 2023.

Ageing affects the morphology of the skin in several ways. One example is the reduction in the thickness of both the epidermis and dermis, which contributes to a loss of skin elasticity and the formation of wrinkles (**Figure 7**). Additionally, inflammation increases and the rate of differentiation decreases, which further compromises skin structure and function (Rittié & Fisher, 2015). Furthermore, the composition of cells in the skin changes, including a reduction

in melanocytes and Langerhans cells. Overall, ageing of the skin impairs its barrier function and ability to regulate homeostasis (Rittié & Fisher, 2015).

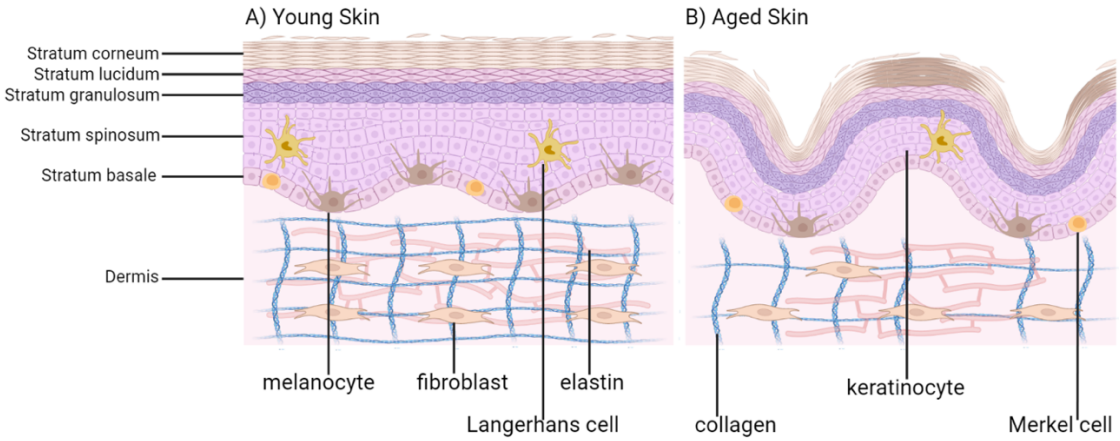

Figure 7: The composition of young and aged human skin.

A) a schematic of cross-sectional young human skin with the layers and cells of the epidermis and the ECM and cells of the dermis. B) a schematic of cross-sectional aged human skin with the same features but with age-related changes such as a reduction of cells, a decreased dermal and epidermal thickness, and a less dense ECM. Created with BioRender.com.

Ageing can occur both intrinsically and extrinsically. Intrinsic or chronological ageing happens naturally over time, and is characterised by fine wrinkles, decreased elasticity, and vascular prominence in the skin (Naidoo & Birch-Machin, 2017; **Figure 8**). Extrinsic ageing or photo-ageing displays similar biochemical features to natural skin ageing but occurs as a result of exposure to ultraviolet radiation (UVR) and other environmental factors such as smoking and air pollution (Lee, 2021). Photo-ageing accelerates the process of intrinsic skin ageing and causes physiologically distinct manifestations (Rittié & Fisher, 2015). These include deep wrinkles, a rough texture, telangiectasia (the appearance of dilated or broken blood vessels on the skin), and pigmentation abnormalities (Naidoo & Birch-Machin, 2017; **Figure 8**).

Figure 8: Clinical appearance of intrinsic and extrinsically aged skin.

Photographs depicting the clinical manifestations of chronological skin ageing compared to photo-ageing by showing photo-exposed and photo-protected areas of the same ageing individual. The photo-exposed skin appears more pigmented and has deep wrinkles in comparison to the photo-protected skin. Images sourced from Seo & Chung, 2006.

1.2.1 Hallmarks of Ageing

This literature review will cover a few of the key hallmarks of ageing in relation to skin pigmentation. Firstly, cellular senescence is well-documented with skin ageing, where senescent cells accumulate in ageing skin and play a key role in driving the ageing phenotypes (Low *et al.,* 2021). Fibroblasts and melanocytes are known to be the most observed senescent cells of the skin, and there is a link between senescence and pigmentary changes that occur with ageing (Kim *et al.,* 2022). Senescent cells lose their proliferative ability and enter a state of permanent cell cycle arrest, where they acquire a senescence-associated secretory phenotype, or SASP (López-Otín *et al.,* 2023). Senescent cells in this state release high levels of pro-inflammatory cytokines, growth factors, and immune modulators, which triggers a chronic state of inflammation known as inflammaging (Tamàs *et al*., 2019). This chronic inflammation induces further cellular dysfunction and premature ageing, even for young individuals with photo-aged skin (Jarrold *et al*., 2022).

Senescent cells can be identified using various biomarkers; Lamin-B1 and high mobility group box 1 (HMGB1) have been identified as markers of cellular senescence in the skin. Whilst Lamin-B1 levels have been observed to decrease *in vitro* during replicative, oncogene-, and UV-induced senescence and *in vivo* in intrinsically aged skin, HMGB1 expression has been seen to decrease in aged skin *in vivo* and senescent fibroblasts *in vitro* (Wang *et al.,* 2022).

Altered intercellular communication is an additional hallmark of ageing that is involved in the time-dependent functional decline of human skin. A dysregulation of the crosstalk between the cells of the skin can be involved in inducing not only ageing phenotypes, but also pigmentary changes (De Los Santos Gomez *et al*., 2024; **Figure 9**). In addition to cell-to-cell interactions, the interactions between cells and their environment are also involved in ageing, and potentially in pigmentation. A 2011 study by Choi *et al.* found that aged senescent fibroblasts were rejuvenated and restored to a more youthful state when cultured with the ECM from young fibroblasts.

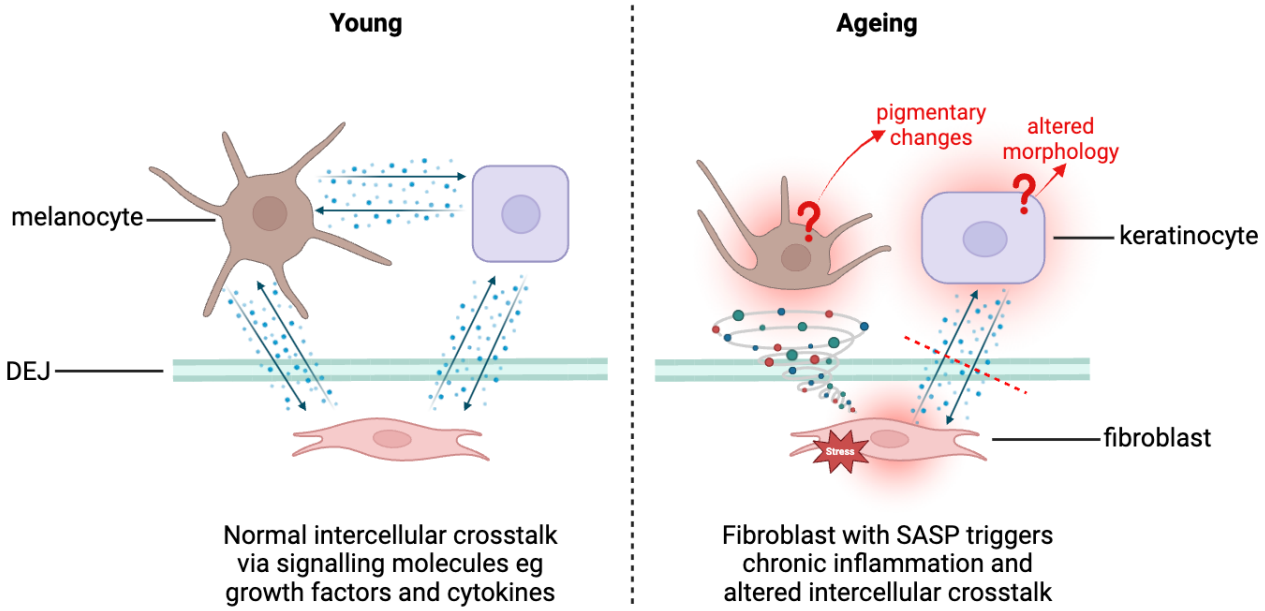

Figure 9: Intercellular crosstalk in young and ageing skin.

A schematic depiction of the crosstalk between a fibroblast and a keratinocyte and melanocyte across the dermal-epidermal junction. The young skin has normal intercellular crosstalk via signalling molecules such as growth factors and cytokines, whereas the ageing skin shows a senescent fibroblast with a SASP phenotype releasing a storm of pro-inflammatory cytokines and other signalling molecules, with an altered intercellular communication. This produces a state of chronic inflammation (inflammaging) and causes the keratinocyte to display altered differentiation and morphology and the melanocyte to have dysregulated melanogenesis, resulting in pigmentary changes. Created with BioRender.com.

Cellular reactive oxygen species (ROS) is produced in both intrinsic and extrinsic skin ageing as a byproduct of cellular processes such as mitochondrial respiration and from environmental stressors such as UVR, and its build up induces oxidative stress (Naidoo & Birch-Machin, 2017; **Figure 10**). The skin is particularly susceptible to ROS-mediated oxidative stress due to its abundance of biological targets for oxidative stress such as lipids and proteins (Lee, 2021). Additionally, since it is a highly metabolically active organ with a high cell turnover, lots of mitochondria are required for sufficient ATP production with high levels of cellular ROS accumulating as a consequence (Sreedhar *et al.*, 2020).

Oxidative stress plays a role in skin pigmentation as the ROS hydrogen peroxide (H_2O_2) is involved in the regulation of tyrosinase, the biological catalyst of melanogenesis (Schallreuter *et al.*, 2008). Consequently, ROS-mediated oxidative stress can cause dysregulated melanin synthesis, which could lead to an altered pigmentary phenotype and has been implicated in both hyper- and hypomelanosis (Lee, 2021). Moreover, oxidative stress is a major cause of genomic instability, another hallmark associated with ageing. Nuclear DNA is susceptible to damage via chemical, physical, and biological agents due to the unstable nature of the genome (López-Otín *et al.,* 2023). DNA damage can accumulate endogenously via ROS and

other byproducts of cellular processes but is accelerated by exogenous factors such as UVR in photo-ageing (Schumacher *et al*., 2021).

Nuclear damage manifests in several ways including point mutations, telomere shortening, and DNA replication errors (López-Otín *et al.,* 2023). Although melanocytes serve a protective function against DNA damage, UVR exposure over time can still induce damage to the nuclear DNA of melanocytes; for example, the upregulation of the MC1R gene that is involved in the regulation of skin pigmentation can be induced by UVR exposure (García-Borrón *et al.,* 2005). Additionally, the production of ROS as a byproduct of melanogenesis leaves melanocytes susceptive to oxidative stress and therefore DNA damage (Jenkins & Grossman, 2013).

Furthermore, the DNA repair mechanisms become decreasingly efficient with age, which exacerbates the accumulative genomic damage (López-Otín *et al.,* 2023). The build-up of oxidative stress and DNA damage accentuates other hallmarks of ageing including cellular senescence, telomere attrition, mitochondrial dysfunction, proteostatic stress, and epigenetic alterations (Schumacher *et al*., 2021). Changes to the epigenome are one of the several hallmarks of ageing that has been linked to the control of skin pigmentation. The methylation of DNA plays a role in the regulation of the genes involved in melanogenesis including TRP1, TRP2 and MITF (Zhou *et al.,* 2021).

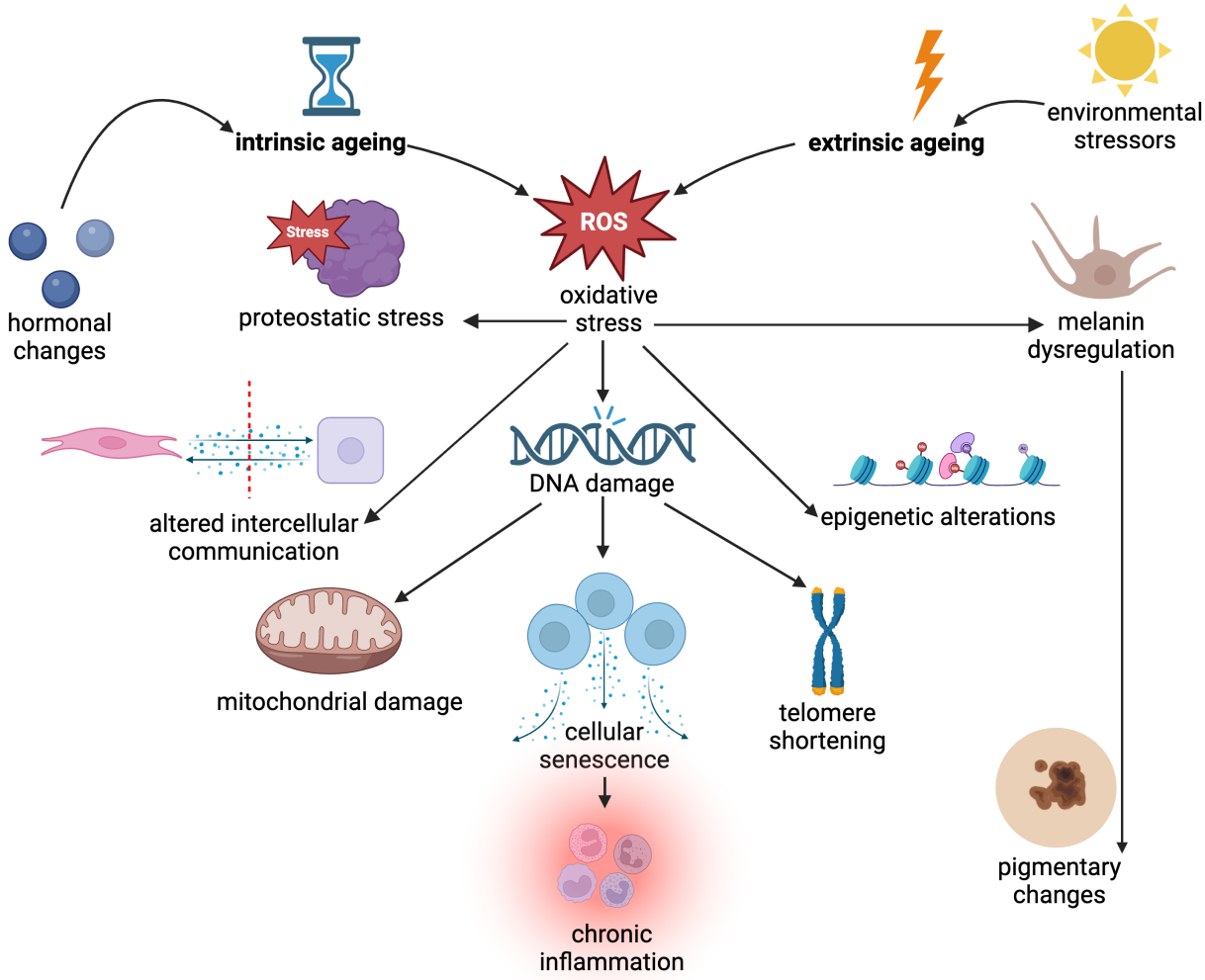

Figure 10: Schematic overview of the hallmarks of ageing implicated in intrinsic and extrinsic skin ageing.

Intrinsic ageing occurs naturally with the passing of time and is induced by internal factors such as hormonal changes, whereas extrinsic ageing is induced by environmental factors such as UV radiation. Both forms of ageing cause ROS-mediated oxidative stress, which causes DNA damage as well as proteostatic stress, altered intercellular communication, and epigenetic alterations. Oxidative stress also leads to melanin dysregulation, which ultimately causes pigmentary changes. DNA damage also contributes to telomere shortening, mitochondrial damage, and cellular senescence, which induces a state of chronic inflammation. All of these hallmarks are intricately interlinked and not all hallmarks are included in the diagram, so it should be noted that this schematic is a highly simplified overview of the processes involved in skin ageing, and also causing pigmentary changes. Created with BioRender.com.

Overall, the twelve hallmarks of ageing are intricately interlinked (**Figure 10**). Although they are all associated with ageing, none of them solely cause or are caused by ageing; rather, they encompass a complex network of molecular and cellular factors that interact with one another, and a resultant ageing phenotype can be observed. There is evidence that several of these hallmarks of ageing are also linked with pigmentation, which indicates that skin ageing and pigmentation influence one another.

1.2.2 Morphology of Ageing Skin

In ageing skin, the primary function of providing a barrier from the external environment becomes impaired (Farage *et al*., 2013), and therefore the ability to regulate homeostasis becomes compromised (Rittie & Fisher, 2015). Although an impaired skin barrier is associated with an increase in trans epidermal water loss (TEWL), there is contradictory evidence in current literature to support how TEWL is affected in ageing human skin. For example, a systematic review and meta-analysis conducted by Kottner *et al*. (2013) suggests that TEWL values in subjects aged 65 and above are significantly lower than in middle aged individuals. Therefore, TEWL values are not necessarily a reliable measurement of epidermal barrier integrity.

A reduction in epidermal thickness is another characteristic of skin ageing (Fenske and Lober, 1986; Waller and Maibach, 2005), which can partially be attributed to an impairment of keratinocyte proliferation (Ding *et al*., 2021). The percentage of cells expressing the Ki67 marker declines with age, which indicates a decrease in the proliferative activity of ageing keratinocytes (Shamitova *et al*., 2018). This age-related impairment of keratinocyte proliferation may have various causes, including the loss of junctional structures anchoring basal keratinocytes to the basement membrane, interrupting the communication between keratinocyte and fibroblasts and therefore reducing the proliferative capacity of basal stem cells (Langton *et al*., 2016). Additionally, high epidermal calcium concentrations have been hypothesised to inhibit keratinocyte proliferation in ageing skin (Tomitaka *et al*., 2003).

Several other studies found that a loss of p63 induces cellular senescence and accelerated ageing (Li *et al.*, 2023; Keyes & Mills, 2006; Keyes *et al.*, 2005). However, there is conflicting literature on the change in expression of the proliferation marker p63 in ageing skin. Some studies have found an increase in p63 expression with skin ageing. For example, a 2006 study by Sommer *et al.* found that in transgenic mice with an overexpression of ΔNp63&alpha, an accelerated ageing phenotype such as reduced cell proliferation and a decrease in epidermal thickness was observed, along with a drastic reduction in longevity. Either way, these collective findings do infer that p63 is somewhat involved in the process of ageing, and that keeping levels of its expression consistent is important for healthy skin ageing.

Additionally, there are changes in the composition of the cornified envelope with skin ageing. As well as a decrease in involucrin expression (Dos Santos *et al*., 2016), there is a decline in loricrin in old age, with no significant difference between young and middle-aged skin (Rinnerthaler *et al*., 2013). The changes in expression of these cornified envelope precursors

and barrier markers could also relate to the compromised integrity of the skin barrier with ageing. However, there is evidence that some of the barrier proteins such as involucrin and periplakin show no change in expression on a transcriptional or translational level in aged skin. This suggests that these proteins may not play a key role in driving skin ageing (Rinnerthaler *et al*., 2015). These proteins are also biomarkers of differentiation, in addition to kytokeratins such as k14. A 2008 study by Oender *et al*. found that the expression of the k14 gene did not change with skin ageing, suggesting that although k14 is an important marker of differentiation, it is not a major driving force of ageing in human skin.

Changes in the composition of the dermis are known to occur in ageing human skin. From a person's twenties or thirties, the activity of fibroblasts declines, and the synthesis of the ECM is reduced; collagen production decreases by around 1 % - 1.5 % every year (Reilly & Lozano, 2021). According to a 2014 study by Sibilla & Borumand, there is a peak in collagen content between the ages of 25-34 years old. As the subjects age, a gradual reduction in collagen occurs, with an estimated decrease of 25 % over the next 40 years. This is consistent with the ageing-related decline in collagen content seen in several studies using a range of measurements and methodologies. It is generally agreed that this loss of collagen is a key factor in the appearance of ageing skin, such as the presence of fine lines and wrinkles and decreased skin firmness and elasticity seen in both intrinsic and extrinsic skin ageing (Reilly & Lozano, 2021). Fibronectin expression is also downregulated with skin ageing, particularly in senescent fibroblasts (Cho *et al.,* 2022), which further reduced the ECM density.

ECM remodelling occurs in both intrinsically and extrinsically ageing skin, where the extracellular matrix becomes increasingly disorganised with an uneven distribution of its proteins (Naylor *et al*., 2011). Furthermore, the degradation of collagen and elastin increases via the upregulation of collagenases such as matrix metalloproteinases 1 and 3 (MMP1 and MMP3). This causes extracellular collagen and elastin to become fragmented, further contributing to the reduced elasticity and wrinkle formation associated with ageing skin (Chambers & Vukmanovic-Stejic, 2020).

Another way in which ageing changes the skin is that the morphology of cells can change; senescent skin cells *in vitro* display a flattened morphology and enlarged nuclei (Chin *et al*., 2023). Additionally, an altered composition of cells is observed in aged skin. For example, there is known to be a 10 % - 20 % reduction in melanocytes every decade in association with skin ageing (Rittie & Fisher, 2015). This would imply that ageing skin has a decrease in pigmentation and is more susceptible to sunburn and damage induced by UVR exposure.

1.2.3 Intrinsic Ageing

Intrinsic skin ageing occurs naturally with the passage of time, as a consequence of physiological age-related alterations such as hormonal changes that lead to the accumulation of cellular ROS and impairment to DNA damage repair systems (Farage *et al.,* 2008; **Figure 10**). There is also highly suggestive (although not yet conclusive) evidence that cellular senescence is a key driver of intrinsic skin ageing (Low *et al*., 2021)

A histological and morphometric analysis study by Arnal-Forné *et al.* (2024) found that intrinsic ageing on photo-protected areas of skin had profound influences on the composition and morphology of human skin. The number of cells, vessels, and appendages decreased throughout a person's lifetime, which is depicted in **Figure 11**. Additionally, the epidermal thickness decreases, the dermal-epidermal junction becomes flattened, and the reticular dermis becomes less dense as elastin fibres diminish.

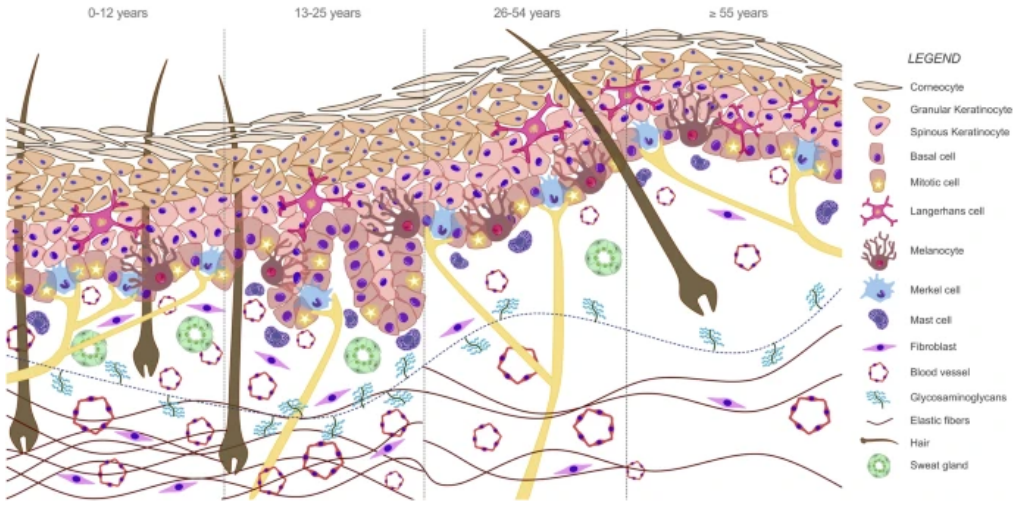

Figure 11: Changes in skin composition with intrinsic ageing.

A schematic of the histological structure of skin and its evolution in photo-protected areas caused by intrinsic ageing. Variations in all parameters investigated in a 2024 study by Arnal-Forné et al. between the age groups: group 1 (0-12 years; n = 5), group 2 (13-25 years; n = 5), group 3 (26-54 years; n = 10), group 4 (≥ 55 years; n = 5). Diagram sourced from Arnal-Forné et al., 2024.

The resultant characteristics typical of chronological skin ageing include a loss of elasticity, fine wrinkles, and aberrant pigmentation (Low et al., 2021). A reduction in pigmentation can be caused by the loss of melanocytes with intrinsic ageing (Ho & Dreesen, 2021). Additionally, melanogenesis can be regulated by intrinsic factors such as changes in the hormonal

environment and inflammation, which can cause a deviation in normal skin pigmentation (Serre *et al.*, 2018).

Several endocrinal changes occur with skin ageing, most notably changes in sex steroids such as oestrogen. The levels of oestrogen decline dramatically during the menopause, and an acceleration of the ageing processes can be experienced during this time. These hormonal changes are characterised by a decreased dermal collagen content and a reduced skin thickness, and the subsequent appearance of wrinkles (Ho & Dreesen, 2021).

There is some evidence to support the notion that there is a correlation between this ageing-related hormonal decline and hyperpigmentary disorders, such as melasma. Current *in vitro* data shows that oestrogen can stimulate melanocytes and therefore play a role in modulating pigmentation. Although sex steroid hormones can initiate hyperpigmentation in melasma, it is hypothesised that it does so by amplifying the influence of UVR on melanogenesis (Cario, 2019). Therefore, these pigmentary changes are likely caused by both extrinsic and intrinsic skin ageing.

The protective role of oestrogen has been demonstrated in various studies, such as a 2008 study by Tsukahara *et al.,* where ovariectomised mice displayed a deterioration in skin properties compared to the control, which was made worse with UVR exposure. Additionally, there is a link between an oestrogen decline and increased inflammation, as uncontrolled inflammation has been observed in the skin of postmenopausal women (Makrantonaki *et al*., 2010). This suggests that oestrogen also plays an anti-inflammatory role.

There is also a potential connection between inflammation and pigmentary changes. The pro-inflammatory cytokines secreted by senescent fibroblasts in intrinsically aged skin could be involved in stimulating pigmentation abnormalities. Such ROS-mediated inflammatory responses have been proposed as key mechanisms in driving post-inflammatory hyperpigmentation (PIHP) in darkly pigmented skin (Markiewicz *et al.,* 2022). This provides a further link between altered skin pigmentation and the hallmarks of ageing, namely chronic inflammation.

1.2.4 Extrinsic Ageing

Environmental ageing is the premature, accelerated skin ageing that occurs as a result of one's lifestyle and exposure to external stressors (Low *et al*., 2021). One of the most significant

exogenous factors that induces environmental ageing is UVR, which reaches the skin in two main forms: UVA and UVB. Both UVA and UVB rays are able to penetrate the epidermal layer, but UVA is better able to penetrate through the dermis (Song *et al.*, 2024). UVB rays are more responsible for burning, whereas UVA rays are more highly implicated in skin ageing (**Figure 12**). Ageing induced by exposure to UVR is referred to as photo-ageing.

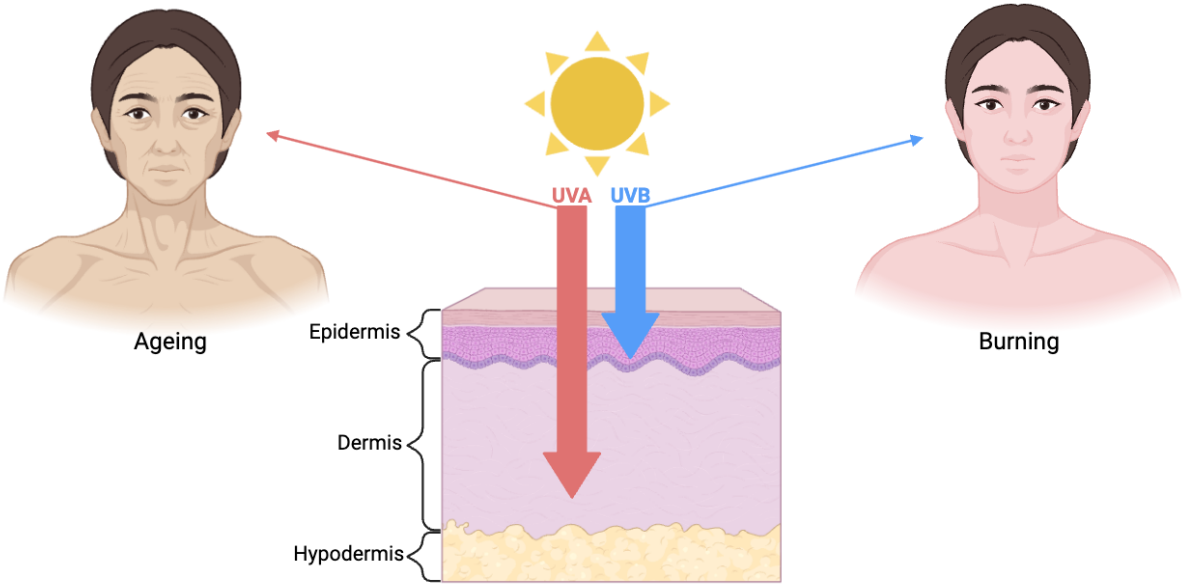

Figure 12: The effects of UVA and UVB rays.

A diagrammatic representation of the depth of skin penetration of UVA rays compared with UVB rays, and the physiological effect of exposure to UVA and UVB. UVA rays penetrate into the dermis and are implicated in skin ageing, whereas UVB rays reach the epidermis and cause sunburn. Created with BioRender.com.

Exposure to UVR causes DNA damage in a photobiochemical reaction via two different mechanisms. Firstly, UVR can produce cellular ROS, leading to oxidative damage that can alter the normal structure and function of DNA (Barnard *et al.*, 2018). Secondly, DNA photoproducts including cyclobutene pyrimidine dimers (CPDs) and 6-4 photoproducts are emitted when UVR is absorbed by the DNA, which can cause structural changes to the DNA helix and therefore disruptions to the processes of transcription and translation (Song *et al.*, 2024). In extrinsically aged skin, cellular senescence can be prematurely induced by exposure to UVR and the resultant DNA damage. A study by Wang *et al.* (2017) found that with UV exposure, senescence is induced in keratinocytes *in vitro* and *in vivo* (mouse model), characterised by a reduction in the marker lamin B1.

There are visible morphological differences in photo-exposed skin, even in young individuals (**Figure 13**). A quantitative morphometrics analysis by Costello *et al.* (2023) found that young photo-exposed skin was comparable to ageing photo-protected skin. Both groups display a

similar ageing morphology, such as the flattening of the DEJ. This supports the hypothesis that photo-ageing accelerates the process of skin ageing, even prematurely, and that changes in the DEJ contribute to changes in epidermal thickness in ageing skin.

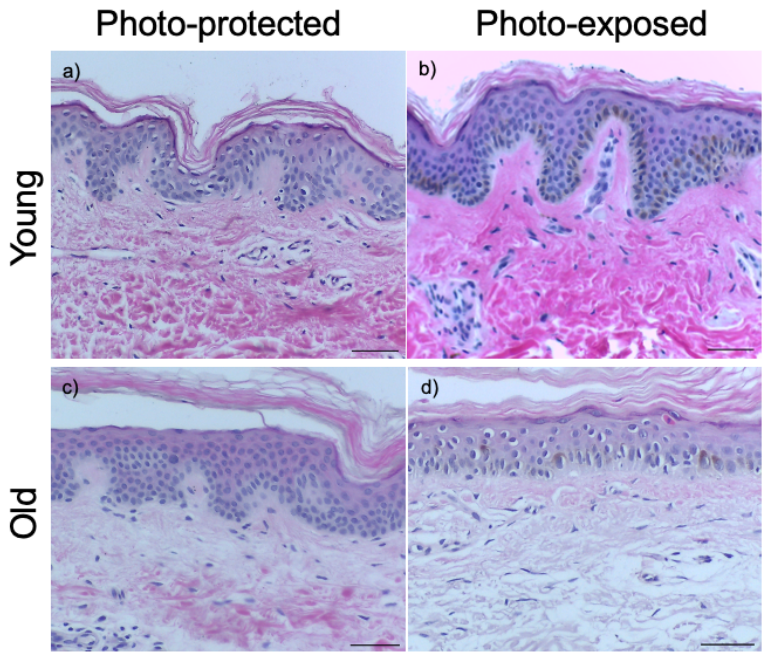

Figure 13: Histological analysis of ex vivo human skin tissue.

Representative H&E staining images of human tissue samples taken from female donors. a) biopsy sample from the photo-protected buttocks of a young (~ 20 yo) female donor, and b) from the photo-exposed arm of the same young female donor. c) biopsy sample from the photo-protected buttocks of an ageing (~ 60 yo) female donor, and d) from the photo-exposed arm of the same ageing female donor. Scale bar: 50 µm. Magnification: x20. Human skin sections kindly provided by Procter & Gamble.

The morphological changes in photo-aged skin differ to chronologically aged skin in several ways. For example, the organisation of collagen fibres becomes disordered compared with young, healthy human skin, and the degradation of collagen is exacerbated (Reilly & Lozano, 2021). Additionally, unlike in chronological ageing, the corneodesmosomes fail to degrade correctly, resulting in an increased epidermal thickness, with a thicker stratum corneum (Low *et al*., 2021). The phenotypic appearance of extrinsically aged skin is therefore characterised by deep wrinkles, skin laxity, roughness and telangiectasia (Naidoo & Birch-Machin, 2017). Pigmentary changes are another key clinical sign of photo-ageing, and they are better characterised and more well studied than the changes in pigmentation in intrinsically ageing skin (Low *et al*., 2021). This may in part be due to the loss of well-functioning melanocytes and disrupted communication between melanocytes and keratinocytes (Brenner & Hearing, 2008).

1.3 Skin Pigmentation

Skin pigmentation is fundamental in protecting human skin against harmful UVR (Goncalves *et al.*, 2023). The broad spectrum of pigmentation observed in human skin is determined by melanin content. Melanin is a tyrosine-derived pigment existing in the yellow/red pheomelanin and brown/black eumelanin forms. Individuals with higher ratios of eumelanin will have a darker skin tone, whereas those with a higher proportion of pheomelanin will have a lighter skin tone. Eumelanin absorbs and scatters UVR, therefore it has photoprotective properties. However, pheomelanin is photo-unstable and phototoxic, thus promoting photo-ageing (Lee, 2021).

1.3.1 Melanogenesis

Skin pigmentation occurs as a result of a series of processes: melanogenesis, melanin transport within melanocytes, melanin transfer to adjacent keratinocytes, and internalisation of melanin by keratinocytes (Moreiras *et al.,* 2021). Melanogenesis is the biosynthesis of melanin that occurs within melanosomes, membrane-bound organelles in melanocytes. This process involves the hydroxylation of tyrosine into dihydroxyphenylalanine (DOPA), which is then oxidised into dopaquinone (Rawlings, 2006). The rate-limiting enzyme of this series of reactions is tyrosinase (Hearing, 2011).

Once melanin has been synthesised, melanosomes are transferred from melanocytes to keratinocytes via the dendritic extensions of melanocytes (Kolarsick *et al.,* 2011). This is thought to occur via a coupled exocytosis/phagocytosis of the melanosome (Hall *et al.,* 2022). Melanosomes then accumulate in the perinuclear region to form supranuclear caps, which provide innate protection against DNA damage from UVR exposure (**Figure 14**). When exposed to an increase in UVR, an increase in melanin production and transfer to keratinocytes occurs, thus maximising the protection of the nuclei from harmful radiation (Kolarsick *et al*., 2011). The tanning effect can be observed when this occurs (Goncalves *et al.*, 2023).

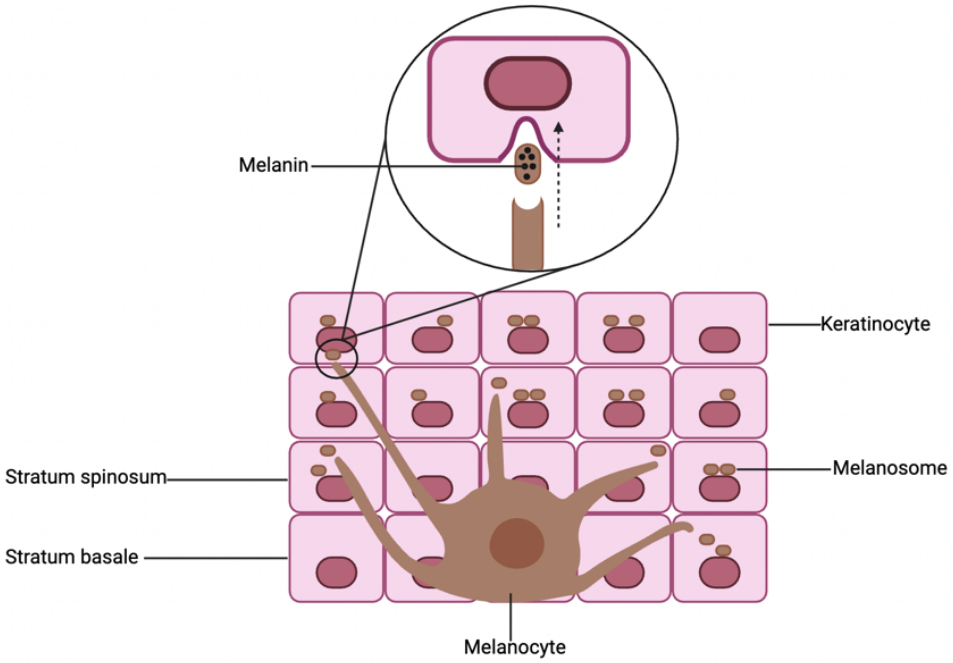

Figure 14: Melanogenesis and melanin transfer.

A diagram representing the synthesis of melanin by melanocytes and the transfer of melanin-containing melanosomes from the melanocytes into keratinocytes. Supranuclear caps can be visualised above the nuclei of keratinocytes. Created with BioRender.com

Melanogenesis is under tight regulation via multiple mechanisms. This is mainly with expression of the genes encoding tyrosinase, tyrosinase-related proteins such as TRP1, and microphthalmia-associated transcription factor (MITF) (Lee, 2021). On top of this, melanin synthesis is also under epigenetic control, as DNA methylation regulates the expression of genes involved in the regulation of melanogenesis including TRP1, TRP2 and MITF (Zhou *et al.,* 2021). A further gene involved in the regulation of skin pigmentation is melanocortin-1 receptor (MC1R), which is expressed by melanocytes and modulates the quantity and type of melanin synthesised (García-Borrón *et al*., 2005).

Gaining a deeper understanding of the functions of melanin and its regulation in relation to health and disease is important not only with regards photoprotection and skin cancers, but also in terms of pigmentary disorders (Goncalves *et al.*, 2023).

1.3.2 Pigmentary Changes with Ageing

As mentioned in Section 1.1.4, pigmentary disorders can arise when there is a dysregulation in the crosstalk between cell types (Bastonini *et al.*, 2016; **Figure 9**). The signalling between melanocytes, fibroblasts and keratinocytes is vital in the processes of melanogenesis, melanin transfer, and correct localisation of melanin in photoprotective supranuclear caps (De Los

Santos Gomez *et al*., 2024). However, current *in vitro* approaches do not accurately recapitulate the complexity of these processes as they occur in native human skin.

There is a strong correlation between the dysregulation of melanin synthesis and cellular senescence, which indicates that pigmentary changes can be related to ageing. For example, senescent fibroblasts can disrupt the processes involved in melanogenesis and subsequently cause age-related pigmentation abnormalities (Kim *et al*., 2022; **Figure 9**). In fact, a higher proportion of senescent fibroblasts have been detected in hyperpigmented lesions, indicating a strong link between skin ageing and pigmentation abnormalities (Yoon *et al.*, 2018). Additionally, in senescent melanocytes, TRP-1, TRP-2 and MITF are downregulated, therefore melanin production is reduced, giving the phenotypic outcome of hypopigmentation (Lee, 2021). All of this provides evidence that dysregulation of the processes involved in the production of melanin can give rise to skin pigmentation abnormalities.

Oxidative stress is a further hallmark of ageing that is thought to be involved in pigmentary irregularities. ROS is produced during melanogenesis, and melanocytes are susceptible to oxidative stress caused by the increased levels of intracellular ROS; this may even increase the risk of melanoma formation (Jenkins & Grossman, 2013). In addition, there is a strong correlation between these ageing-related pigmentary changes and extrinsic skin ageing. Multiple pigmentary disorders including senile lentigo are typically signs associated with photo-ageing (Kim *et al*., 2022). Furthermore, the MC1R gene is upregulated by UVR exposure (García-Borrón *et al.,* 2005). This suggests an association between pigmentation abnormalities and photo-ageing.

Dark spots, or solar lentigines, are characterised by the excessive production and deposition of melanin, causing lesions of hyperpigmentation (Jdid *et al*., 2024). Dark spots are often associated with photo-ageing, particularly in Chinese populations where they are perceived as a more prominent sign of ageing than wrinkles and sagging (Porcheron *et al*., 2014). On the contrary, the number of melanocytes is known to deplete in intrinsically ageing human skin, which may reduce melanin production. This can result in phenotypic outcome of lesions of hypopigmentation (Ho & Dreesen, 2021).

It is thought that melanocytes become more unevenly distributed within the basal layer with age, causing some regions to have a reduced number of melanocytes and some areas to have an increased number of melanocytes (Yaar *et al*., 2002). This is likely a key factor responsible for the combination of hyperpigmentation and hypopigmentation seen with ageing. The reduction of melanocytes in certain areas would also make the skin more susceptible to

UV-induced environmental damage, which would, in turn, exacerbate the phenotypic effects of photo-ageing (Yaar *et al*., 2002).

Overall, age-related pigmentation abnormalities have been seen to arise in the form of hypopigmentation and hyperpigmentation, however more research is needed to uncover the biological mechanisms that determine this.

1.3.3 Ageing in Ethnically Diverse Skin

When discussing the requirement for more complex models of skin ageing and pigmentation, it is fundamental to address the need for the research to be representative of diverse populations. Most skin ageing research focusses on Fitzpatrick phototypes I-III (lightly pigmented skin), whilst little emphasis is placed on more darkly pigmented skin tones with Fitzpatrick phototypes V-VI (Langton *et al*., 2019). Unfortunately, an understanding of skin of colour is lacking in the current scientific landscape, even though ethnically diverse skin makes up the majority of our global population (Rawlings, 2006).

A 2019 study by Langton *et al.* found that in a black African American sample, both intrinsic and extrinsic ageing significantly affected the structure and function of skin. This highlights that all racial groups are subjected to the process of photo-ageing, even though individuals with darker skin tones have a higher cellular content of photoprotective eumelanin and therefore increased natural photoprotection. This study is highly commendable given the lack of other research on skin of colour, and it emphasises the need for further research and improved public health advice regarding the harmful consequences of exposure to UVR.

However, unlike to the numerous large-scale studies on lighter skin tones, the study is limited by its smaller sample size, with only 21 participants in the young group and 18 in the old group. This is a frequent limitation of skin research in ethnically diverse populations, with another limitation being that the existing studies show conflicting results (Rawlings, 2006). For example, a study by Corcuff *et al*. (1991) found that desquamation was increased in black subjects. Conversely, a study by Warrier *et al*. (1996) found that desquamation was greater in Caucasian individuals, and a study by Manuskitti *et al*. (1998) found no differences in desquamation between women with lightly or darkly pigmented skin. Additionally, these studies are outdated and were carried out decades ago, which reflects the state of the literature on skin of colour. Besides, not all of these studies focus specifically on the processes involved in skin ageing.

Despite these limitations, there are a few studies that show the phenotypic differences of ageing skin between ethnic groups. A comparative pilot study between Chinese and French women found that although wrinkle onset occurs around 10 years earlier in French women, the intensity of dark spots was more prominent and significant as a sign of ageing in Chinese women (Nouveau-Richard *et al.,* 2005). The women in the French and Chinese populations did not differ in the assessment of lifelong sun exposure, therefore the differences were likely caused by photo-ageing but presented differently across the different ethnic groups. The differences in characteristics of facial ageing between racial groups are depicted in a 2016 paper by Vashi *et al.* (**Figure 15**).

Figure 15: The differences in characteristics of facial ageing between racial groups.

Women over 60 years old displaying the difference in characteristic features of facial aging between ethnic groups. a) Caucasian, b) Hispanic, c) East Asian, d) African. Images sources from Vashi et al., 2016.

A more comprehensive knowledge of the structural and functional differences in ethnic skin is fundamental in understanding the differences in the processes of ageing. There is evidence of differences in the composition of the stratum corneum, such as differences in the water and lipid content and barrier function between multiple ethnic groups (Black, Asian, Hispanic, White). In black skin, there is evidence of an increased number cornified cells in skin with the

same epidermal thickness as white skin, and so a more compact stratum corneum (Rawlings, 2006). These differing physiological characteristics are likely to affect the processes of ageing in various ways.

Individuals with darker skin are believed to have an increased skin firmness in comparison to individuals of the same age with lighter skin, and these manifestations of ageing typically occur around 10 years later in skin of colour (Vashi *et al.*, 2016). This may be due to dermal differences between ethnic groups. The thickness of the dermis has been found to be proportional to the level of pigmentation, with black and Asian skin having a more compact dermis with an increased dermal thickness compared with white skin (Montgana *et al.*, 1993). This may be because the fibroblasts have been found to be larger, more numerous and multinucleated in black skin, forming smaller collagen fibre bundles which contributes to a preserved skin elasticity (Montgana & Carlisle, 1991).

The most obvious difference between ethnic groups is differences in skin pigmentation, with an increase in age-related pigmentary changes in those with darker skin (Vashi *et al.*, 2016). Ethnic differences in pigmentation can be attributed to an increase in TRP1-mediated tyrosinase activity and therefore increased melanin synthesis (Talakoub & Wesley, 2009). The increased melanin content in darker skin tones leads to dyschromias with ageing, but a greater degree of photoprotection and less pronounced photo-ageing compared with lighter skin (Vashi *et al.*, 2016). However, public awareness and education of healthy skin ageing and photoprotection remains important across all racial groups. Skin conditions can present differently on different skin tones, leading to unequal opportunity to recognise symptoms and even to misdiagnoses (NHS, 2022).

Overall, research on lightly pigmented skin is not necessarily applicable to ethnically diverse populations. This emphasises the importance of improved scientific research and public awareness and education of protection from the sun across all populations, no matter the skin tone. Furthermore, it is not as simple as black or white; there is a whole diversity of skin tones that all need representation in science to help bridge the gap in medical care. Therefore, there is a need to implement more diverse skin model systems going forward, such as with the incorporation of cells derived from donors with skin of colour, for example using darkly pigmented melanocytes.

1.4 Studying Skin Ageing and Pigmentation

Model systems are fundamental in studying the processes of ageing and pigmentation in the skin. There are multiple model platforms that may be used, each with their own advantages and disadvantages, which are outlined in **Table 1**.

Table 1: An overview of different skin models.

A description of the current approaches for studying skin ageing and pigmentation and their advantages and disadvantages.

Model	Description	Advantages	Disadvantages
2D assay *in vitro*	Culturing 2D homogeneous fibroblasts or keratinocytes on a plastic substrate	• Cost effective • High-throughput assay • Quick	• Lacks thorough characterisation • Not representative of human skin • Variation in cell behaviour and morphology
Animal model *in vivo*	Studying ageing in model organisms with an ageing phenotype	• Allows systemic effects to be studied	• Differences to human skin • Animal testing prohibited
Human skin sample/explant *ex vivo*	Full thickness skin biopsy samples taken from human volunteers	• Human skin tissue containing all relevant cell types and appendages	• Limited tissue availability • Tissue heterogeneity • Viability issue
3D skin model *in vitro*	Bioengineered tissue model with a dermal and epidermal compartment	• Representative of native human skin including its microenvironment • Robust • Reproducible • Highly characterised • Can mimic an ageing or pigmented phenotype	• Currently only contain 2-3 cell types • Lack appendages of human skin • Current models do not combine ageing and pigmented phenotypes • Heterogeneity
Human clinical trials	Testing drugs or cosmetics on human volunteers	• Necessary for pharmaceutical and cosmetic testing	• Expensive • Time-consuming

1.4.1 2D *in vitro* Assay

The most basic skin model types are 2D *in vitro* assays, which involve culturing a monolayer of homogeneous fibroblasts or keratinocytes. The use of conventional 2D cell culture has

facilitated various developments in ageing research, such as the discovery of the SASP-associated secretome in ageing fibroblasts (Waldera Lupa *et al.*, 2015). Skin pigmentation has also been studied using a 2D *in vitro* methodology where human epidermal keratinocytes and melanocytes were co-cultured with the addition of tyrosine and ammonium chloride, and melanogenesis was successfully induced (Branquinho *et al.*, 2020).

Additionally, these 2D models are highly useful for performing quick, cost-effective, high-throughput assays; however, they lack the complexity of human skin since they are limited to just one cell type. Human skin is multi-layered and multicellular, and the stratified and differentiated structure cannot be replicated by culturing a homogenous cell population in 2D (Costello *et al.*, 2022). Furthermore, the microenvironment of these models does not mimic that of human skin, and cells can be observed to have an altered physiological behaviour versus *in vivo*. This is due to factors including a flattened morphology, compromised intercellular interactions and disrupted apical-basal polarity (Baker & Chen, 2012). Ultimately, this means that 2D *in vitro* skin cannot be used to successfully study how ageing affects pigmentation.

1.4.2 *in vivo* Animal Model

The animal ageing model is another platform for studying skin ageing, which allows for the systemic effects to be studied. The mouse model has enabled several breakthroughs in skin and ageing research. This model is often used in mice with ageing phenotypes, since they are mammals and therefore display a more similar age-related functional decline compared with more simple organisms (Costello, 2019). In a 2016 study by Baker *et al.*, mice were genetically engineered to induce apoptosis in cells expressing secretory phenotype $p16^{Ink4a}$, and thereby studying its effect on cellular senescence. This is a typical example of the use of the mouse model system to study skin ageing.

The mouse model has also been used to study skin pigmentation. For example, a murine model of post-inflammatory hyperpigmentation (PIH) was established by Nakano *et al.* (2021). An increase in melanin was observed, amongst other characteristics attributed to PIH. This model was produced by inducing chronic contact dermatitis in transgenic mice with melanocytes in their epidermis, which had previously been developed by Kunisada *et al*. in 1998 to more closely mimic human skin.

However, animal models are not entirely representative of human anatomy. For instance, murine and human skin differ in epidermal thickness and hair follicle distribution, among other factors (Wong *et al.*, 2011). Above all, animal testing is prohibited in cosmetic research by the European Union legislation, and several initiatives are working to develop ethical alternatives to animal testing, including reconstructed human skin equivalents (European Union, 2009). Therefore, it is imperative to move away from the use of animal models in skin studies, especially where the output is to benefit the cosmetics industry.

1.4.3 *in vivo* Human Clinical Trials

Human clinical trials are mandatory when testing compounds and topical formulations in industry. This is, of course, the most accurate model system, and is useful for looking at clinical and phenotypic manifestations of ageing and pigmentary disorders. In a 2012 study by Lagarrigue *et al.,* the researchers developed an *in vivo* method to assess the effects of age and UV radiation on skin pigmentation, comparing photo-exposed and photo-protected anatomical areas using reflectance confocal microscopy. Their methodology allowed the epidermal pigmentation to be quantified, as well as the dermis papilla density measured at the DEJ as a marker of skin pigmentation.

Non-invasive studies such as this provide some useful measurements of skin pigmentation in relation to ageing, however specific markers cannot be analysed using immunofluorescence analysis and other molecular techniques. Despite being essential to later stages of compound testing after they have already been tested on other model systems, the process of clinical trials is expensive and time-consuming, and therefore not necessarily suitable for routine skin ageing and pigmentation studies.

1.4.4 *ex vivo* Human Skin Explant

Human skin explants are a highly useful model type because they are fully representative of human skin; they are inclusive of all appendages and cell types, including melanocytes for the potential to quantify pigmentary changes (Costello, 2019). A 2023 study by Costello *et al.* used *ex vivo* skin samples from ageing individuals to conduct a quantitative morphometric analysis of chronological ageing and photo-ageing. This was achieved by comparing skin biopsies from photo-exposed and photo-protected anatomical sites from young and ageing individuals. This study found that the thickness of the epidermis decreased with both age and photo-exposure, and that the changes were not attributed to changes in cellular proliferation. Instead, the

findings of this study highlight the importance of the presence of the dermal-epidermal junction within a model platform, since age-related changes in epidermal thickness were attributed to alterations in the DEJ. Additionally, the young photo-aged skin in this study was comparable to old intrinsically aged skin across several parameters, cementing the notion that exposure to UVR accelerates skin ageing.

Ex vivo skin explants can be cultured, often obtained as a surplus from plastic surgery. These samples can remain viable for up to 14 days and can be a safe and efficient tool that generates data that is reproducible and consistent with clinical trials, such as for the topical application of personal care products (Zhou *et al*., 2023). However, tissue explants do not remain viable for sufficiently long periods of time, and there is a shortage of tissue available for these models (Costello, 2019), especially during times where there is a decrease in plastic surgery such as during the summer. Additionally, tissue heterogeneity is a challenge when working with skin explants, even amongst punch biopsies derived from the same donor; there are significant structural differences such as the epidermal thickness in samples taken from different donors (Wurbs *et al*., 2024). For these reasons, it is not always feasible to use this model platform.

1.4.5 3D *in vitro* Skin Model

3D *in vitro* skin human skin equivalents (HSEs) are highly physiologically relevant model platforms as they are representative of human native skin (Roth-Carter *et al*., 2022). In addition, these models reproduce the microenvironment of human skin more accurately than in traditional 2D cell culture, therefore cellular signalling, behaviour, and morphology are more representative of the conditions *in vivo* (**Figure 16**). However, unlike human skin, 3D skin models only contain a few of the cell types and lack the appendages and vascularity of human skin (Yamada & Cukierman, 2007), therefore their complexity needs to be increased.

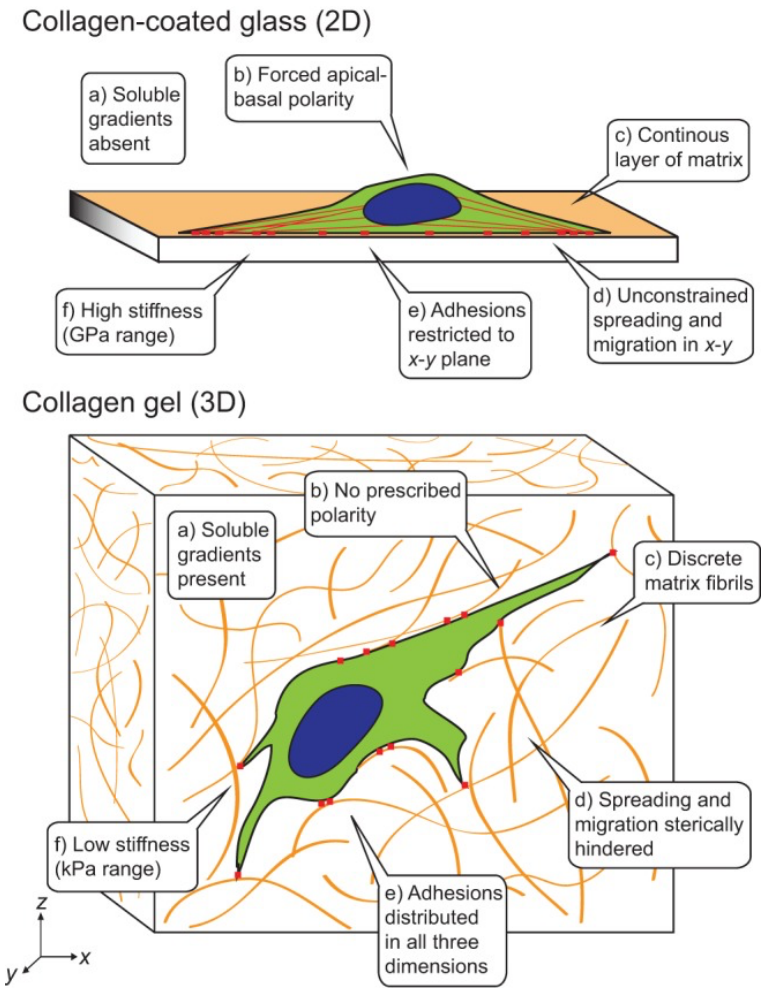

Figure 16: The differences in cellular behaviour and morphology in 2D and 3D cell culture.

Environmental cues and resultant differences in the behaviour and morphology of cells in 2D (collagen-coated glass) vs 3D (collagen gel) cell culture. Diagram sourced from Yamada & Cukierman, 2007.

An example of a 3D skin model is the organotypic skin culture, which is constructed by seeding keratinocytes onto a collagen plug (often containing fibroblasts), and then raising the model to the air-liquid interface to encourage keratinocyte differentiation. Pigmented skin models have been generated using this methodology, with the incorporation of melanocytes seeded alongside the keratinocytes in 3D *in vitro* skin models (Roth-Carter *et al.*, 2022).

In several studies, such 3D skin equivalents have been used as a platform to investigate skin ageing. Multiple papers have incorporated senescent fibroblasts to produce an ageing phenotype in their 3D *in vitro* models. For example, Diekmann *et al.* (2016) constructed a 3D ageing model by co-culturing fibroblasts and keratinocytes on a collagen-glycosaminoglycan-chitosan scaffold and inducing senescence by exposing fibroblasts to the chemotherapy drug Mitomycin-C. The senescent fibroblasts in this study were responsible for some ageing-associated changes, such as a reduction in collagen and elastin expression and a decrease

in epidermal filaggrin, however no difference in the epidermal thickness was observed (Diekmann *et al*., 2016).

In another ageing model of senescence, a 3D organotypic skin model was used where senescent fibroblasts were cultured in a collagen-based matrix (Weinmüllner *et al.,* 2020). It was found that several hallmarks of intrinsic skin ageing were induced by the presence of these senescent fibroblasts; a reduction of the epidermal thickness was observed, as well as a decrease in the proliferation of basal keratinocytes, reduced differentiation of keratinocytes, and impaired barrier function (Weinmüllner *et al.,* 2020). However, such models of skin ageing that incorporate senescent cells hold some limitations. For example, they are often used with neonatal keratinocytes, or intrinsically aged skin cells that are not age matched. In addition, the exogenous ECM proteins in the collagen-based system may confound the results, and the artificial induction of senescence, a singular hallmark of cellular ageing, may confine our understanding of the intricate, multifaceted ageing process.

3D *in vitro* skin equivalents are not limited to collagen-based model systems; there are several other examples of 3D skin models. For example, dermal and epidermal models of ageing and pigmentation have been bioengineered, where the fibroblasts or keratinocytes (and melanocytes in pigmented models) are seeded onto a scaffold. 3D *in vitro* epidermal models have been generated by seeding keratinocytes onto Millicell® cell culture inserts, using a methodology previously described by Roger *et al.* (2019). Ageing epidermal models have been bioengineered by Costello in 2019, where ageing female keratinocytes were seeded onto the Millicell® insert. Age-related epidermal changes were observed compared with neonatal epidermal equivalents, such as alterations in the morphology of basal keratinocytes.

Pigmented epidermal models have been produced using the same technology, where darkly pigmented melanocytes were seeded alongside keratinocytes. The successful incorporation of melanocytes was confirmed with the melanocyte markers S100 and GP100, and Fontana-Masson staining showed that melanin was deposited across the epidermis, which indicated that melanin was transferred to keratinocytes similar to in human skin. Additionally, the ITA values were reduced in the pigmented models compared with models without melanocytes, indicating an increase in skin pigmentation (Goncalves *et al*., 2023).

Ageing dermal models have been produced using the Alvetex® technology. Alvetex® is an inert porous scaffold upon which fibroblasts can be seeded and cultured, allowing them to secrete the components of the ECM including collagens, fibronectin and elastin (Roger *et al*., 2019). Dermal equivalents constructed using ageing female fibroblasts showed ageing-

associated differences, such as a reduction in the deposition of ECM proteins (Costello, 2019). However, dermal models cannot contain melanocytes, so it is not possible to investigate the effects of ageing on pigmentation using this platform.

It must be noted that these epidermal and dermal equivalents were bioengineered as a simplified model to optimise the development of more complex 3D full thickness skin models prior to their construction (Goncalves *et al*., 2023). Additionally, dermal and epidermal skin equivalents hold the key limitation of the lack of a DEJ, considering the importance of the crosstalk between the two layers. This means that several of the pigmentary and ageing-related changes would not be reproduced to be representative of human skin.

Ageing pigmented 3D *in vitro* HSEs have been generated by Duval *et al*. (2014) using a bovine-based collagen hydrogel system. The dermal compartment was constructed by culturing fibroblasts with bovine type 1 collagen, then keratinocytes and melanocytes were co-seeded in a steel ring placed on top of the dermal compartment. Firstly, they constructed these models with the presence and absence of fibroblasts and found that pigmentation increased drastically in the presence of fibroblasts. This confirms that fibroblasts are important in determining pigmentation, as well as highlighting the importance of dermal-epidermal crosstalk in these processes.

Secondly, Duval *et al*. (2014) compared these models containing foetal versus adult fibroblasts to assess age-related variation in pigmentation. They observed a macroscopic increase in pigmentation in the models containing foetal fibroblasts, which was confirmed by quantitative parameters related to skin colour, melanocyte numbers and melanocyte content. This experiment confirms that fibroblasts are important in influencing the level of skin pigmentation *in vitro*, and the role that altered intercellular communication might play in determining skin pigmentation.

Thirdly, they compared skin models with young fibroblasts (16–21-year-old) from a photo-protected region with natural photo-aged fibroblasts (71–77-year-old). Prior to this experiment, the photo-aged fibroblasts were confirmed to express a senescence profile with a lower rate of proliferation and altered morphological features. In the 3D *in vitro* skin models with photo-aged fibroblasts, a significant increase in skin colour, epidermal melanin content, and melanogenic expression was observed, which shows that photo-ageing and related pigmentary changes could be linked to modifications of dermal fibroblasts that occur over time.

However, this 3D *in vitro* model that combines skin ageing and pigmentation hold some limitations and requires some optimisation to better understand how the two attributes affect one another in human skin. For example, the age of the adult female keratinocytes used in this study was not specified or age matched to the corresponding fibroblasts. Additionally, the melanocytes were neonatal and originated from moderately pigmented Caucasian donors, which may have limited the pigmentation levels observed across all models and is not particularly representative of the pigmentary phenotypes observed across our diverse global population. Furthermore, the seeding ratio of keratinocytes: melanocytes was not specified or optimised, therefore it may not have reflected the proportion of these cell types in human skin. A further limitation of their study is that the bovine collagen hydrogels lack several of the features of human skin, such as a DEJ and an endogenous ECM network. Therefore, the potential to investigate how ageing affects pigmentation using 3D *in vitro* HSEs platforms has not yet been fully explored.

1.5 Bioengineering 3D in vitro Full Thickness Human Skin Models

A novel *in vitro* 3D full thickness model is bioengineered using neonatal cells by culturing a dermal component on an Alvetex® scaffold and subsequently seeding keratinocytes onto the dermis, then raising the model to the air-liquid interface. These models are robust, reproducible, and highly characterised, containing an ECM-producing dermal component and stratified epidermal component (**Figure 17**), as well as the presence of a dermal-epidermal junction (Costello *et al*., 2024). It accurately mimics the structure, function, and cellular processes of human skin, making it an extremely useful tool for studying skin ageing and pigmentation (Roger *et al.,* 2019).

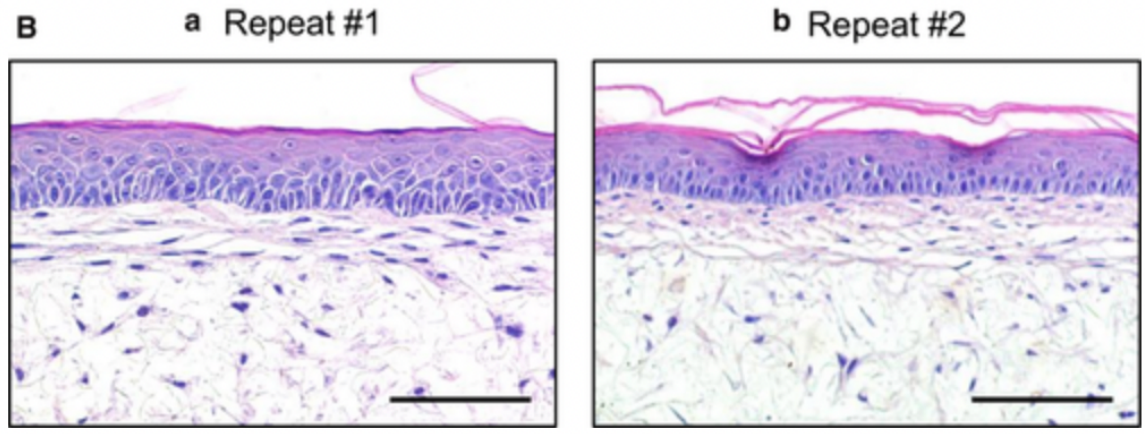

Figure 17: The reproducible and robust 3D in vitro full thickness skin models using Alvetex® technology.

Each repeat was performed by researchers from different labs independently of one another. The dermal component was cultured for up to 35 days and the model was raised to the air-liquid interface for 14 days. Scale bar: 50 μm. Image sourced from Roger et al, 2019.

However, it is important to acknowledge the limitations of the Alvetex®-based full thickness skin model. While these models are largely representative of human skin, they do not yet include skin appendages such as sebaceous glands, hair follicles, and vascular components, lacking the complete anatomical complexity of human skin (Simpson *et al*., 2024). Additionally, most skin equivalents are constructed using neonatal fibroblasts and keratinocytes, which can limit the direct extrapolation to adult skin unless ageing is engineered (Low *et al.*, 2024).

Nevertheless, in a 2024 study by Low *et al*., this model platform was used to address skin ageing by incorporating senescent fibroblasts. An ageing phenotypic outcome was observed; the dermal-epidermal crosstalk reproduced in this model caused the senescent fibroblasts to affect the structure and function of the epidermis with neonatal keratinocytes. These findings further highlight the importance of a 3D environment (Low *et al.*, 2024).

This methodology has also been used to construct ageing 3D *in vitro* full thickness skin models using cells from ageing donors. These models have been piloted and optimised, showing an ageing morphology such as a thinning viable epidermis compared with models made using cells from a young donor (Costello, 2019; **Figure 18**). The researchers in a study by Costello *et al.* (2024) created a 3D full thickness skin model by coculturing ageing fibroblasts from a 60-year-old donor with neonatal keratinocytes using the Alvetex® technology. It was determined that ageing fibroblasts secreted SASPs, which significantly decreased the epidermal thickness and altered the morphology of healthy neonatal keratinocytes that were in the 3D *in vitro* full thickness skin model.

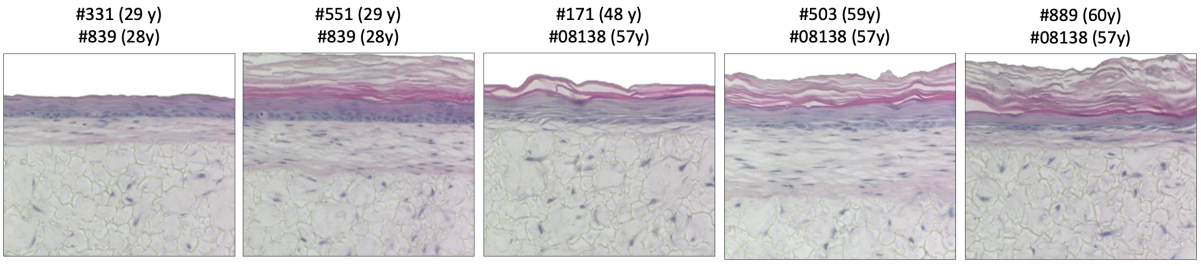

Figure 18: An ageing morphology is observed in ageing 3D in vitro full thickness skin models compared to young skin models.

Primary cells taken from young and ageing adult female donors. Age of the donor from which primary cells are derived is in brackets above images. Images sourced from Costello, 2019.

Due to the multifactorial nature of ageing and its heterogeneity between individuals, it is extremely challenging to study and understand ageing in the laboratory. Although several studies of skin ageing have attempted to overcome this obstacle, many of them incorporate senescent cells, which are only reflective of one hallmark of cellular ageing and, whilst it is still valuable to understand each of the hallmarks of ageing in isolation, this narrows the insights available from such research. Some studies have used cells from an ageing donor to overcome this and, although this does not overcome the issue of heterogeneity, it is more representative of native human skin and encapsulates the broad spectrum of hallmarks of ageing that have occurred in a real person. However, no study has matched the age of different cell types, which would increase the level of complexity of the model.

Multiple separate studies by Hall *et al.* (2022), Goncalves *et al.* (2023), and De Los Santos Gomez *et al*. (2024) used the same protocol and Alvetex® technology to generate and validate pigmented 3D full thickness skin models. These studies showed that melanocytes can be successfully incorporated into 3D full thickness models to produce uniformly distributed pigmentation comparable to human skin, which was confirmed across various parameters (**Figure 19**). The 2023 study by Goncalves *et al.* and 2024 study by De Los Santos Gomez *et al.* investigated the effects of exposure to UVR and revealed a tanning effect similar to human skin in the pigmented skin models, demonstrating that the protective function of melanocytes is retained *in vitro*. These studies also emphasised the significance of the fibroblasts and communication across the DEJ in determining epidermal pigmentation.

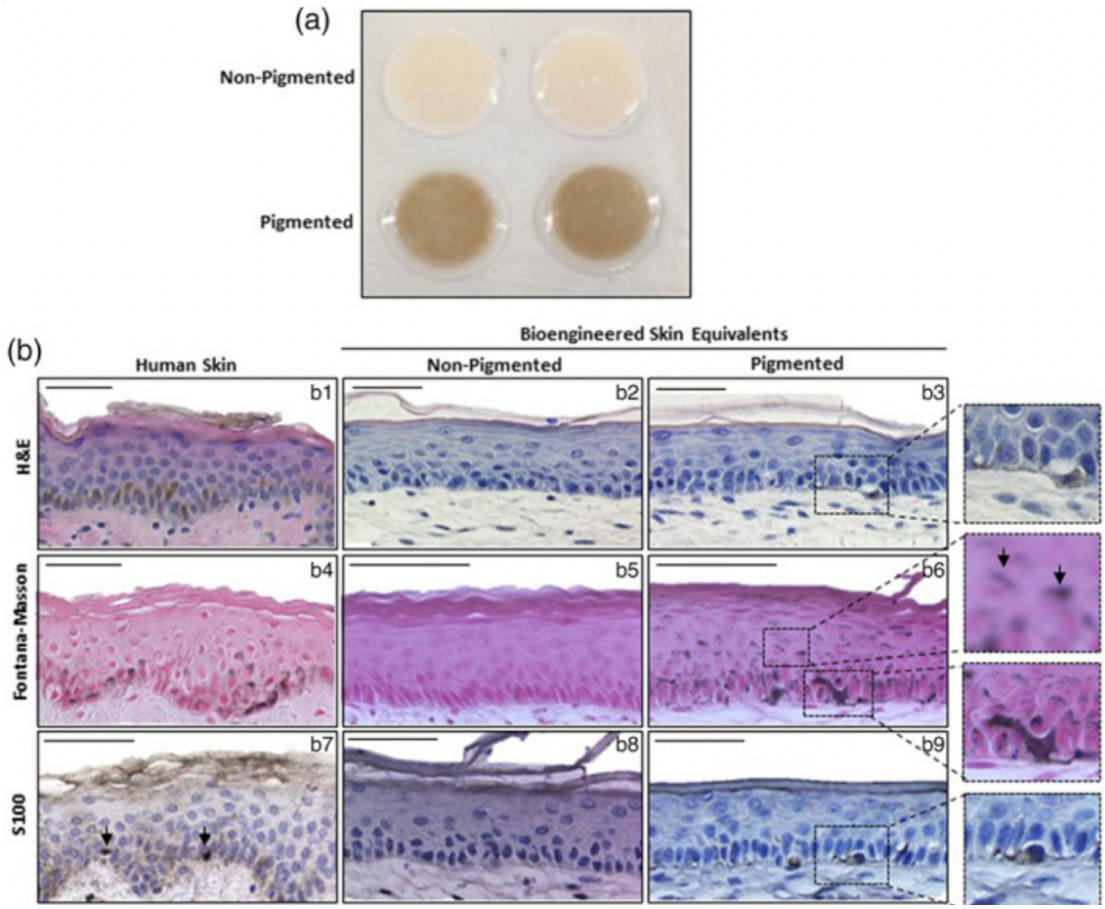

Figure 19: Melanocytes are successfully incorporated into 3D full thickness skin models to produce a uniformly distributed pigmentation comparable to human skin.

A) gross appearance models display a pigmented phenotype in pigmented models. B) H&E staining shows pigmentation comparable to human skin in pigmented models; Fontana-Masson staining shows even melanin dispersion comparable to human skin; and immunohistochemistry of S100 shows melanocytes distributed and aligned in the epidermis comparable to human skin. Images sourced from Goncalves et al, 2023.

Ultimately, only a limited number of ageing pigmented 3D *in vitro* HSEs have been developed, resulting in a restricted amount of available data. As a result, we are unable to fully grasp the complexities of the processes underlying the observed age-related pigmentary changes. There is a need to develop more complex models that integrate both ageing and pigmented phenotypes to explore how the two interact with one another. While it is known that photo-ageing can cause pigmentation abnormalities (Naidoo & Birch-Machin, 2017), the phenotypic outcome in *in vitro* 3D full thickness model systems, specifically whether hyperpigmentation or hypopigmentation, remains unknown.

1.6 Conclusion

The development of 3D full thickness skin models has been a groundbreaking advancement in dermatological research, offering a valuable tool for studies within the cosmetics and

pharmaceutical industries (Roger *et al*., 2019). The Alvetex® model platform has been used to create distinct skin models that exhibit both an ageing morphology (Costello, 2019; Low *et al.*, 2024; Costello *et al*., 2024) and a pigmented phenotype (Goncalves *et al*., 2023; De Los Santos Gomez *et al*., 2024), with the potential to combine these two features. Furthermore, the Alvetex® system offers several advantages over previously established models, including reproducibility, well-characterized structure, support for an endogenous extracellular matrix (ECM), and similarity to native human skin tissue. Its inclusion of a dermal-epidermal junction (DEJ) makes it an ideal platform for investigating dermal- epidermal interactions, which have been implicated in both skin ageing and pigmentation. Addressing the gap in research regarding how ageing influences pigmentation abnormalities
in vitro is crucial to advancing our understanding of this complex process.

Creating a more intricate model system that combines both ageing and pigmentation would be highly advantageous for studying how ageing impacts skin pigmentation. While it is known that ageing affects pigmentation, further investigation is needed to elucidate the biological mechanisms driving these changes. Additionally, increasing the complexity of skin models is essential for advancing this research. Melanocytes, key cells in human skin, interact with other cell types such as keratinocytes and fibroblasts, and play a significant role in the ageing process. Using age-matched skin cells from adult donors *in vitro* would offer a more accurate representation of native human skin compared to using primary neonatal cells, thus enhancing the complexity of these models.

Finally, in light of the global demographic shift toward an ageing population with diverse skin tones, it is crucial for scientific research to reflect this diversity. As such, prioritising research on ageing and skin of colour is imperative for ensuring that scientific findings are inclusive and relevant to the broader population.

1.7 Aims and Objectives

This project aims to utilise bioengineered 3D *in vitro* full thickness skin models to investigate the effects of skin ageing on pigmentation. These full thickness models are constructed using primary human cells and established Alvetex® technology. Alvetex® is an inert porous scaffold upon which fibroblasts can adhere and grow to form the dermal equivalent. Keratinocytes can then be seeded on, with the addition of melanocytes to construct pigmented models, to form the epidermal equivalent. The model is then raised to the air-liquid interface and maintained in this state for at least 14 days. This produces robust, reproducible *in vitro* 3D full thickness

skin equivalents which consistently mimic the structure and function of native human skin tissue (Roger *et al.,* 2019).

This model has been used to generate pigmented models; melanocytes were successfully incorporated into full thickness skin models, resulting in a uniformly distributed pigmentation comparable to human skin (Goncalves *et al.*, 2023). Ageing models have also been constructed using this platform. This was achieved by culturing fibroblasts and keratinocytes from ageing females, which produced skin models in which an ageing morphology such as reduced epidermal thickness could be observed (Costello, 2019). Both the ageing and pigmented full thickness skin models are physiologically relevant to human skin compared to neonatal non-pigmented models; however, the two attributes have not yet been combined *in vitro*.

The aim of this project is to construct and analyse novel ageing pigmented female 3D full thickness human skin models to investigate how ageing affects pigmentation. Firstly, it is hypothesised that melanocytes will be successfully integrated into the ageing 3D *in vitro* full thickness skin equivalents to produce pigmented models of aged human skin. Secondly, it is hypothesised that there will be phenotypic effects on pigmentation in relation to ageing, including a reduction of overall pigmentation and the appearance of hyperpigmented lesions, or dark spots. The main objectives of this project are:

- To construct ageing pigmented 3D *in vitro* full thickness skin models using the Alvetex® technology.
- To confirm whether the ageing pigmented HSEs can successfully be produced.
- To perform biometrics analysis to identify the hallmarks of skin ageing.
- To obtain detailed analyses of pigmentation within the ageing HSEs.
- To compare the differences in pigmentation between neonatal and ageing HSEs.

2 Materials and Methods

2.1 2D Cell Culture

2.1.1 Primary Cells and Cell Maintenance

Commercially available cells were used in the bioengineering of human skin models, as detailed in **Table 2**. The primary cells used to make neonatal skin equivalents included human neonatal dermal fibroblasts (HDFn), human neonatal epidermal keratinocytes (HEKn), and darkly pigmented human neonatal epidermal melanocytes (HEMn-DP). The primary cells used to construct ageing skin equivalents were human adult dermal fibroblasts (HDFa), human adult epidermal keratinocytes (HEKa), and HEMn-DP. Darkly pigmented human adult epidermal melanocytes (HEMa-DP) were only analysed using 2D immunostaining and were not used for the generation of human full thickness skin equivalents. The cells were cultured in the appropriate supplemented media, as shown in **Table 3**.

Table 2: Primary cells.

Primary cell information and maintenance.

Cell Type	Cell Line	Company	Age	Sex	Pigmentation Level	Media	Time for confluency
Fibroblast	HDFn #1366434	Thermo Fisher Scientific	Neonatal	Male	Caucasian origin	Supplemented Dulbeccco's Modified Eagle Medium (DMEM, Thermo Fisher Scientific)	6-7 days
	HDFa #80124171	Thermo Fisher Scientific	48-year-old (middle aged)	Female	Caucasian origin		7-8 days
	HDFa #19TL170889	Thermo Fisher Scientific	60-year-old (old aged)	Female	Caucasian origin		7-8 days
Keratinocyte	HEKn #2289109	Thermo Fisher Scientific	Neonatal	Male	Caucasian origin	Supplemented EpiLife® (Thermo Fisher Scientific)	6-7 days
	HEKa #2391965	Thermo Fisher Scientific	47-year-old (middle aged)	Female	Caucasian origin		7-8 days
	HEKa #08138	Thermo Fisher Scientific	57-year-old (old aged)	Female	Caucasian origin		7-8 days
Melanocyte	HEMn-DP #2077650	Thermo Fisher Scientific	Neonatal	Male	Darkly pigmented	Supplemented Medium 254®	10-12 days

	HEMa-DP #21TL076028	Lonza	48-year-old (middle aged)	Female	Hispanic	(M254, Thermo Fisher Scientific)	10-15 days

Table 3: Supplemented complete media.

Composition of supplemented complete media and final concentration.

Complete Media	Reagents	Volume	Final Concentration
Supplemented DMEM	DMEM medium	500 mL	10 % FBS 2 mM L-Glutamine
	Foetal Bovine Serum (FBS, Thermo Fisher Scientific)	50 mL	
	200 mM (100x) L-glutamine (Thermo Fisher Scientific)	5 mL	
Supplemented Epilife®	Epilife® medium	500 mL	0.2 % Bovine pituitary extract, 0.01 µg mL^{-1} Recombinant human insulin-like growth factor-I, 0.18 µg mL^{-1} Hydrocortisone, 5 µg mL^{-1} Bovine transferrin, 0.2 ng mL^{-1} Human epidermal growth factor
	100x Human Keratinocyte Growth Supplement (HKGS, Thermo Fisher Scientific)	5 mL	
Supplemented M254	Medium 254®	500 mL	0.2 % Bovine pituitary extract, 0.5 % FBS, 0.01 µg mL^{-1} Recombinant human insulin-like growth factor-I, 0.18 µg mL^{-1} Hydrocortisone, 5 µg mL^{-1} Bovine transferrin, 3 ng mL^{-1} Basic fibroblast growth factor, 3 µg mL^{-1} Heparin, 10 ng mL^{-1} Phorbol 12-myristate 13-acetate
	100x Human Melanocyte Growth Supplement (HMGS, Thermo Fisher Scientific)	5 mL	
Antibiotics	Penicillin/Streptomycin (Pen Strep, Thermo Fisher Scientific) 10,000 U mL^{-1} penicillin 10,000 µg mL^{-1} streptomycin	5 mL in 500mL media	100 U mL^{-1} penicillin 100 µg mL^{-1} streptomycin

2.1.2 Revival of Cells

Cell stocks were stored in liquid nitrogen or in a freezer at -150 °C. To generate working cell stocks, vials of cells were thawed in a water bath at 37 °C until only a small ice crystal remained. Cells were then resuspended with a 1 mL pipette to ensure that they were evenly

distributed so that they could be seeded at their correct density (2.5 x 10^3 cm^{-2} for fibroblasts and keratinocytes, 5 x 10^3 cm^{-2} for melanocytes) into a T175 flask (Sigma-Aldrich) with 25 mL specific complete media. Flasks were tilted in a cross-like motion to ensure even distribution across the flasks. The flasks were then transferred to a 37 °C incubator at 5 % CO_2 with a 95 % relative humidity environment. A media change was completed the next day to remove the cryopreservative, then subsequently changed every 3 days until cells reached 80 % confluency as shown in **Figure 20**.

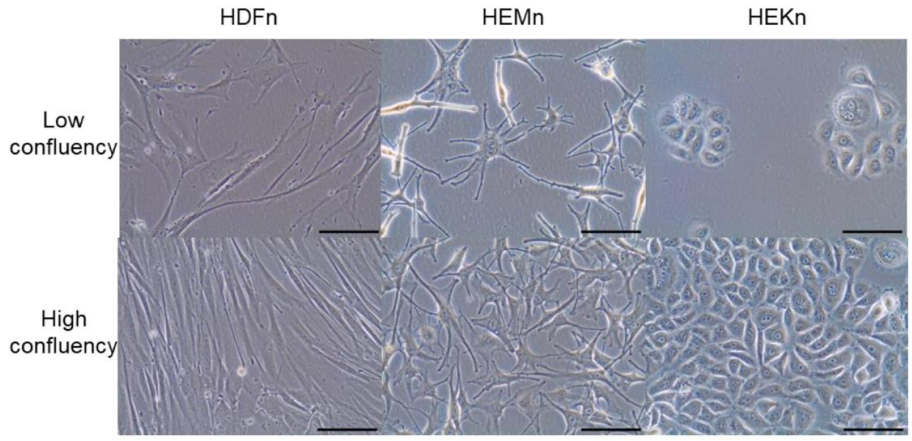

Figure 20: Neonatal human dermal fibroblasts, epidermal melanocytes, and epidermal keratinocytes grown in culture.

HDFn #1366434 at P4, HEMn #2077650 at p5, and HEKn #2286109 at P3 shown at low confluency and high confluency using the 40x objective lens on the EVOS phase contrast microscope. Scale bar: 100 µM. Image taken from De Los Santos Gomez, 2023.

2.1.3 Enzymatic Passaging of Cells

When cells reached 80 % confluency, they were enzymatically passaged. The media was aspirated, and the flasks were washed with 5 mL versene. For trypsinisation, adhered cells were rinsed with a solution of trypsin-EDTA (TE, Thermo Fisher Scientific) in versene (0.25 % TE diluted 1 in 10 with versene), then transferred to the incubator for 2-10 minutes. When all cells became detached, 5 mL trypsin neutraliser (TN, Thermo Fisher Scientific) or media containing FBS was added to the flasks and the cell suspension was moved into a 50 mL falcon centrifuge tube (Thermo Fisher Scientific). The flasks were rinsed with a further 10 mL trypsin neutraliser, which was then transferred to the falcon tube to ensure that all cells were removed from the flask. Cells were then centrifuged for 5 minutes at 200 g, then the supernatant was carefully aspirated, and the pellet was resuspended in 1 mL growth media. 10 µL cell suspension was then added to 90 µL trypan blue solution (Lonza) for a 1:10 dilution and viable cells were counted using a haemocytometer (Marienfeld Superior). The cells were

then re-seeded at the correct density into T175 flasks with 25 mL growth media. In preparation for 2D immunostaining, cells were seeded at the correct density with 2 mL media into a 12-well plate containing circular glass coverslips (Thermo Fisher Scientific). They were then placed in the 37 °C incubator at 5 % CO_2 with a 95 % relative humidity environment and the media was changed every 3 days.

2.1.4 Cryopreservation of Cells

If a surplus of cells were available after subculturing, they were banked at a passage of P4-5 for fibroblasts, P2-3 for keratinocytes and P3-5 for melanocytes. After trypsinisation and counting of cells, 20 mL media was added to the falcon tube containing the cell suspension, which was then centrifuged at 200 g for 5 minutes. The supernatant was then aspirated and the pellet was resuspended in either 10 % dimethyl sulphoxide (DMSO, Sigma-Aldrich) in specific complete media or Synth-a-Freeze™ cryopreservation media (Thermo Fisher Scientific). A volume of this cell suspension at an appropriate density was seeded into 1.8 mL cryogenic vials, which were transferred into a Mr Frosty ™ containing isopropanol and placed in a freezer at -80 °C overnight. This ensured that cells were frozen down slowly at a rate of -1 °C per minute, which maintained the viability of cells. The following day, the cryogenic vials were moved to and stored long-term in liquid nitrogen or a -150 °C freezer.

2.2 3D Cell Culture

2.2.1 Construction of 3D *in vitro* Full Thickness Skin Equivalents

Human dermal fibroblasts were seeded onto 12-well Alvetex® scaffold inserts (Reprocell Europe) to generate the dermal component of the full thickness skin models, as described in Roger *et al*. (2019). The cells were incubated for two hours to allow the attachment of cells to the scaffold, before the media was added. The media for the dermal component comprised of supplemented DMEM with 100 U mL^{-1} penicillin/100 µg mL^{-1} streptocycin (Pen Strep, Thermo Fisher Scientific) as detailed in **Table 3**, 5 ng ml^{-1} transforming growth factor (TGFβ1, Thermo Fisher Scientific), and 100 µg mL^{-1} ascorbic acid (Sigma-Aldrich). The media was changed twice per week for 21 days in neonatal models and 28 days in ageing models.

Once the dermal equivalents had formed, human epidermal keratinocytes and melanocytes were seeded onto the dermis, as detailed in Goncalves *et al.* (2023). Media was added after

a 2-hour incubation to promote proliferation of keratinocytes. The media consisted of supplemented EpiLife® media with Pen Strep (**Table 3**), keratinocyte growth factor (KGF, Thermo Fisher Scientific), 100 µg mL^{-1} ascorbic acid (Sigma-Aldrich), and 200 µM $CaCl_2$ (Sigma-Aldrich). After 2 days, the skin models were raised to the air-liquid interface (ALI) by transferring them to an Alvetex® well insert holder (Reprocell Europe) on the medium height setting in a deep dish (VWR). Models at the ALI were cultured in the same media as previously described, but with an increased $CaCl_2$ concentration of 1.7 mM. The skin equivalents were maintained in this state for 21 days with 2 media changes per week. This process of generating 3D *in vitro* full thickness skin equivalents is outlined in **Figure 21**.

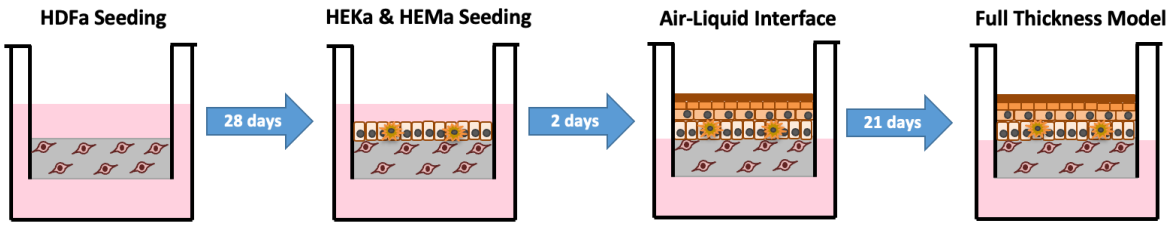

Figure 21: Schematic overview of the methodology used to bioengineer ageing pigmented 3D in vitro full thickness skin equivalents.

This methodology utilises the Alvetex® technology. HDFa were seeded onto the inert porous Alvetex® scaffold 12-well and cultured in supplemented DMEM for 28 days. HEKa and HEMa were then seeded and cultured, submerged in the supplemented Epilife® media, then raised to the air-liquid interface after 2 days. Ageing pigmented models were then cultured in this phase for 21 days when they were ready to be harvested.

2.3 Clinical Analyses

2.3.1 Trans-epidermal Water Loss Readings

The skin models were unclipped from the inserts and transferred to a flat surface. Trans-epidermal water loss (TEWL) values were obtained as an indicator of skin barrier function using a VapoMeter device (Delfin Technologies; **Figure 22**). The dermatological tool was held to the surface of each skin equivalent until the reading appeared on the screen. The device needed to re-equilibrate between readings. Three repeats of these readings were obtained per skin model and the mean values were calculated.

Figure 22: Vapometer.

The Vapometer device is a dermatological tool that quantifies trans-epidermal water loss in 3D human skin equivalents. Available at/image taken from https://delfintech.com/products/vapometer/

2.3.2 Melanin Index and Individual Typology Angle Readings

The skin models were unclipped from the inserts and transferred to a flat surface. Measurements of the Melanin Index (MI) and Individual Typology Angle (ITA) were obtained using a SkinColorCatch colourimeter (Delfin Technologies). This device was held to the surface of each skin equivalent until the readings appeared on the screen, as shown in **Figure 23**. Three repeats of these readings were obtained per skin model and the mean values were calculated.

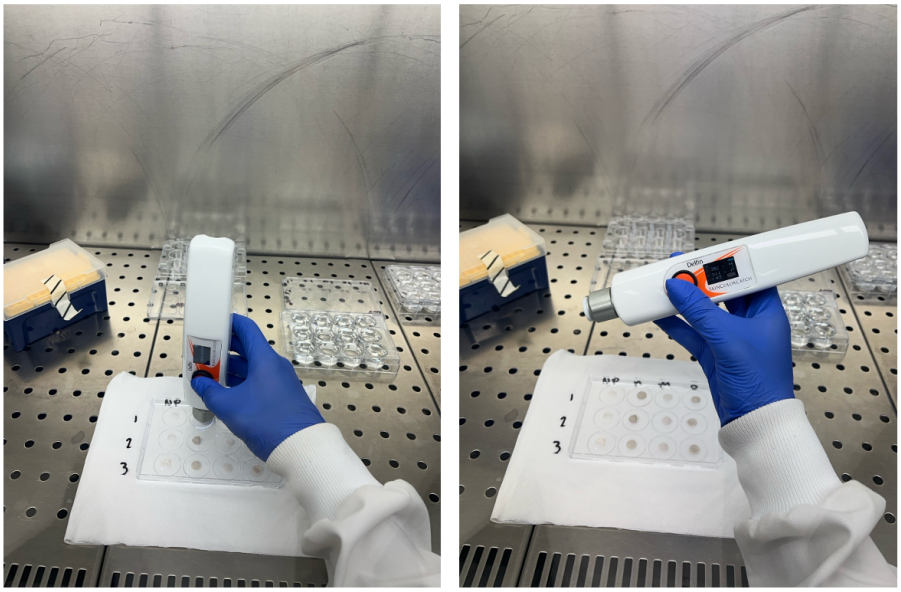

Figure 23: SkinColorCatch.

The SkinColorCatch device is a dermatological tool that quantifies skin tone and pigmentation. This colourimeter is used to obtain the MI and ITA readings of the human skin equivalents. Available at www.delfintech.com/skincolorcatch/

2.4 Histology

2.4.1 Paraffin Embedding and Sectioning of Skin Equivalents

After the harvest, the models were suspended in 4 % paraformaldehyde solution (PFA, Sigma-Aldrich) and fixed for 2 hours at room temperature or overnight at 4 °C. Following this, the samples were washed twice in PBS prior to embedding.

The models were dehydrated through 30 %, 50 %, 70 %, 80 %, 90 % and 95 % ethanol, each for 10 minutes, then in 100 % ethanol for 30 minutes. The samples were then placed in labelled tissue processing cassettes (Solmedia Ltd.) and submerged in Histoclear 2 (National Diagnostics) for 30 minutes in the fume hood. Molten wax (Cell Path) was then added to the beaker to make the ratio up to 1:1 Histoclear:Wax. The beaker was then placed into the oven at 65 °C for 30 minutes until the wax had melted. The Histoclear:Wax mixture was then disposed of and 100 % molten wax was poured into the beaker and placed in the oven for at least 1 hour. The models were then embedded into a plastic mould (Cell Path) filled with molten wax with the flat edge facing downwards, then covered by a tissue cassette. They were then left overnight to solidify at room temperature.

Samples were sectioned at 5 μM using a Leica RM2125RT rotary manual microtome (Leica Biosystems) with MB DynaSharp microtome blades (Thermo Fisher Scientific). The sections were then transferred to a water bath at 37 °C then mounted onto charged Superfrost Plus microscope slides (Thermo Fisher Scientific), before being placed on a 30 °C heated slide rack to dry for at least 2 hours.

2.4.2 Haematoxylin and Eosin Staining

The purpose of haematoxylin and eosin (H&E) staining was to observe the histology of human skin equivalents and to measure the thickness of the epidermis. The slides were deparaffinised in Histoclear 1 (Thermo Fisher Scientific) for 5 minutes, then transferred to 100 % ethanol for 2 minutes. They were then rehydrated in 95 % ethanol, then 70 % ethanol, then distilled water, each for 1 minute, before being stained in Mayer's haematoxylin (Sigma-Aldrich) for 5 minutes. The sections were then washed in distilled water, moved to alkaline alcohol to blue the nuclei, dehydrated in 70 % alcohol and then 95 % alcohol, then stained in Eosin (Sigma-Aldrich), each for 30 seconds. Following this, the samples were dehydrated in 95 % ethanol twice, for 10 seconds each time. Next, they were transferred to 100 % ethanol

for 15 seconds, then again for 30 seconds. The samples were then cleared in Histoclear 1 twice, for 3 minutes each time. The slides were left in Histoclear 1 until ready to mound on a coverslip using Omnimount (SLS NAT1328) or Histomount (SLS NAT 1308). The slides were left to dry in the fume hood until ready for bright-field imaging using a Leica ICC50HD microscope.

2.4.3 Sirius Red Staining

Sirius Red staining was performed to visualise the total collagen content produced by fibroblasts in the human skin equivalents. The slides were deparaffinised in Histoclear 1 for 5 minutes, then transferred to 100 % ethanol for 2 minutes. They were then rehydrated in 95 % alcohol, then 70 % alcohol, then distilled water, each for 1 minute. The nuclei were then stained with Weigert's haematoxylin working solution for 8 minutes. Next, the slides were washed in running tap water for 10 minutes. The samples were then stained in picro-Sirius Red (Direct Red 80, Sigma-Aldrich) for 1 hour. Following this, the slides were washed twice in acidified water then shaken to physically remove most of the water. Then, they were dehydrated in 3 changes of absolute alcohol and then cleared in Histoclear ready to be mounted. Bright-field images were obtained using the Leica ICC50HD microscope.

2.4.4 Fontana-Masson Staining

Fontana-Masson staining was conducted to detect melanin, confirming successful melanin synthesis by melanocytes and transfer to keratinocytes in the human skin equivalents. Fontana-Masson staining was performed using a commercially available kit and according to the manufacturer's instructions (Abcam, ab150669) containing 0.2 % gold chloride solution, 10 % silver nitrate solution, and 5 % thiosulphate solution. The sections were deparaffinised in Histoclear 1 for 5 minutes, then rehydrated through 100 %, 95 % and 75 % ethanol each for 2 minutes, and then in distilled water. In the meantime, a coplin jar and a glass bottle was washed with acetone to ensure there were no residues. Ammonical Silver solution was then made up in the fume hood by combining 27 mL distilled water with one 9 mL vial of silver nitrate solution in the clean glass bottle, then 27 % ammonium hydroxide (Sigma-Aldrich) was added dropwise, swirling after each drop. The solution turned dark brown and then gradually turned colourless with a layer of sediment. When the sediment dissolved, the solution was transferred to the clean coplin jar ready for use. This was then placed in a water bath at 60 °C in the fume hood for around 15 minutes until the temperature had equilibrated, which was

confirmed by placing a thermometer in a second coplin jar in the water bath filled with the same volume of dH_2O. The slides were then incubated in the Ammonical Silver solution for 30 minutes, then rinsed several times in distilled water. The slides were then placed on a tray and the samples were covered in 0.2 % Gold Chloride Solution at room temperature for 30 seconds. The sections were then washed several times in distilled water in the coplin jar. Next, the samples were incubated in 5 % Sodium Thiosulphate Solution for 1-2 minutes at room temperature, then rinsed for 2 minutes under running dH_2O from the tap. Nuclear Fast Red Solution was then added to the slides and incubated for 5 minutes, then rinsed under running tap water for a further 2 minutes. The samples were then rapidly dehydrated in drops of fresh absolute alcohol, then cleared in Histoclear 1 for 5 minutes ready to be mounted. Bright-field images were obtained using the Leica ICC50HD microscope.

2.5 Immunofluorescence Analysis

2.5.1 Immunofluorescence Staining of 2D Cells

The coverslips in a 12-well plate were permeabilised in 0.1 % Triton-X-100 in PBS for 10 minutes on ice. This solution was then aspirated using a Pasteur pipette and a blocking buffer of 10 % NCS in 0.1 % Tween20 in PBS was added to samples and blocked for 60 minutes. The appropriate concentration of the desired primary antibody (**Table 4**) was pipetted as 50 µL droplets onto labelled Parafilm (Thermo Fisher Scientific) in a plastic tray, and coverslips were removed from the wells and placed on the antibody solutions and incubated for 1 hour at room temperature. For the control samples, the coverslips were placed on 50 µL blocking buffer without the primary antibody. The coverslips were then washed 3 times for 10 minutes by moving them to 50 µL drops of blocking buffer on the parafilm. The coverslips were then placed onto 50 µL of the appropriate secondary antibodies at the correct concentration (**Table 5**) for 60 minutes. Coverslips were then washed again as previously described. To mount the coverslips, the excess blocking buffer was blotted carefully and 5 µL Vectashield Antifade Mounting Medium (Vector Laboratories) was placed on a SuperFrost Plus slide. The coverslip was then placed onto the Vectashield on the slide, sealed with nail varnish, then allowed to dry and stored at 4 °C until ready for bioimaging.

2.5.2 Immunofluorescence Staining of 3D Skin Equivalents

The sections were deparaffinised in Histoclear 1 for 15 minutes, then hydrated in 100 % ethanol, then 70 % ethanol, then PBS, each for 5 minutes. The slides were then transferred to citrate buffer in a 95 °C water bath for 20 minutes for antigen retrieval. Cold tap water was then added to the slides to cool, and distilled water was added to the reservoir of the slide tray. The 20 % NCS blocking buffer was prepared by mixing 1 mL NCS with 4 mL 0.4 % Triton-X-100 solution. The samples were then circled using a hydrophobic pen and 100 µL blocking buffer was added. The sections were then left to incubate for 1 hour at room temperature. The primary antibody solution was prepared at the appropriate dilution (**Table 4**) with the blocking buffer and 100 µL was added to each sample. For the control samples, 100 µL blocking buffer was applied without the primary antibody. They were then left to incubate for 1 hour at room temperature or refrigerated overnight at 4 °C.

Following the incubation period, the slides were washed in PBS 3 times, each for 10 minutes. The secondary antibody solution was prepared at a 1:1,000 dilution (**Table 5**) with the blocking buffer and Hoechst 33342 Fluorescent Stain (Thermo Fisher Scientific) at a 1:10,000 dilution. 100 µL secondary antibody solution was then added to the samples and they were left to incubate in the dark for 1 hour at room temperature. After this incubation, the slides were washed 3 times in PBS, for 10 minutes each. They were then mounted using Vectashield Antifade Mounting Medium (Vector Laboratories) and the coverslips were sealed with nail varnish. The slides were stored in a coverslip book in the fridge at 4 °C ready for imaging using a confocal microscope.

2.5.3 Epidermal Whole Mount Staining

Following the harvest, the models were rinsed in PBS then punch biopsies were made using a 5 mM Kai sterile dermal biopsy punch (Selles Medical Ltd) and placed in a well plate. 200 µL 3.8 % ammonium thiocyanate (Sigma-Aldrich) in PBS was added to each punch biopsy to separate the dermis from the epidermis for 20 minutes at room temperature. The epidermis was then separated from the dermis using forceps and then washed in PBS. After this, the models were fixed in a 1:1 solution of methanol (Thermo Fisher Scientific) and acetone (Thermo Fisher Scientific) at -20 °C for 20 minutes. Next, the models were washed in PBS 3 times and stored at 4 °C ready for immunostaining.

The models were blocked on parafilm in 50 µL blocking buffer (20 % NCS in 0.4 % Triton X-100 in PBS) for 2 hours at room temperature. After this incubation, 50 µL primary antibody solution (TRP1) at the correct concentration was added followed by a 2-hour incubation at

room temperature. For the control samples, 50 µL blocking buffer was applied without the primary antibody. The punch biopsies were then washed in blocking buffer 3 times, for 10 minutes each time. 50 µL secondary antibody solution without Hoechst was then added and left to incubate for 1 hour at room temperature. The samples were then mounted with 10 µL Vectashield antifade mounting medium below the epidermis and 10 µL on top, with the stratum corneum on the coverslip and the basal layer facing upwards onto the coverglass. The coverslips were not sealed with nail varnish in case the position of the epidermis needed to be corrected.

Table 4: Primary antibodies.

Primary antibodies used in immunofluorescence analysis and their details.

Marker	Antibody	Code	Manufacturer	Species	Dilution
Extracellular matrix	anti-collagen 1	ab24821	Abcam	Goat	1:100
	anti-fibronectin	ab32419	Abcam	Rabbit	1:100
Skin differentiation	anti-cytokeratin10	ab76318	Abcam	Rabbit	1:100
	anti-cytokeratin14	ab7800	Abcam	Mouse	1:100
	anti-loricrin	ab85679	Abcam	Rabbit	1:100
	anti-involucrin	ab53112	Abcam	Rabbit	1:100
	anti-periplakin	ab131269	Abcam	Rabbit	1:100
Proliferation	anti-Ki67	ab16667	Abcam	Rabbit	1:250
	anti-p63	ab124762	Abcam	Rabbit	1:100
Senescence	anti-HMGB1	ab79823	Abcam	Rabbit	1:250
	anti-Lamin-B1	ab16048	Abcam	Rabbit	1:100
Cytoskeletal	anti-alpha SMA	ab7817	Abcam	Mouse	1:100
Melanocyte	anti-TRP1	ab190709	Abcam	Mouse	1:100
	anti-S100	ab14849	Abcam	Mouse	1:100
	anti-Gp100	ab137078	Abcam	Rabbit	1:100
	anti-MITF	ab122982	Abcam	Mouse	1:100

Table 5: Secondary antibodies.

Secondary antibodies used in immunofluorescence analysis and their details.

Antibody	Code	Manufacturer	Dilution
Donkey Anti-Mouse IgG Alexa Fluor™ 488	A-21202	ThermoFisher Scientific	1:1000

Donkey Anti-Rabbit IgG Alexa Fluor™ 488	A-21206	ThermoFisher Scientific	1:1000
Donkey Anti-Mouse IgG Alexa Fluor™ 594	A-21207	ThermoFisher Scientific	1:1000
Donkey Anti-Rabbit IgG Alexa Fluor™ 594	A-21203	ThermoFisher Scientific	1:1000
Donkey Anti-Goat IgG Alexa Fluor™ 488	A-11055	ThermoFisher Scientific	1:1000

2.6 Melanin Quantification Assay

The melanin content was quantified using a methodology published by Fernandes *et al* (2016). This protocol measures the fluorescence from melanin after oxidation with H_2O_2. At harvest, the remaining part of the models were stored in a lysis buffer of 500 µL of 1 M NaOH containing 10 % DMSO (Sigma-Aldrich) at -80 °C until ready for melanin assay. The standard curve of *Sepia officinalis* melanin (Sigma-Aldrich) was prepared in parallel with the models. All samples were then transferred to a water bath at 80 °C for 1 hour, vortexing every 20 minutes. The samples were then centrifuged for 5 minutes at 3000 g, then 300 µL per sample was added to 450 µL 50 % hydrogen peroxide solution (Sigma-Aldrich), making a final concentration of 30 %. They were then incubated at room temperature for 4 hours in the dark with the lids of the falcon tubes unscrewed. The falcon tubes were then centrifuged at 3000 g for 5 minutes. 100 µL per sample was then pipetted in a 96-well plate 3 times and bubbles were popped with a needle. The fluorescence was then measured using the excitation wavelength as 470 nM and the emission wavelength as 550 nM. This was achieved using the BioTek Synergy H1 Microplate Reader (Agilent). The data was plotted using Microsoft Excel, where a standard curve was plotted and the equation of the trendline was used to calculate the melanin quantity in the samples (**Figure 24**).

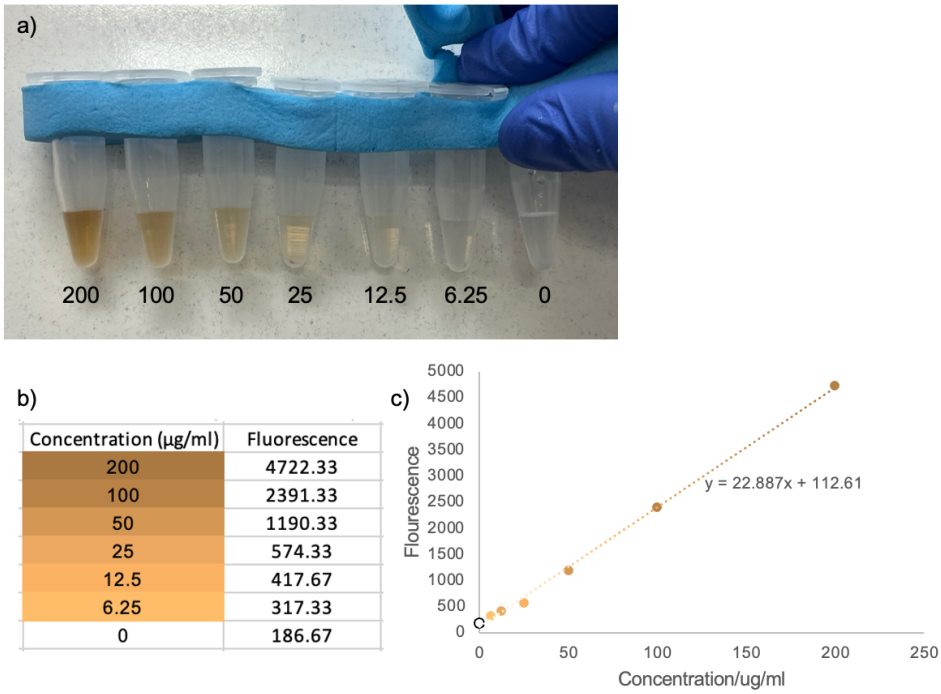

Figure 24: Melanin quantification assay.

a) a photograph of the melanin standards prepared for the melanin quantification assay. b) a table of the standard curves and their corresponding fluorescence readings in Microsoft Excel. c) the standard curve plotted in Microsoft Excel with trendline linear equation displayed on the chart.

2.7 Flow Cytometry

The growth media was removed from cells and the cells were washed in sterile PBS then trypsinised as described in section 2.1.3. Cells were then centrifuged at 200 g for 5 minutes. The supernatant was aspirated, and the pellet was fixed in 1 mL 4 % PFA for 20 minutes on ice. The pellet was then resuspended in 1 mL PBS at 4°C, then centrifuged at 200 g for 5 minutes. This PBS wash was repeated twice, then the pellet was resuspended in 1ml of a 0.2 % Triton-X-100 in PBS permeabilization buffer for 15 minutes. The cell pellet was then suspended in 1ml of a 0.1 % Bovine Serum Albumin (BSA, Sigma) in PBS blocking buffer and centrifuged at 200 g for 5 minutes. This was repeated twice, and the final cell suspension was stored on ice.

To begin the immunostaining process for flow cytometry, 100 µL cell suspension was pipetted into the wells of a round-bottomed 96-well plate (Greiner Bio-one), and the plate was centrifuged at 1,000 rpm at 4 °C for 3 minutes. The appropriate primary antibody was diluted in flow buffer at the correct concentration, and 50 µL primary antibody was added to each well and the cell pellets resuspended in the primary antibody solution. The plate was then

incubated for one hour on ice. The plate was then centrifuged for 3 minutes at 1,000 rpm at 4 °C. The appropriate secondary antibody was then diluted at the correct concentration in flow buffer, and 50 µL secondary antibody was added to each well, the pellets being resuspended. Following this, the plate was centrifuged at 1,000 rpm for 3 minutes at 4 °C and the pellets were resuspended in flow buffer. This was repeated twice, the cell pellets being suspended in 200 µL flow buffer in the final wash.

The plate was then transferred to the Guava Technologies EasyCyte Plus flow cytometer and plates were read using the Guava Express Pro software according to the manufacturer's instructions. The flow cytometry data was then analysed using the Cytosoft software.

2.8 Microscopy

2.8.1 Brightfield Imaging

A Leica ICC50 High-Definition Camera (Leica Microsystems) mounted onto a DM500 Leica Microscope (Leica Microsystems) with 4x, 10x, 20x and 40x objective lenses was used to image histology samples. The Leica LAS EZ software was used to capture images with an image size of 2048 x 1536 pixels. Images were processed using the Fiji software. The scale used in the captured images are shown in **Table 6**. For each magnification, 'set scale' was selected and the corresponding scale value was inputted for 1 pixel. 'Global' was selected to set this scale for all histology images opened using the Fiji software.

Table 6: Scale bar values used for brightfield images.

Objective lens and corresponding scale in µm per pixel.

Magnification	Scale/µm per pixel
4x	1.582
10x	0.6328
20x	0.3164
40x	0.157

2.8.2 Confocal Fluorescence Imaging

High-resolution images were obtained using the Zeiss 880 and 800 confocal fluorescence laser scanning microscope (Carl Zeiss AG). The Zeiss Zen software was used to capture images, which were then processed using the Fiji software. 'Autoscale' was selected when opening images using Fiji.

2.9 Biometrics Analysis

2.9.1 Measuring Epidermal Thickness

Analyses were completed using the Fiji software (version: ImageJ 1.54f). For each image, 'set measurements' was selected and only 'perimeter' was ticked. 'Transform' then 'rotate' then 'straighten' were selected and the epidermis was straightened for each image. A grid was used to measure at 50-micron intervals and measurements were taken on a zoomed in screen. To take measurements, the line tool was used to draw a vertical line across the viable epidermis (**Figure 25**) and 'M' was pressed on the keyboard. 10 measurements were taken per image at regular intervals and repeated for each of 10 images for a total of 100 measurements per condition. The values were copied and pasted into Microsoft Excel and the mean epidermal thickness values were calculated.

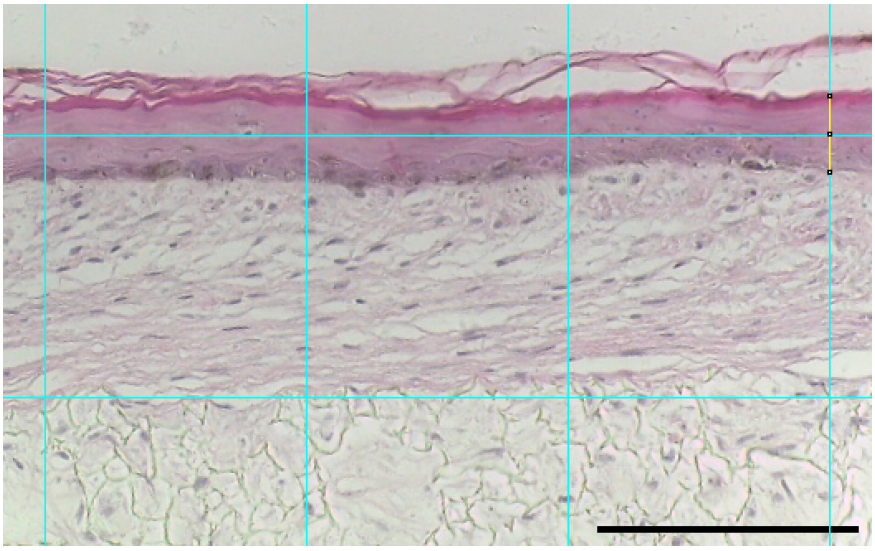

Figure 25: Biometrics analysis of epidermal thickness.

A representative schematic of a H&E stained skin equivalent where the epidermal thickness is measured using the Fiji software. Image acquired using the 20x objective lens on a brightfield microscope. Grid area: 50 μM^2. Scale bar: 50 µM.

2.9.2 Measuring Cells and Nuclei

Analyses were completed using the Fiji software (version: ImageJ 1.54f). Images at a 40x magnification ensured the most accurate measuring of cells and nuclei. ‘Set measurements’ was selected, and ‘area’, ‘perimeter’, ‘Ferret’s diameter’, and ‘bounding rectangle’ were selected. The cells or nuclei were outlined as shown in **Figure 26**, and ‘M’ was pressed on the keyboard to take measurements. This was repeated for all cells/nuclei, then all values and column names were copied and pasted into Microsoft Excel.

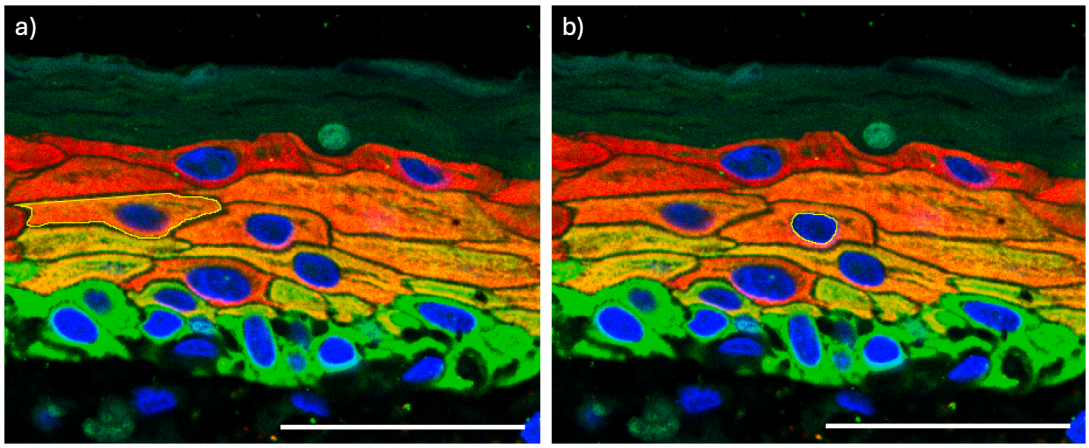

Figure 26: Measuring cells and nuclei.

A representative schematic of outlining a) cells and b) nuclei to be measured using the Fiji software. Image shows cells stained for k10 (red) and k14 (green) and nuclei stained for Hoechst (blue). Scale bar: 50 μM.

2.9.3 Measuring Epidermal Proliferation

Immunostaining was performed for the marker keratinocyte proliferation markers Ki67 and p63 for the quantification of epidermal proliferation. Several images were captured across the basal layer of the epidermis of each of 3 skin models per age group. To count Ki67 or p63 positive cells in the epidermis, the multipoint tool in the Fiji software was used by clicking on each nucleus expressing this protein (green). The number of Hoechst-stained (blue) nuclei were also counted using this method (**Figure 27**). The same method was used to determine the percentage of HMGB1 positive cells to quantify cellular senescence.

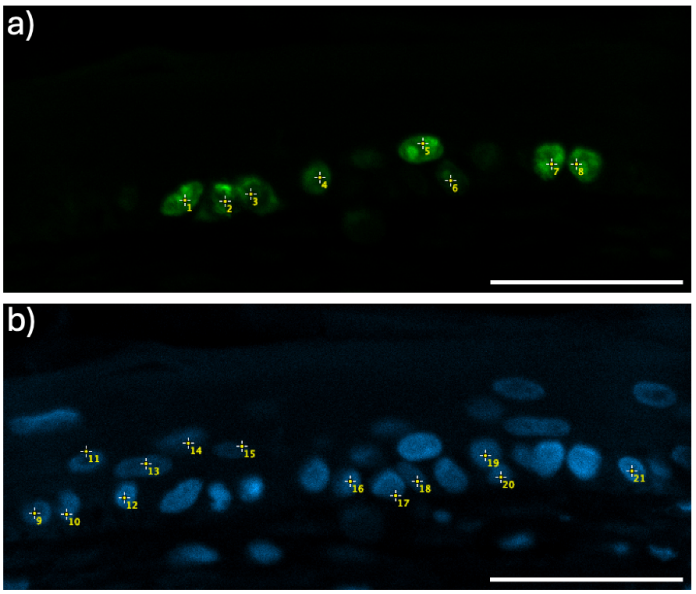

Figure 27: Biometrics Analysis of Epidermal Proliferation.

A representative schematic of the proportion of Ki67-positive cells being determined using the multipoint tool to count cells in the Fiji software. Skin equivalents immunostained for the Ki67 keratinocyte proliferation marker. Channels split into a) ki-67 positive cells (green) and b) Hoechst-stained nuclei (blue). Image obtained using the 40x objective lens on the confocal immunofluorescence microscope. Scale bar: 50 μM.

2.9.4 Determining Melanocyte Density

Three Z-stack images at a x20 magnification were acquired per model. To process Z-stacks in the Fiji software, 'image' was selected, then 'stacks', then 'Z-projects'. The start slice was set as 1 and the stop slice was set as 5, with the projection type set as 'max intensity'. The processed image was then saved as a Tiff in a new folder. Starting zoomed in in one quarter, the multipoint tool was used to count each cell by clicking on them (**Figure 28**). This was repeated in each quarter, then 'count' was selected and the new file with the counts was saved. Using Microsoft Excel, a table of counts was made per quantification per model/condition. A table of the image height in μm, then converted to mm and squared to calculate the area in mm. The number of melanocytes was then divided by the area to calculate the melanocyte density in melanocytes/mm^2.

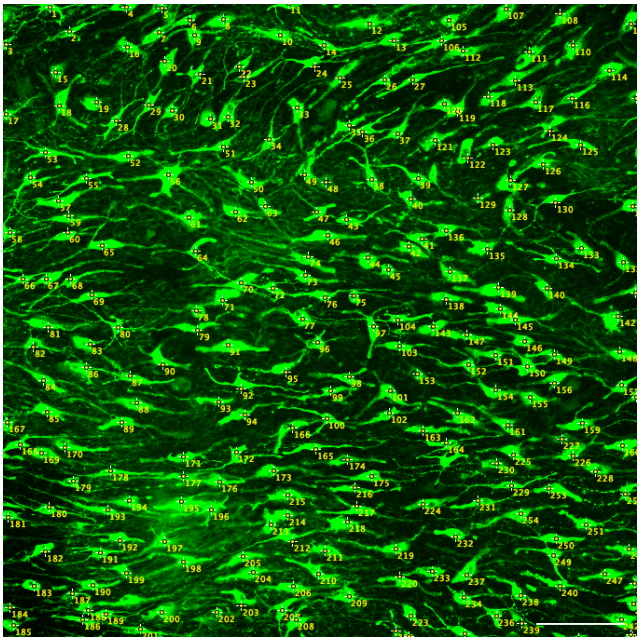

Figure 28: Biometrics Analysis of Melanocytes.

A representative schematic showing the melanocyte count as determined using the Fiji software. The number of melanocytes was needed to subsequently determine the melanocyte density in 3D full thickness skin equivalents. An epidermal whole mount stain was performed and the melanocyte marker TRP1 was immunostained. Images were taken from different areas across 5 mM punch biopsies of skin models. Confocal immunofluorescence image captured at a 20x magnification. Scale bar: 100 μM.

2.9.5 Quantifying Fluorescence Intensity of the ECM

Immunofluorescence staining was carried out for markers of ECM components collagen 1 and fibronectin. All sections were stained together, and confocal images were acquired at x20 magnification across the length of the skin models. Acquisition parameters were kept constant during imaging to ensure that signal levels were comparable. Images were analysed using the Fiji software. For each image, the entire dermis was selected for analysis using the freeform tool. ‘Set measurement’ was selected from the ‘analyse’ dropdown menu. The parameters ‘area’, ‘min & max grey value’, ‘integrated density’, and ‘mean grey value’ were selected and ‘measure’ was selected from the analyse menu.

2.10 Statistical Analysis

The GraphPad Prism version 10 software (GraphPad Software) was used to conduct statistical analyses. The statistical test used was one-way analysis of variance (ANOVA) using Tukey’s post-test for multiple comparisons, under the assumption that the standard deviations between groups was not significantly different ($P < 0.05$). Where the standard deviations between groups was significantly different ($P > 0.05$), the statistical significance was determined by the

Brown-Forsythe and Welch one-way ANOVA tests, followed by the Dunnett T3 post-test for multiple comparisons when n < 50 per group, or the Games-Howell post-test for multiple comparisons where n > 50 per group. Statistically significant differences were noted as * if P < 0.05, ** if P < 0.01, *** if P < 0.001, or **** if P < 0.0001 above bars. No significant statistical difference was noted as 'ns' above bars.

2.11 Human Tissue Information

Human tissue samples that have been sectioned and stained have been included in this thesis. Punch biopsies of young and ageing skin were obtained from Caucasian females. These human tissue samples were collected by Procter & Gamble USA under a clinical protocol that has been approved by the Institutional Review Board in compliance with local laws and regulations. Informed consent documents were signed by all tissue donors for the procurement of the tissue biopsy or surgical waste samples. A material transfer agreement (MTA) was drawn up to cover the transfer of human tissue to Durham. The tissue was processed following relevant rules and guidelines under the UK Human Tissue Act 2004.

3 Results

3.1 Characterisation of 2D Human Epidermal Melanocytes and Keratinocytes

2D analyses were carried out on epidermal melanocytes and keratinocytes to visualise differences in morphology and protein expression in neonatal and ageing primary cells. The data obtained from these analyses are an indicator of how ageing cells may behave in 3D *in vitro* skin models compared with neonatal cells, as well as facilitating the selection of suitable cell populations to include in the 3D skin equivalents.

3.1.1 Neonatal and ageing human epidermal melanocytes express melanocytes marker TRP1

Neonatal and ageing 2D human epidermal melanocytes were analysed to determine which population of melanocytes to include in the ageing pigmented 3D *in vitro* full thickness skin models. Both populations of melanocytes were grown to confluency in flasks were enzymatically passaged as described in Section 2.1.3, then cells were seeded into a 12-well plate containing coverslips. Cells were grown for 7 days on the cover slips, with 3 media changes per week as usual. 2D immunostaining was then performed as detailed in Section 2.5.1 using the melanocyte marker TRP1 to characterise these 2D primary cells.

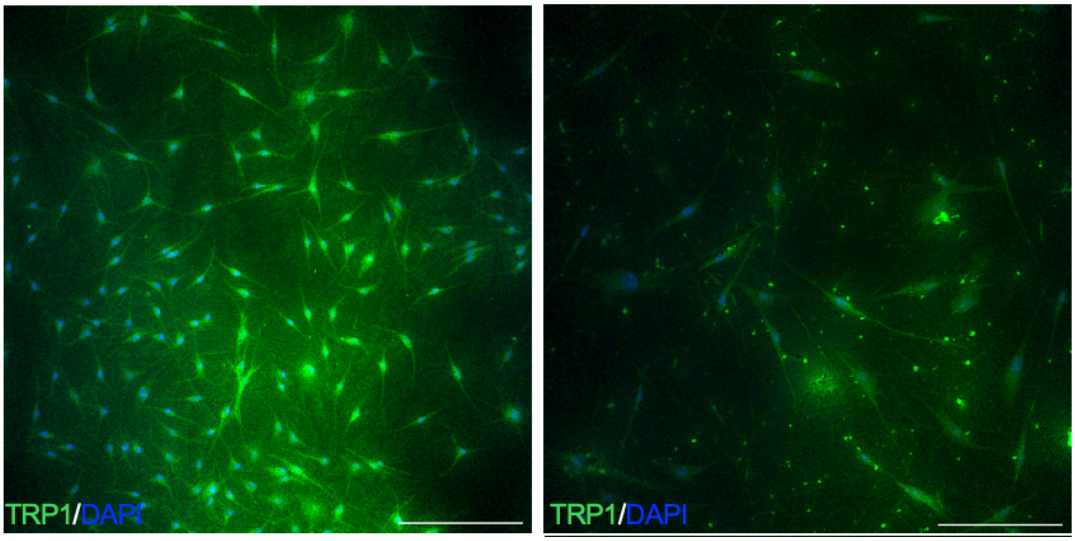

Figure 29: Immunofluorescence analysis of TRP1 protein expression in 2D human epidermal neonatal and ageing melanocytes.

Representative immunofluorescence staining micrographs of TRP1 expression in neonatal (left) and ageing (right) melanocytes. Magnification: x10. Scale bar: 200 µm.

Figure 29 demonstrates that TRP1 is expressed in both populations of human epidermal melanocytes. The morphology of the neonatal and ageing melanocytes are normal, and dendritic extensions can be visualised. Although the cell populations were each grown for the same number of days, expression of TRP1 and confluency of cells was much higher in the neonatal melanocytes compared with the ageing melanocytes. These neonatal primary melanocytes were therefore used to construct the neonatal and ageing pigmented 3D full thickness skin models.

3.1.2 Neonatal and ageing human epidermal keratinocytes express proliferation markers Ki67 and p63

Flow cytometry was used to quantitatively determine cell expression markers and indicate how the different human epidermal keratinocytes might behave in 3D *in vitro* models. Flow cytometry was performed on fixed neonatal, middle aged, and old aged keratinocytes (Section 2.7) for the keratinocyte proliferation markers p63 and Ki67.

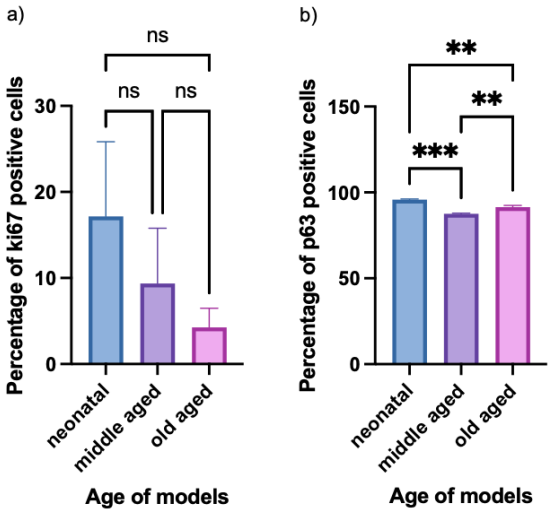

Figure 30: Flow cytometry data for neonatal and ageing human epidermal keratinocytes.

Data are representative of the percentage of cells expressing the keratinocyte proliferation markers a) Ki67 and b) p63 in neonatal, middle aged, and old aged keratinocytes. Three readings were taken per group per marker. The GraphPad Prism 10 software was used to generate the graphs displaying the mean ± SEM. Statistical significance was determined by an ordinary one-way ANOVA followed by Tukey's multiple comparisons post-test. The standard deviation values between groups were not significantly different ($P < 0.05$). Statistically significant differences were noted as ** if $P < 0.01$ or *** if $P < 0.001$ above bars. No statistical difference was noted as 'ns' above bars.

In **Figure 30a**, the bars show a decrease in the percentage of Ki67 positive cells with age. However, the difference between the groups is not statistically significant and the standard error bars are large. According to **Figure 30b**, there is a slight decrease in the percentage of p63 positive cells in both populations of ageing keratinocytes compared with neonatal keratinocytes, which has been determined as statistically significant. There is a slight increase in the percentage of p63 positive cells in old aged vs middle aged populations of keratinocytes, which is statistically significant ($P < 0.01$).

3.2 Clinical Analyses of 3D *in vitro* Full Thickness Skin Models

Gross appearance images and various clinical analyses using dermatological tools were performed at the harvest of 3D *in vitro* skin models to observe visible changes in skin pigmentation in ageing full thickness equivalents, as well as to indicate that the skin models have a normal barrier function.

3.2.1 Incorporation of melanocytes into ageing full thickness bioengineered skin produces ageing pigmented skin equivalents

Neonatal and ageing pigmented 3D *in vitro* full thickness skin models were constructed as described in Section 2.2.1, with the aim of investigating the effects of ageing on pigmentation. Skin equivalents were harvested and unclipped and placed in the lid of a 12-well plate on top of a piece of white roll. A photograph was taken on an iPhone 13 to highlight the differences in skin pigmentation between the neonatal and ageing models.

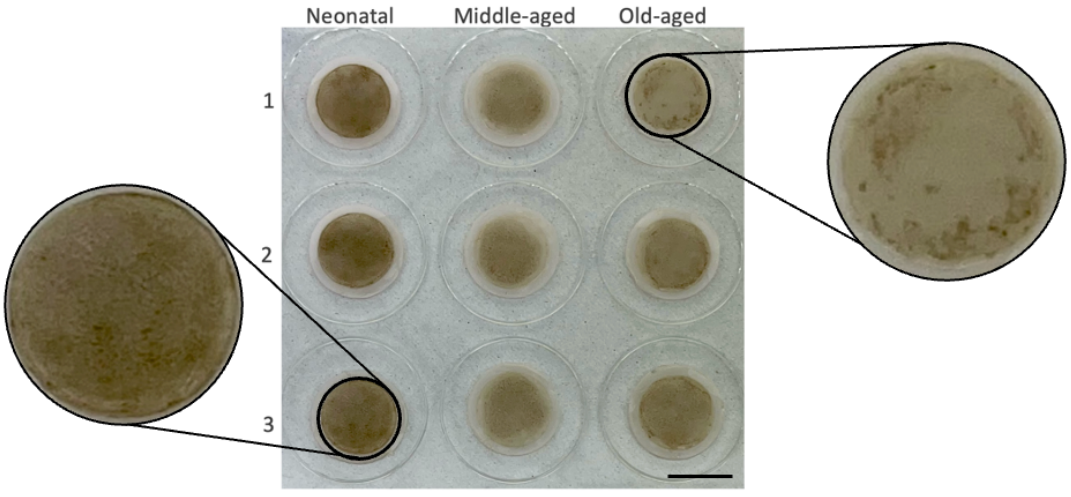

Figure 31: Gross appearance images of neonatal and ageing pigmented 3D in vitro full thickness skin models.

Gross appearance images of a triplicate of neonatal, middle aged, and old aged pigmented full thickness skin models. Skin equivalents constructed from the following primary cells: Neonatal: HDFn34, HEKn109; Middle Aged: HDFa171 (48yo), HEKa 965 (45yo); Old Aged: HDFa 889 (60yo), HEKa 08138 (57yo); Melanocytes: HEMn-DP 650. Image captured at harvest. Scale bar: 1 cm.

Figure 31 shows that with the incorporation of melanocytes into ageing full thickness bioengineered skin, pigmented ageing full thickness skin models were successfully produced, where ageing has an effect on pigmentation. Pigmentation appears to be reduced in ageing models compared with neonatal models, with the appearance of dark spots in the old aged skin models.

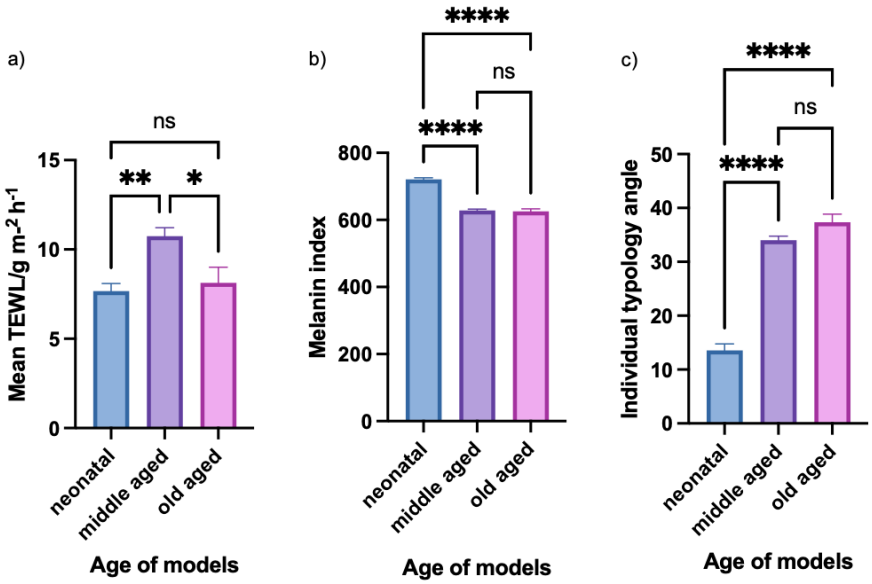

Figure 32: Analyses of neonatal and ageing pigmented 3D in vitro full thickness skin models using clinical devices at harvest.

a) Trans-epidermal water loss values in g m^{-2} h^{-1} measured using Vapometer device. b) melanin index and c) individual typology angle values measured using SkinColorCatch device. Measurements taken using 3 representative counts from each set of models per age group. GraphPad Prism 10 software was used to generate the graphs displaying the mean ± SEM with 3 skin equivalents per condition. Statistical significance was determined by an ordinary one-way ANOVA followed by Tukey's multiple comparisons post-test. The standard deviations between groups was not significantly different ($P < 0.05$). Statistically significant differences were noted as * if $P < 0.05$, ** if $P < 0.01$, or **** if $P < 0.0001$ above bars. No statistical difference was noted as 'ns' above bars.

3.2.2 Ageing pigmented full thickness skin models have a normal skin barrier function

TEWL readings were taken at harvest using the Vapometer device as described in Section 2.3.1. TEWL is a measure of skin barrier function, where a lower TEWL value indicates a higher integrity of the skin barrier. 3 representative measurements were obtained per model. According to **Figure 32a**, all TEWL values are < 18 g m^{-2} g^{-1}, which is an indicator that the skin equivalents are successful and robust with a functioning skin barrier. There is a difference in

mean TEWL values between all groups. There is a slight increase in mean TEWL in old aged vs neonatal skin equivalents, however this difference is not statistically significant. There is a statistically significant increase ($P < 0.01$) in the mean TEWL readings for middle aged models compared with neonatal models, and a significant decrease ($P < 0.05$) in old aged vs middle aged skin models.

3.2.3 Pigmentation is reduced in ageing skin models compared to neonatal bioengineered skin equivalents

MI and ITA readings were obtained at harvest using the SkinColorCatch colourimeter device, as detailed in Section 2.3.2. These are clinical spectrophotometric measurements used to assess human skin tone and pigmentation, where the ITA is dependent upon the MI. 3 representative readings were taken per model. According to **Figure 32b**, the mean melanin index significantly decreases ($P < 0.0001$) in ageing skin equivalents compared with neonatal skin equivalents, with no significant difference between middle aged and old aged skin models. These data are supported by **Figure 32c**, where the mean individual typology angle values significantly increase ($P < 0.0001$) for all ageing models vs neonatal models, with a slight increase but no significant decrease between middle aged and old aged skin equivalents. Overall, there is a decrease in melanin index and an increase in individual typology angle in ageing models in comparison with neonatal models, and therefore a reduction in pigmentation with age. These findings are highlighted in **Figure 31** appearance, and the quantitative data in **Figure 32** confirms this observation.

3.3 Histological Analyses of 3D *in vitro* Full Thickness Skin Models

Histological analyses were conducted to visualise whether 3D in vitro full thickness skin models have successfully been developed, and any changes in the morphology and epidermal thickness of the ageing skin equivalents.

3.3.1 An organised epidermis was formed upon a fibroblast-rich dermis in ageing pigmented 3D full thickness skin models

H&E staining was performed on ageing pigmented full thickness skin models that had been paraffin embedded and sectioned. Samples were stained as detailed in Section 2.4.2.

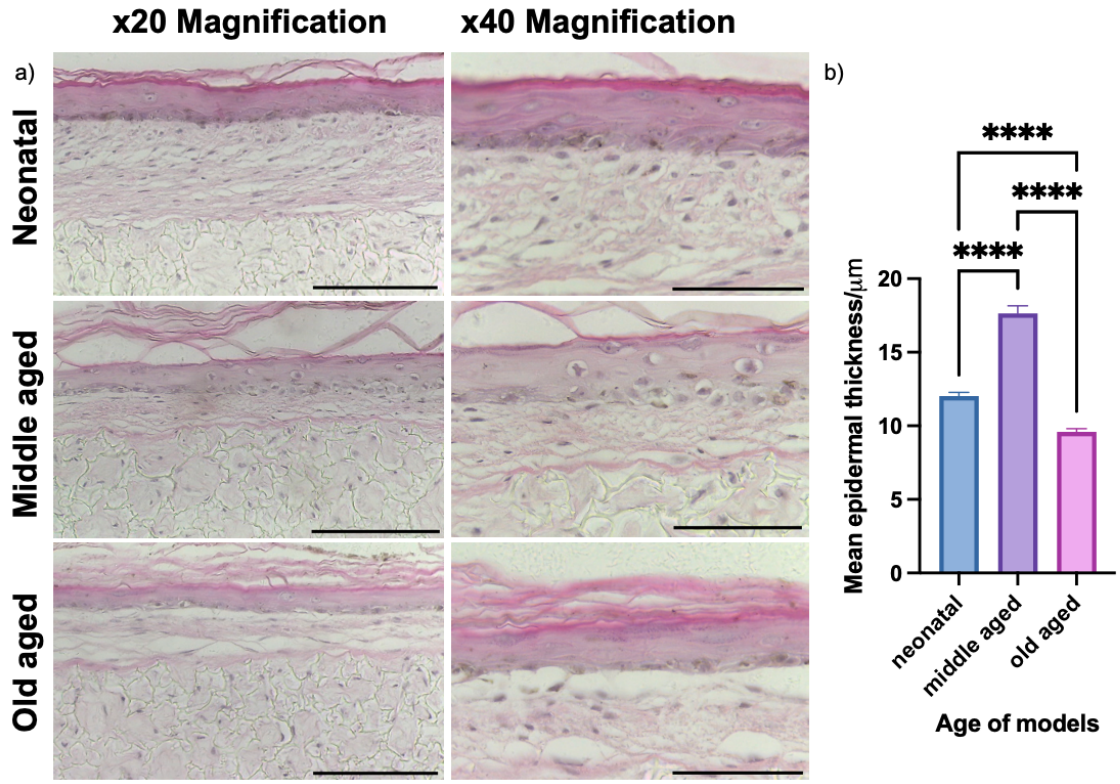

Figure 33: Histological analysis of 3D in vitro full thickness skin models.

a) Representative H&E staining images of pigmented neonatal, middle aged, and old aged full thickness skin models. Scale bar: 50 µm for x20 magnification, 25 µm for x40 magnification. b) Mean epidermal thickness in µm for neonatal, middle aged, and old aged full thickness skin models. GraphPad Prism 10 software was used to generate the graphs displaying the mean ± SEM with 3 skin equivalents per condition. Values as an average of > 60 representative counts from each set of models were taken per age group. Upon performing the ordinary one-way ANOVA test and Tukey's post-test for multiple comparisons, it was determined that the standard deviations between groups were significantly different ($P > 0.05$). The statistical significance was therefore determined by the Brown-Forsythe and Welch one-way ANOVA tests, followed by the Games-Howell post-test for multiple comparisons where $n > 50$ per group. Statistically significant differences were noted as **** where $P < 0.0001$ above bars.

Figure 33a reveals that successful epidermal stratification was achieved in the ageing pigmented full thickness skin equivalents, where keratinocytes successfully differentiated to produce viable layers with minimal infiltration into the Alvetex® scaffold. There is a polarised basal layer, and the epidermis has differentiated to form a stratum corneum, which indicates successful differentiation. Similarly to native human skin, the histology shows an organised epidermis upon a fibroblast-rich dermis.

3.3.2 The epidermal thickness decreases in old aged pigmented skin models compared with neonatal full thickness skin equivalents

The thickness of the epidermis was measured and quantified as described in Section 2.9.1. According to Figure **33b**, there is a decrease in epidermal thickness in old aged skin models compared with both neonatal and middle aged models. However, there is an increase in

epidermal thickness in the middle aged skin equivalents compared with the neonatal models. All differences between groups were determined to be statistically significant ($P < 0.0001$).

3.4 Pigmentation Analyses of 3D *in vitro* Full Thickness Skin Models

In order to determine whether melanin content and melanocyte density are affected in ageing skin models, the skin pigmentation was analysed and quantified using various techniques. These analyses also enable the observation of uniform pigmentation in well-constructed neonatal pigmented skin equivalents.

3.4.1 Melanin is successfully produced and transferred by melanocytes in ageing pigmented full thickness skin equivalents

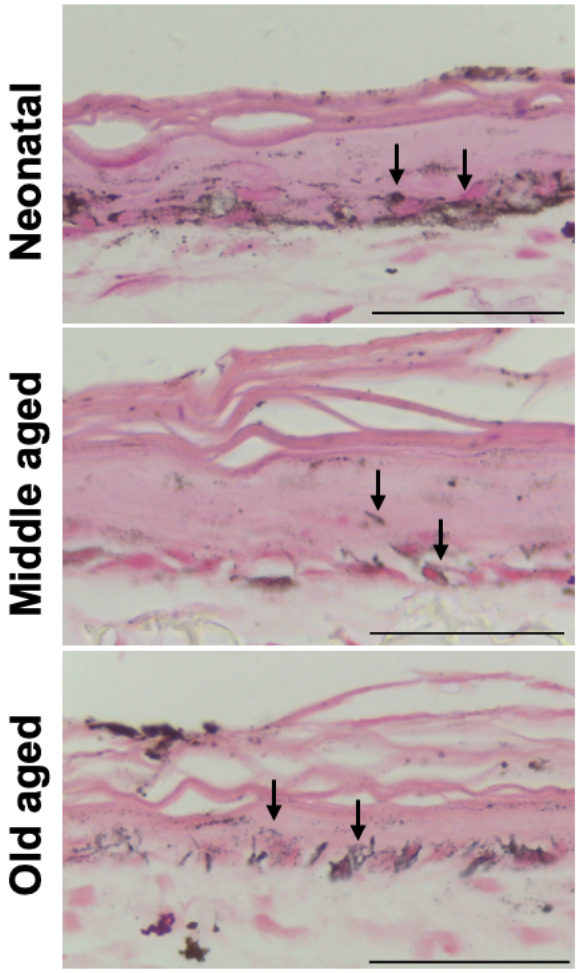

Figure 34: Fontana-Masson staining of 3D in vitro full thickness skin models.

Representative images of pigmented neonatal, middle aged, and old aged skin models with Fontana-Masson melanin staining. Arrows highlight a supranuclear cap and melanocyte. Scale bar: 50 µm. Magnification: x40.

In order to visualise the distribution of melanin, melanocytes, and supranuclear caps, Fontana-Masson staining was achieved as detailed in Section 2.4.4. **Figure 34** reveals that melanocytes are correctly positioned within the epidermis and are able to produce and transfer melanin to keratinocytes, producing pigmented tissue comparable to native human skin. The melanin can be visualised in the suprabasal layers, as well as the stratum corneum. Additionally, the melanin content appears to have decreased in ageing models compared with neonatal models.

3.4.2 Melanocytes are uniformly distributed across the area of the epidermis

The epidermises were detached from the dermises and stained for the melanocyte marker TRP1 as detailed in Section 2.5.3. The TRP1 marker allowed the melanocytes and any differences in their distribution to be visualised.

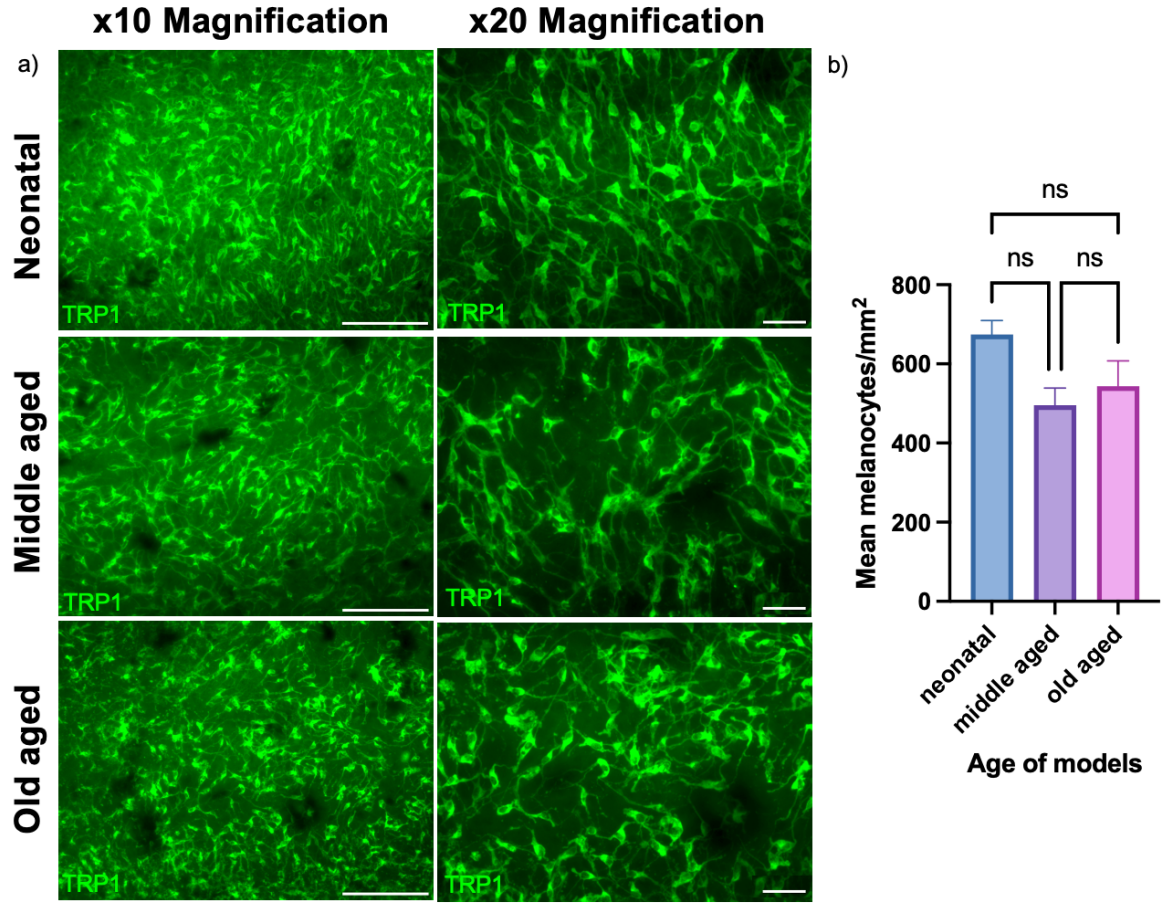

Figure 35: Immunofluorescence analysis of TRP1 protein expression in 3D in vitro full thickness skin models.

a) Representative epidermal whole mount immunostaining images for melanocyte marker TRP1 in pigmented neonatal, middle aged, and old aged full thickness skin models. Scale bar: 500 µm. b) Mean melanocyte density in melanocytes per mm^2 for neonatal, middle aged, and old aged full thickness skin models. GraphPad Prism 10 software was used to generate the graphs displaying the mean ± SEM with 3 skin equivalents per condition. Measurements taken using 3 representative counts from each

set of models per age group. Statistical significance was determined by an ordinary one-way ANOVA followed by Tukey's multiple comparisons post-test. The standard deviations between groups was not significantly different ($P < 0.05$). No statistical difference was noted as 'ns' above bars.

Figure 35a reveals that melanocytes are uniformly distributed across the entire area of the epidermis, particularly in the neonatal models compared to ageing models. Melanocytes also have a normal morphology with dendrites.

3.4.3 There is a decrease in melanocyte density in ageing pigmented bioengineered skin equivalents compared with neonatal pigmented skin equivalents

The density of melanocytes was quantified as described in Section 2.9.4. According to **Figure 35b**, there is a decrease in melanocyte density in ageing models compared with neonatal skin equivalents, despite melanocytes being seeded at the same density. However, the difference between the groups is not significant.

3.4.4 Ageing pigmented full thickness skin models contain a quantifiable melanin content

A melanin quantification assay based on the protocol by Fernandes *et al* (2016) was performed as outlined in Section 2.6. This assay was performed to measure the content of cellular melanin in the ageing pigmented skin equivalents.

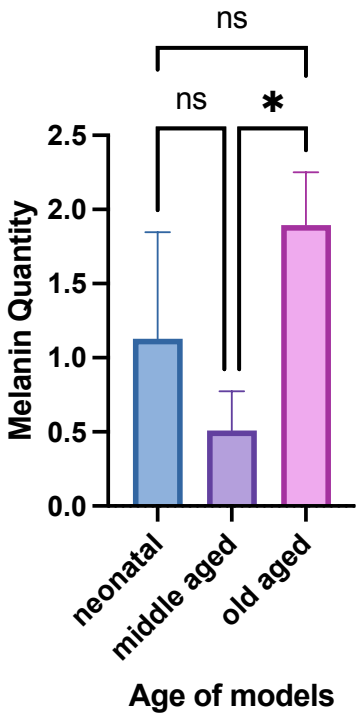

Figure 36: Melanin quantification assay.

Melanin quantity (arbitrary unit) determined by melanin assay. Upon performing the ordinary one-way ANOVA test and Tukey's post-test for multiple comparisons, it was determined that the standard deviations between groups were significantly different ($P > 0.05$). The statistical significance was therefore determined by the Brown-Forsythe and Welch one-way ANOVA tests, followed by the Dunnett T3 post-test for multiple comparisons when $n < 50$ per group, or the Games-Howell post-test for multiple comparisons where $n > 50$ per group. Statistically significant differences were noted as * if $P < 0.05$ above bars. No statistical difference was noted as 'ns' above bars.

Figure 36 shows that the neonatal and ageing pigmented full thickness skin models contain a quantifiable melanin content. The melanin quantity is significantly higher in the old aged skin equivalents compared with the middle aged specimens. This shows a different effect to the SkinColorCatch analysis, where there is no significant difference in pigmentation levels between the old aged and middle aged skin models. However, the means and standard error values are highly variable.

3.5 Dermal Analyses

The dermis of full thickness skin equivalents was analysed to measure changes in the quantity and organisation of components of the ECM such as collagen 1 and fibronectin.

3.5.1 Collagen is successfully synthesised by fibroblasts in ageing pigmented full thickness skin equivalents

Neonatal and ageing pigmented full thickness skin models were stained to visualise the total collagen content using Sirius Red staining, which was achieved using the protocol described in Section 2.4.3.

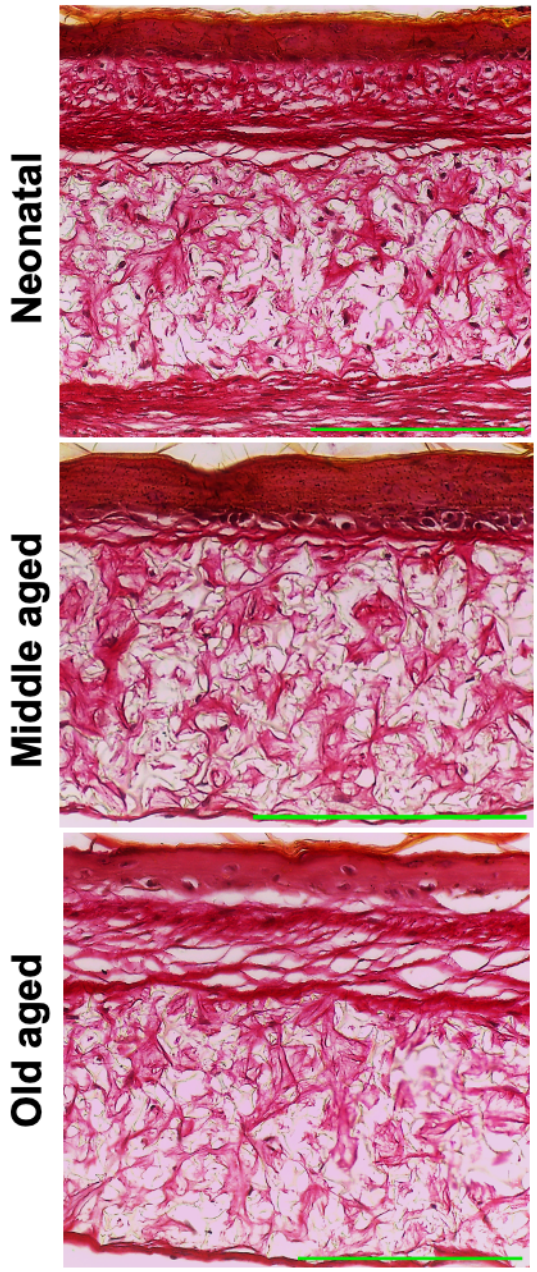

Figure 37: Sirius Red staining of 3D in vitro full thickness skin models.

Representative images of pigmented neonatal, middle aged, and old aged skin models with Sirius Red staining. Scale bar (green): 200 µm. Magnification: x20.

Figure 37 shows that the fibroblasts in all models are involved in the successful synthesis of collagen fibres, and that the density of overall collagen content appears to decrease with age.

3.5.2 ECM components collagen 1 and fibronectin are expressed in ageing pigmented full thickness skin equivalents

Immunofluorescence analysis of ECM proteins was completed to determine any structural changes to the ECM in ageing skin models, and changes in the expression of these proteins. Neonatal and ageing pigmented full thickness skin models were immunostained as described in Section 2.5.2 for extracellular matrix markers collagen 1 and fibronectin, and nuclear marker DAPI.

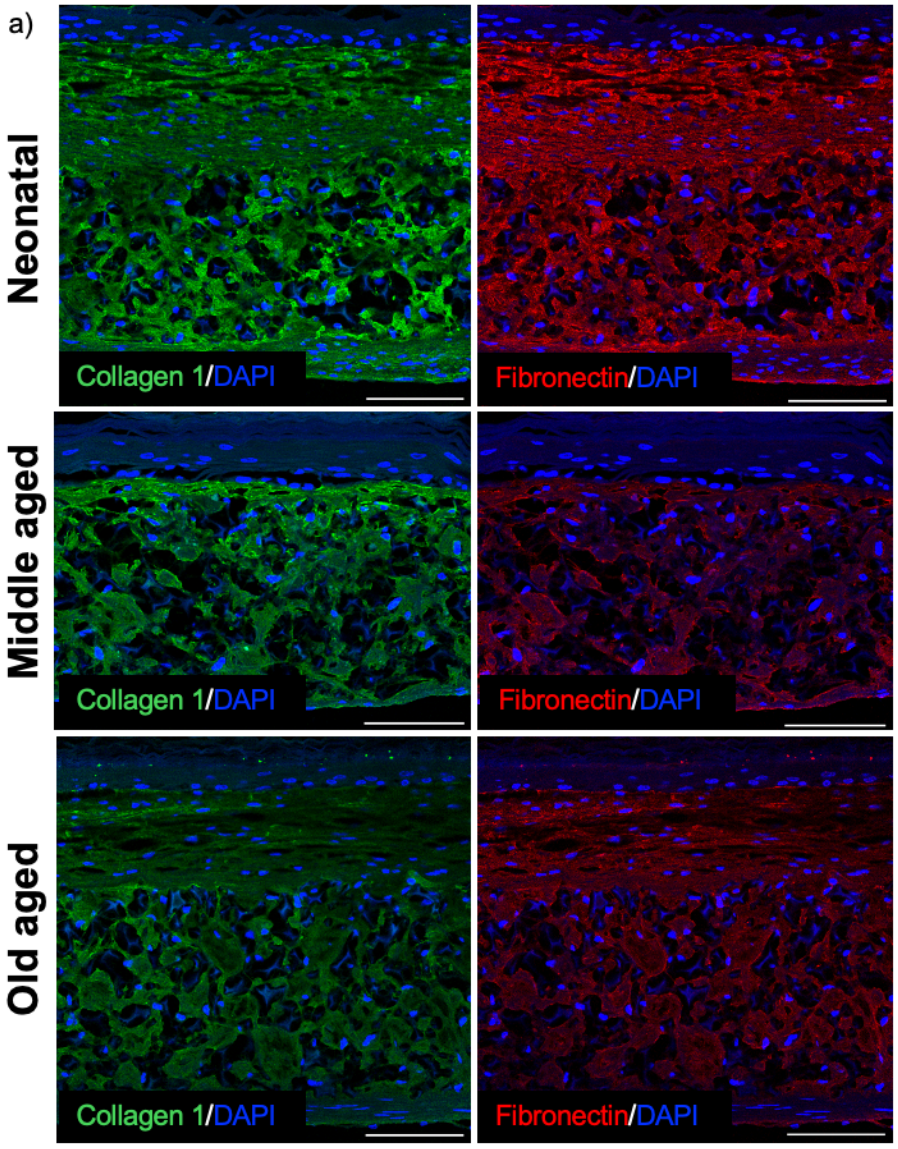

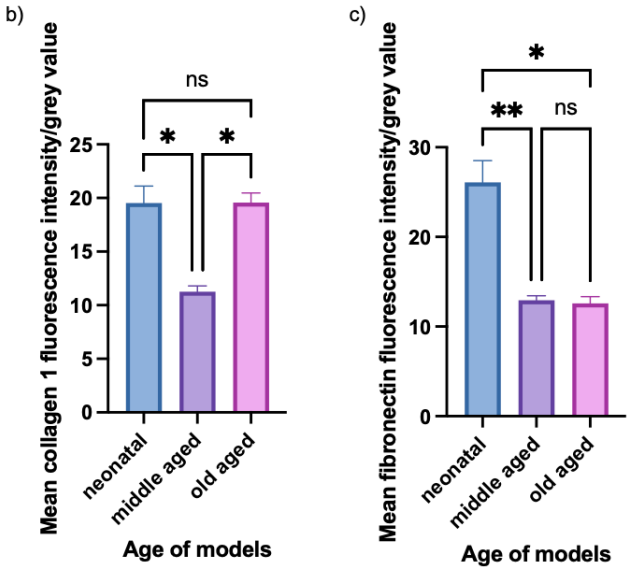

Figure 38: Immunofluorescence analysis of extracellular matrix protein expression in 3D in vitro full thickness skin models.

a) Representative immunostaining images for collagen 1 (green), fibronectin (red), and DAPI (blue) in neonatal, middle aged, and old aged pigmented full thickness skin equivalents. Scale bar: 100 µm. Magnification: x20. b) Mean grey value as a measure of collagen 1 staining fluorescence intensity across the entire dermis. GraphPad Prism 10 software was used to generate the graphs displaying the mean ± SEM with 3 skin equivalents per condition. Statistical significance was determined by an ordinary one-way ANOVA followed by Tukey's multiple comparisons post-test. The standard deviations between groups was not significantly different ($P < 0.05$). Statistically significant differences were noted as * where $P < 0.05$ above bars. No statistical difference was noted as 'ns' above bars. c) Mean grey value as a measure of fibronectin staining fluorescence intensity across the entire dermis. GraphPad Prism 10 software was used to generate the graphs displaying the mean ± SEM with 3 skin equivalents per condition. Statistical significance was determined by an ordinary one-way ANOVA followed by Tukey's multiple comparisons post-test. The standard deviations between groups were not significantly different ($P < 0.05$). Statistically significant differences were noted as * where $P < 0.05$ or ** where $P < 0.01$ above bars. No statistical difference was noted as 'ns' above bars.

Figure 38a demonstrates that collagen 1 and fibronectin are expressed, therefore the fibroblasts in all skin models are involved in producing a robust ECM. The intensity of staining appears to become weaker in ageing models, indicating that the quantity of ECM fibres perhaps decreases with age. Additionally, there appears to be clumping of the ECM components in the ageing models. This clumping appears to be most prominent in the old aged samples, which indicates that the structure of the collagen 1 and fibronectin fibres may have a more irregular organisation in the ageing skin models.

3.5.3 Changes in the ECM are observed in ageing vs neonatal full thickness skin models

The intensity of immunofluorescence staining of the ECM components was quantified as described in Section 2.9.5. According to **Figure 38b**, the intensity of collagen 1 staining is not significantly different between neonatal and old aged models, but that of middle aged models is significantly decreased ($P < 0.05$) compared with neonatal and old aged models. **Figure 38c** shows that there is a significant decrease in the fluorescence intensity of fibronectin in

ageing models, where P < 0.05 between neonatal and old aged models and P < 0.01 between neonatal and middle aged models. There is no significant difference between the fibronectin fluorescence intensity across the two ageing groups.

3.6 Epidermal Characterisation

Immunofluorescence analyses were carried out for markers of proliferation, differentiation, and barrier function in the epidermal equivalent of 3D full thickness skin models. The objectives of this were to observe any changes in cellular and nuclear morphology and expression of the epidermal markers in the ageing pigmented models.

3.6.1 The suprabasal and basal cells express differentiation markers k10 and k14, respectively, in ageing pigmented bioengineered skin

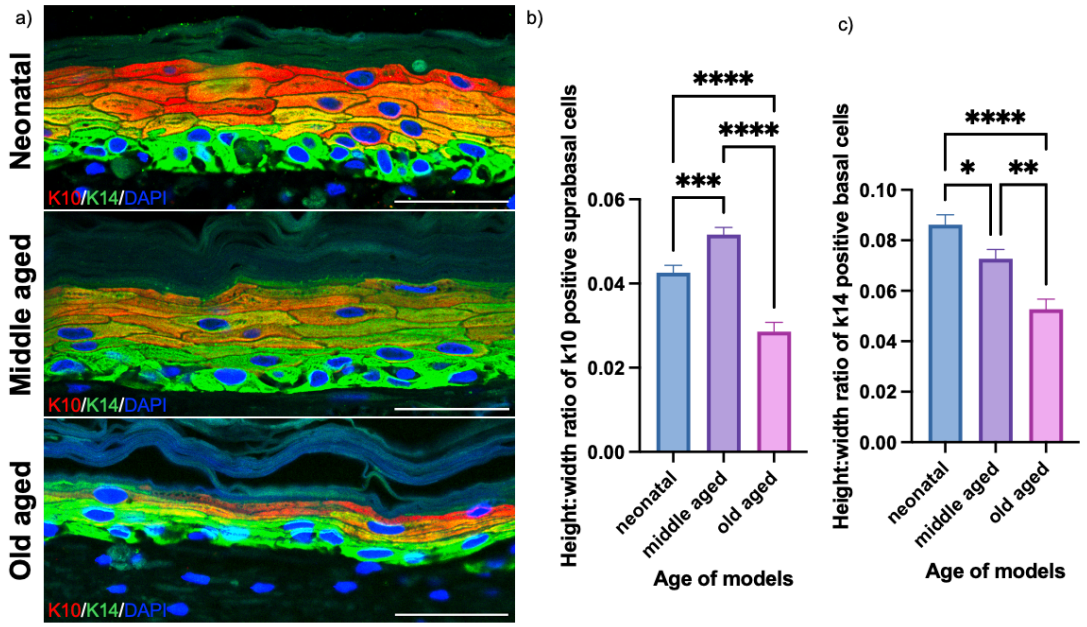

Figure 39: Immunofluorescence analysis of k10 and k14 protein expression in 3D in vitro full thickness skin models with measurements of suprabasal and basal cell morphology.

a) Representative immunostaining images for differentiation markers k10 and k14 and nuclear marker DAPI in neonatal, middle aged, and old aged 3D full thickness skin models. Scale bar: 50 µm Magnification: x20. b) Flatness as a ratio of height:width of k10 positive cells in the suprabasal layer of the epidermis for neonatal, middle aged, and old aged full thickness skin models. Measurements taken using counts from across the entire epidermis of each set of models per age group. GraphPad Prism 10 software was used to generate the graphs displaying the mean ± SEM with 3 skin equivalents per condition. Statistical significance was determined by an ordinary one-way ANOVA followed by Tukey's multiple comparisons post-test. The standard deviations between groups was not significantly different (P < 0.05). Statistically significant differences were noted as *** if P < 0.001, or **** if P < 0.0001 above bars. c) Flatness as a ratio of height:width of k14 positive cells in the basal layer of the epidermis for neonatal, middle aged, and old aged full thickness skin models. GraphPad Prism 10 software was used to generate the graphs displaying the mean ± SEM with 3 skin equivalents per condition. Measurements taken using counts from across the entire epidermis of each set of models per age group. Upon performing the ordinary one-way ANOVA test and Tukey's post-test for multiple comparisons, it was determined that the standard deviations between groups were significantly different (P > 0.05). The statistical significance was therefore determined by the Brown-Forsythe and Welch one-way ANOVA tests, followed by the Dunnett T3 post-test for multiple comparisons when n < 50 per group. Statistically significant differences were noted as * if P < 0.05, ** if P < 0.01, or **** if P < 0.0001 above bars.

Neonatal and ageing pigmented full thickness skin models were immunostained as described in Section 2.5.2 for differentiation markers k10 and k14 and nuclear marker DAPI (**Figure 39a; Figure 40a**). Basal keratinocytes expressed the differentiation marker k14 (green) and suprabasal keratinocytes expressed the k10 marker (red). Differences in the epidermal thickness, number of viable cells, and changes in cellular and nuclear morphology between the models can also be visualised in the representative micrograph images; the cells appear flattened in the images, which is confirmed by the quantitative data.

3.6.2 The cellular morphology of k10 positive suprabasal keratinocytes becomes flattened in ageing vs neonatal pigmented full thickness skin models

To visualise any changes in the morphology of suprabasal cells in the ageing pigmented skin equivalents, the height and width of k10 positive suprabasal cells was measured using the Fiji software, then the height to width ratio was calculated as a measure of cellular flatness. According to **Figure 39b**, there is a significant decrease in the height:width ratio in old aged models versus neonatal and middle aged ($P < 0.0001$), therefore the suprabasal keratinocytes in this age group become more flattened. However, there is a significant increase in cell height:width ratio ($P < 0.001$) for the middle aged group compared with the neonatal group.

3.6.3 The cellular morphology of k14 positive basal cells becomes flattened in ageing vs neonatal pigmented full thickness skin models

To visualise any changes in the morphology of basal cells in the ageing pigmented skin equivalents, the height and width of k14 positive basal cells was measured using the Fiji software, then the height to width ratio was calculated as a measure of cellular flatness. There is a significant decrease in height:width ratio ($P < 0.0001$) and therefore a significant increase in cell flatness in the old age group. There is also a significant decrease in height:width ratio between the neonatal and middle aged group ($P < 0.05$) and between the middle aged and old aged group ($P < 0.01$). Overall, the k14 positive basal keratinocytes display an increasingly flattened cellular morphology as the age increases.

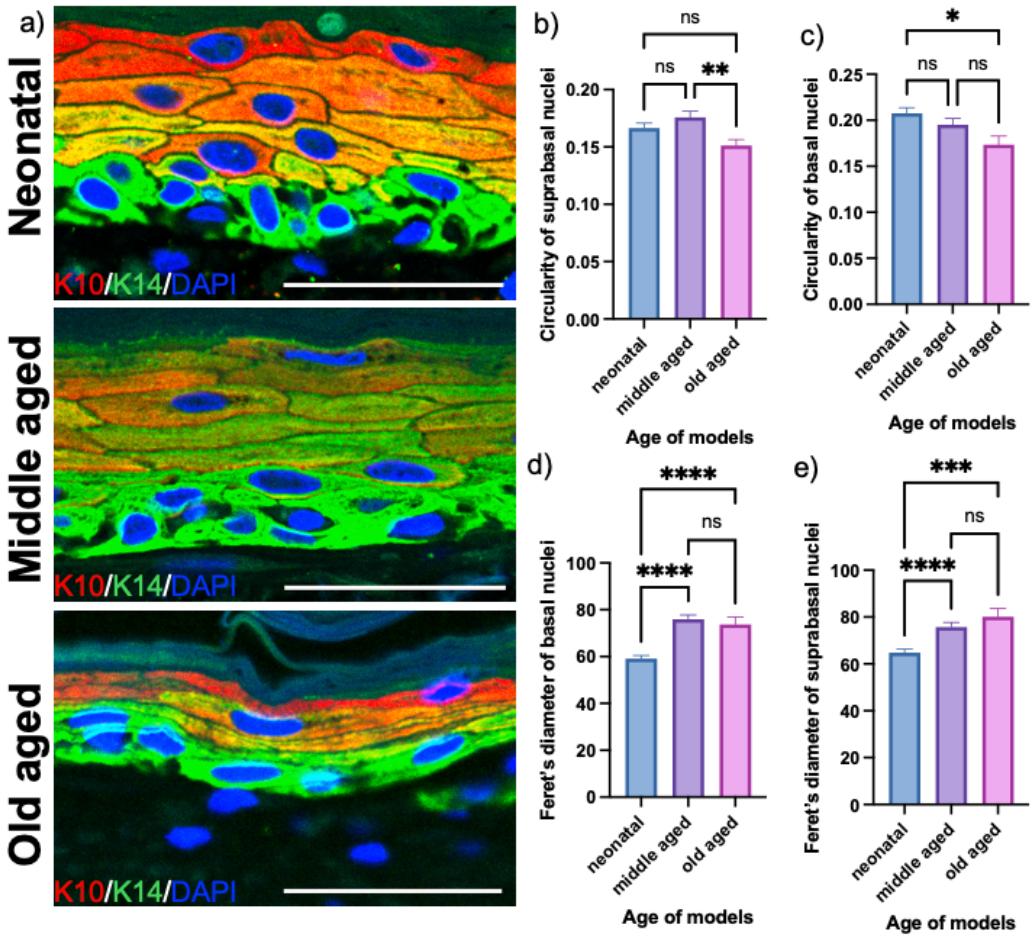

Figure 40: Immunofluorescence analysis of k10 and k14 protein expression in 3D in vitro full thickness skin models with measurements of morphology of nuclei in cells of the suprabasal and basal layers.

a) Representative immunostaining images for differentiation markers k10 and k14 and nuclear marker DAPI. Scale bar: 50 µm Magnification: x20. b) Circularity of the nuclei of k10 positive cells in the suprabasal layer of the epidermis for neonatal, middle aged, and old aged full thickness skin models. c) Circularity of the nuclei of k14 positive cells in the basal layer of the epidermis for neonatal, middle aged, and old aged full thickness skin models. d) Feret's diameter of the nuclei of k10 positive cells in the suprabasal layer of the epidermis for neonatal, middle aged, and old aged full thickness skin models. Statistical significance for c) was determined by an ordinary one-way ANOVA followed by Tukey's multiple comparisons post-test. The standard deviations between groups was not significantly different ($P < 0.05$). Statistically significant differences were noted as * where $P < 0.05$ above bars. No statistical difference was noted as 'ns' above bars. Upon performing the ordinary one-way ANOVA test and Tukey's post-test for multiple comparisons, it was determined that the standard deviations between groups in b), d) and e) were significantly different ($P > 0.05$). The statistical significance was therefore determined by the Brown-Forsythe and Welch one-way ANOVA tests, followed by the Dunnett T3 post-test for multiple comparisons when $n < 50$ per group. Statistically significant differences were noted as ** where $P < 0.01$, *** if $P < 0.001$, or **** if $P < 0.0001$ above bars. No statistical difference was noted as 'ns' above bars. All measurements were taken using counts from across the entire epidermis of each set of models per age group. GraphPad Prism 10 software was used to generate all the graphs displaying the mean ± SEM with 3 skin equivalents per condition.

3.6.4 The nuclear morphology of k10 positive suprabasal keratinocytes becomes flattened in ageing vs neonatal pigmented full thickness skin models

To visualise any changes in the morphology of the nuclei of suprabasal cells in the ageing pigmented skin equivalents, the DAPI-stained nuclei of the k10 positive suprabasal cells were measured. Several parameters were measured using the Fiji software, including the Feret's diameter of the nuclei. The circularity of the nuclei was determined using the equation $4\pi \times$

Area/Perimeter^2. According to **Figure 40b**, there was no significant difference in nuclear circularity for neonatal versus middle aged or old aged k10 positive suprabasal cells. However, there was a significant decrease in circularity ($P < 0.01$) for old aged nuclei compared with middle aged nuclei. According to **Figure 40d**, there is a significant increase in the Feret's diameter ($P < 0.0001$) of the nuclei in the ageing groups compared with the neonatal group. There is no significant difference in the Feret's diameter of the nuclei between the middle aged and old aged suprabasal keratinocytes. This indicates that the morphology of the nuclei become flattened in the ageing skin models.

3.6.5 The nuclear morphology of k14 positive basal cells becomes flattened in ageing vs neonatal pigmented full thickness skin models

To visualise any changes in the morphology of the nuclei of basal cells in the ageing pigmented skin equivalents, the DAPI-stained nuclei of the k14 positive basal cells were measured. Several parameters were measured using the Fiji software, including the Feret's diameter of the nuclei. The circularity of the nuclei was determined using the equation $4\pi \times$ Area/Perimeter^2. According to **Figure 40c**, there was no significant difference in the circularity of nuclei between the k14 positive keratinocytes in the middle aged group and the neonatal or old aged groups. However, there was a significant decrease in circularity in the old aged group versus the neonatal group. According to **Figure 40e**, there is a significant increase in the Feret's diameter ($P < 0.0001$) of the nuclei in the ageing groups compared with the neonatal group. There is no significant difference in the Feret's diameter of the nuclei between the middle aged and old aged suprabasal keratinocytes. This indicates that the morphology of the nuclei become flattened in the ageing skin models.

3.6.6 Ageing pigmented full thickness skin equivalents show expression and correct localisation of barrier markers, similar to neonatal models

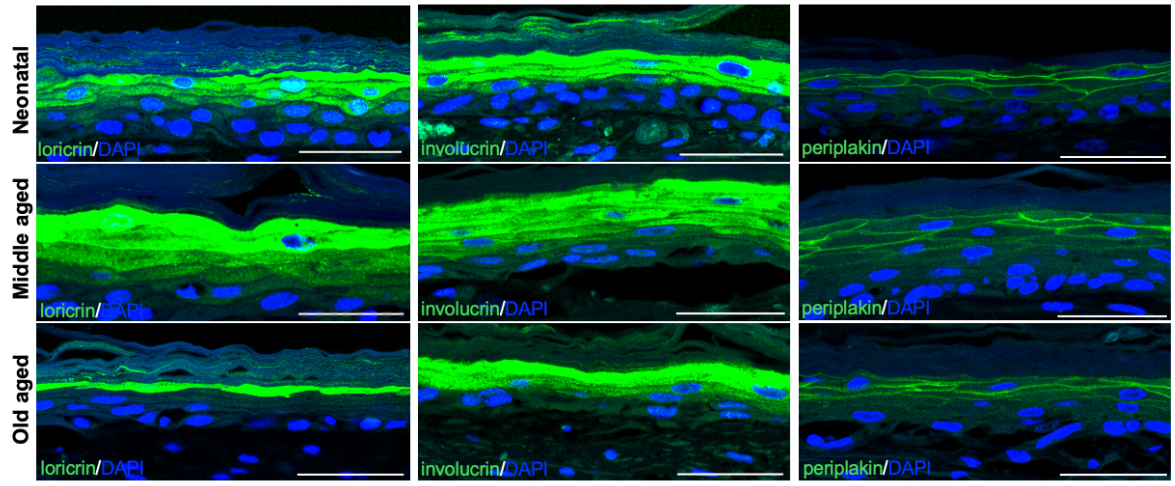

Figure 41: Immunofluorescence analysis of epidermal differentiation protein expression in 3D in vitro full thickness skin models.

Representative immunostaining images for differentiation markers loricrin, involucrin, and periplakin (green), and nuclear marker DAPI (blue) in pigmented neonatal, middle aged, and old aged full thickness skin equivalents. Scale bar: 50 µm. Magnification: x20.

As an indicator of the correct localisation of barrier markers, neonatal and ageing pigmented full thickness skin models were immunostained as described in Section 2.5.2 cornified envelope precursors loricrin, involucrin, and periplakin, and nuclear marker DAPI. **Figure 41** demonstrates that all of the skin models express these markers, and that keratinocytes successfully differentiate to form a stratified epidermis, comparable to native human skin. Additionally, the presence and correct localisation of these markers indicate the formation of the skin barrier.

3.6.7 Ageing pigmented skin models show a decrease in proliferation marker Ki67, but not basal stem cell marker p63, compared to neonatal control models

In order to identify any changes in keratinocyte proliferation in ageing pigmented skin models, neonatal and ageing pigmented full thickness skin models were immunostained as described in Section 2.5.2 for proliferation markers Ki67 and p63, and nuclear stain DAPI.

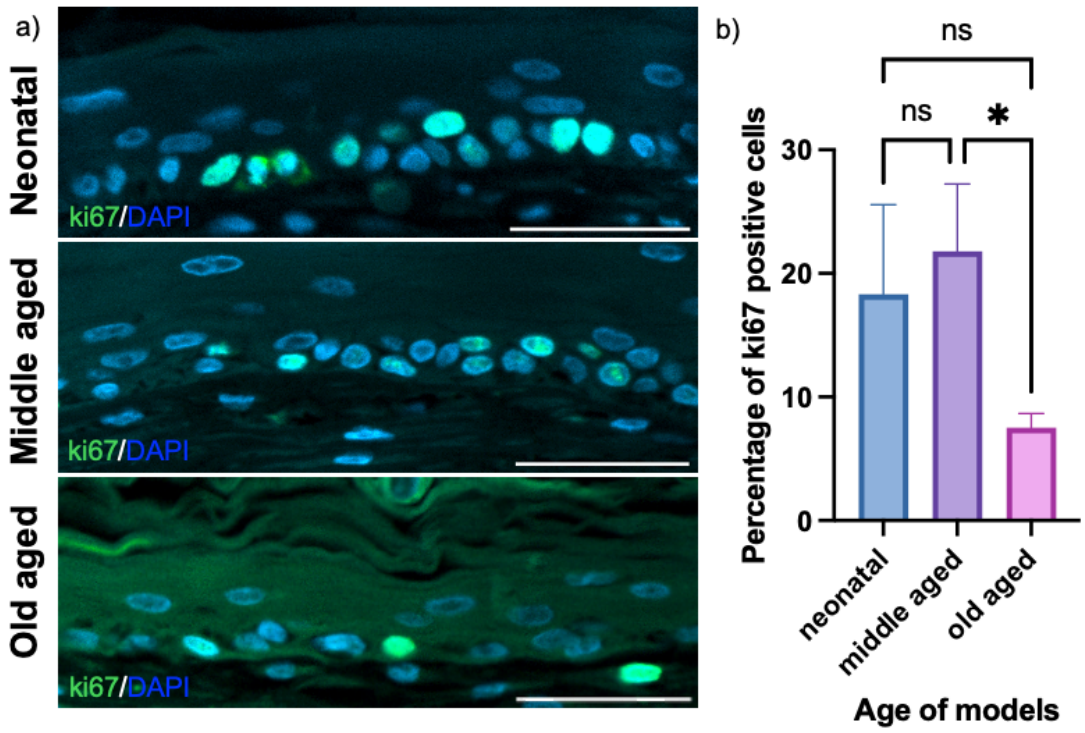

Figure 42: Immunofluorescence analysis of Ki67 protein expression in 3D in vitro full thickness skin models.

a) Representative immunostaining images for proliferation marker Ki67 and nuclear marker DAPI in pigmented neonatal, middle aged, and old aged 3D full thickness skin models. Scale bar: 50 µm Magnification: x20. b) Ki67 count as percentage of Ki67 positive cells for neonatal, middle aged, and old aged pigmented full thickness skin models. Measurements taken using counts from across the entire epidermis of each set of models per age group. GraphPad Prism 10 software was used to generate the graphs displaying the mean ± SEM with 3 skin equivalents per condition. Statistical significance was determined by an ordinary one-way ANOVA followed by Tukey's multiple comparisons post-test. The standard deviations between groups was not significantly different ($P < 0.05$). Statistically significant differences were noted as * where $P < 0.05$ above bars. No statistical difference was noted as 'ns' above bars.

Ki67 is expressed in all of the skin models (**Figure 42a**), which indicates that the keratinocytes are proliferative. According to **Figure 42b**, there is no significant difference in expression of Ki67 between neonatal and ageing pigmented skin models. However, there is a significant decrease in Ki67 expression ($P < 0.05$) in old aged models compared with middle aged ones.

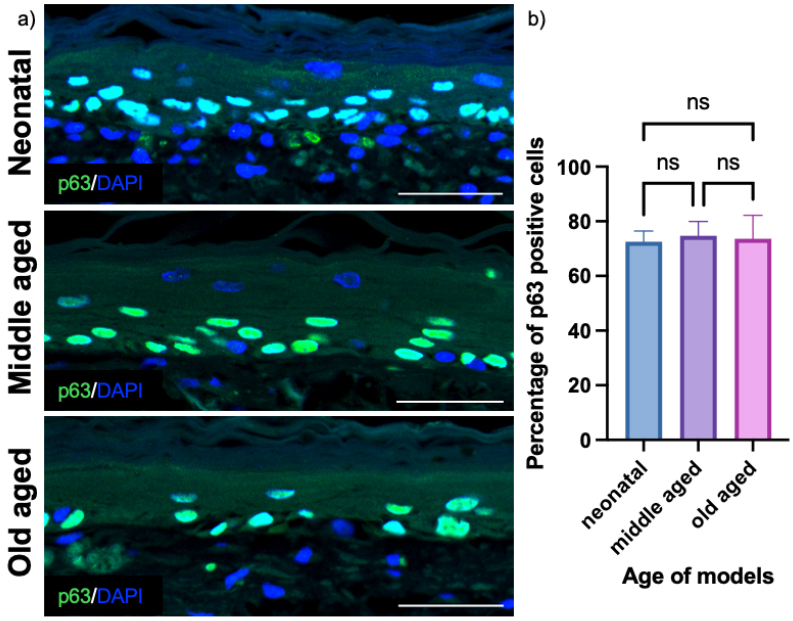

Figure 43: Immunofluorescence analysis of p63 protein expression in 3D in vitro full thickness skin models.

a) Representative immunostaining images for proliferation marker p63 and nuclear marker DAPI in pigmented neonatal, middle aged, and old aged 3D full thickness skin models. Scale bar: 50 µm Magnification: x20. b) p63 count as percentage of p63 positive cells for neonatal, middle aged, and old aged full thickness skin models. GraphPad Prism 10 software was used to generate the graphs displaying the mean ± SEM with 3 skin equivalents per condition. Measurements taken using counts from across the entire epidermis of each set of models per age group. Statistical significance was determined by an ordinary one-way ANOVA followed by Tukey's multiple comparisons post-test. The standard deviations between groups was not significantly different ($P < 0.05$). No statistical difference was noted as 'ns' above bars.

Proliferation marker p63 is expressed in all of the skin models (**Figure 43a**), indicating that keratinocytes are successfully proliferating. According to **Figure 43b**, there is no significant difference in expression of p63 between any groups; the levels of p63 expression are consistent between neonatal and ageing pigmented models.

3.7 Senescence

Immunofluorescence analysis was carried out in order to determine whether the expression of markers associated with cellular senescence change in the ageing pigmented skin equivalents.

3.7.1 Ageing pigmented full thickness skin models express senescence-associated markers HMGB1 and lamin-B1

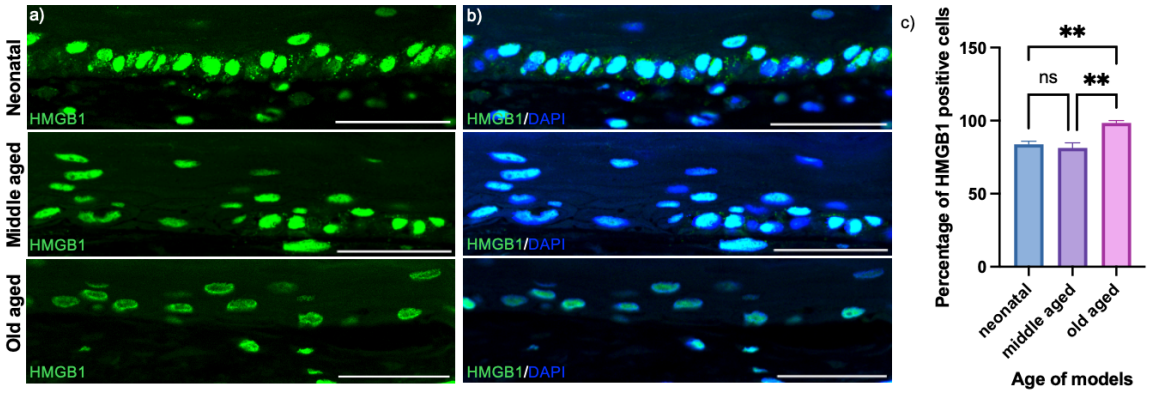

Figure 44: Immunofluorescence analysis of senescence-associated protein HMGB1 expression in 3D in vitro full thickness skin models.

Representative immunostaining images for the ageing and senescence marker HMGB1 (green), b) and nuclear marker DAPI (blue). Scale bar: 50 µm. Magnification: x20. c) HMGB1 count as percentage of HMGB1 positive cells for neonatal, middle aged, and old aged full thickness skin models. GraphPad Prism 10 software was used to generate the graphs displaying the mean ± SEM with 3 skin equivalents per condition. Measurements taken using counts from across the entire epidermis of each set of models per age group. Upon performing the ordinary one-way ANOVA test and Tukey's post-test for multiple comparisons, it was determined that the standard deviations between groups were significantly different ($P > 0.05$). The statistical significance was therefore determined by the Brown-Forsythe and Welch one-way ANOVA tests, followed by the Dunnett T3 post-test for multiple comparisons when $n < 50$ per group. Statistically significant differences were noted as ** where $P < 0.01$ above bars. No statistical difference was noted as 'ns' above bars.

Neonatal and ageing pigmented full thickness skin models were immunostained as described in Section 2.5.2 for senescence-associated markers HMGB1 and lamin-B1 and nuclear stain DAPI. **Figure 44a** shows that the models all express nuclear HMGB1, and **Figure 44b** depicts the marker HMGB1 merged with nuclear marker DAPI. According to **Figure 44c**, there is no significant difference in HMGB1 expression between neonatal and middle aged skin models, however there is a significant increase ($P < 0.01$) in the percentage of HMGB1 positive cells in old aged models compared with neonatal and middle aged skin models. It is worth noting that the percentage of cells is dependent upon the total number of stained cells, which is smaller in the ageing skin models.

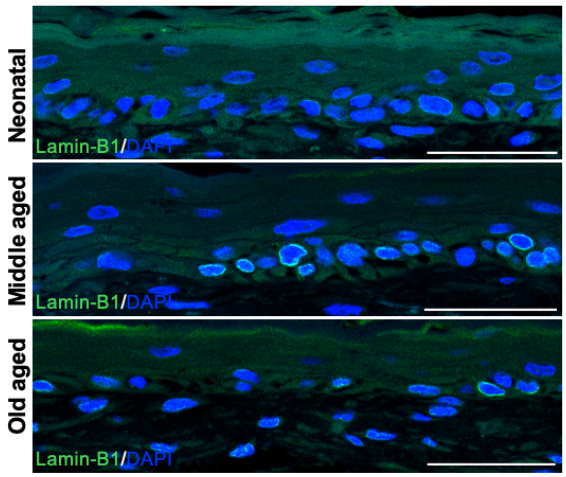

Figure 45: Immunofluorescence analysis of senescence-associated protein Lamin-B1 expression in 3D in vitro full thickness skin models.

Representative immunostaining images for the ageing and senescence marker Lamin-B1 (green) and nuclear marker DAPI (blue) in pigmented neonatal, middle aged, and old aged 3D full thickness skin models. Scale bar: 50 µm. Magnification: x20.

Figure 45 shows that the ageing pigmented skin models express the senescence-associated marker lamin-B1 at the periphery of the nuclei. This expression is highest in middle aged models, and slightly weaker in the neonatal models compared with the old aged models.

4 Discussion

The biological processes involved in skin ageing and pigmentation require a deeper level of understanding, therefore there is a need for more complex ageing pigmented skin model systems. This study utilised the novel bioengineered 3D *in vitro* full thickness skin model platform using the Alvetex® technology to construct ageing pigmented skin equivalents. Neonatal, middle aged, and old aged human dermal fibroblasts were cultured upon the Alvetex® scaffold, before human epidermal keratinocytes of the corresponding ages were seeded upon the dermal layer, along with neonatal human epidermal melanocytes at a 1:10 ratio.

The objectives of this research were, first, to successfully incorporate melanocytes into ageing full thickness skin equivalents, and second, to determine whether ageing induces changes in pigmentation *in vitro*. By meeting these objectives, the hypotheses that melanocytes would be successfully incorporated into ageing models and that changes in pigmentation would be observed could be investigated, and the overall aim of the study would be achieved. The aim of this study was to increase the complexity and diversity of bioengineered skin models to more accurately mimic the microanatomy of native human skin in the context of ageing.

4.1 Ageing Pigmented 3D full thickness Skin Models are Successfully Produced

There is a need for more complex and diverse HSEs to be developed, replicating the multifaceted attributes of human skin such as ageing and pigmentation. In this study, the ageing skin models with the incorporation of neonatal melanocytes were pigmented (**Figure 31**), which indicates that, as hypothesised, ageing pigmented skin models were successfully produced.

The uniformly pigmented models in **Figure 31** resemble those constructed by Goncalves *et al.* (2023) and De Los Santos Gomez *et al.* (2024). The same population of melanocytes (darkly pigmented neonatal human epidermal melanocytes #2077650) were used to generate the neonatal pigmented HSEs using the same protocol in these studies, making this research comparable. In each of these studies, pigmented tissue representative of native human skin was formed, which implies that the models produced in this study were also reliable and reproducible, and structurally and functionally highly similar to human skin. Moreover, the melanocytes were derived from a darkly pigmented donor, thereby increasing the diversity

and therefore the relevance of the skin models to individuals across the global population, a research requirement discussed in Section 1.3.3.

The melanocytes displayed a normal morphology with dendrites reaching into the epidermis to interact with keratinocytes, and they were uniformly distributed across the entire area of the epidermis (**Figure 29; Figure 35**), which can also be observed in 3D *in vitro* pigmented HSEs in other studies (Duval *et al.*, 2014; Goncalves *et al*., 2023; De Los Santos Gomez *et al*., 2024). Additionally, the SkinColorCatch skin tone values (**Figure 32b**; **Figure 32c**) indicate that the ageing skin models are pigmented, and the melanin index values are within a comparable range to those reported in other related studies (De Los Santos Gomez *et al*., 2024).

Furthermore, Fontana-Masson staining in **Figure 34** shows that in the ageing pigmented skin equivalents, melanocytes can successfully synthesise and transfer melanin to adjacent keratinocytes. Melanin can be visualised from the stratum basale to the stratum corneum with a normal distribution, and melanocytes are correctly positioned in the stratum basale, along with formation of supranuclear caps. The same uniform distribution of melanin and melanocytes was observed in other *in vitro* pigmented HSEs (Duval *et al*., 2014; Hall *et al*., 2022; Goncalves *et al*., 2023; De Los Santos Gomez *et al*., 2024). This highlights the importance of the role of fibroblasts in the 3D full thickness models, as their support is essential for the correct localisation of melanin and formation of supranuclear caps (Goncalves *et al.*, 2023).

A quantifiable melanin content was readily solubilised from the ageing pigmented skin models (**Figure 36**), as was the case in pigmented HSEs constructed by De Los Santos Gomez *et al.* (2024). However, the results from the melanin quantification assay designed by Fernandes *et al.* (2016) were highly variable. This is due to an issue with the protocol, where there was excessive effervescence from the reaction of melanin in the samples with hydrogen peroxide, making it difficult for the plate reader to quantify fluorescence. The assay methodology would need to be optimised for a more accurate assessment of melanin content. This would include altering reaction time, reagent concentrations and taking regular readings throughout to assess. Alternatively, a different method of melanin quantification could be used instead, such as image analysis of Fontana-Masson staining, as performed by Duval *et al.* (2014).

The H&E images in **Figure 33a** illustrate that the epidermis was stratified and well-differentiated upon a fibroblast-rich dermis, with no infiltration from keratinocytes observed

across the entire scaffold (data not shown), a key indicator of the success of 3D *in vitro* full thickness skin models constructed using the Alvetex® platform (Roger *et al*., 2019; Hall *et al.*, 2022; Goncalves *et al*., 2023; De Los Santos Gomez *et al*., 2024; Costello *et al*., 2024; Low *et al*., 2024). **Figure 39a** shows that in the ageing pigmented models, differentiation markers k10 and k14 were localised as expected and consistent with findings in other *in vitro* ageing studies (Costello *et al*., 2024; Low *et al*., 2024), indicating that differentiation occurs successfully. The ageing pigmented skin models also express the terminal differentiation markers loricrin, involucrin and periplakin with the correct localisation, which was also observed by Costello *et al*. (2024). As well as being indicative of normal differentiation, this shows that the cornified envelope and skin barrier formation has occurred successfully.

Additionally, the TEWL readings in **Figure 32a** fall within a comparable range to those observed in similar research (Goncalves *et al.*, 2023) and suggest that the ageing pigmented models maintain normal barrier function, which is the primary role of human skin. However, as noted in Section 1.2.2, the effects of ageing on TEWL values are conflicting in the current literature (Kottner *et al*., 2013). Therefore, TEWL values may not necessarily be the most accurate measure of skin barrier function.

Using the benchmark of other successful 3D *in vitro* full thickness skin models, the ageing pigmented skin models can also be deemed as successful. As hypothesised, the melanocytes were incorporated into the bioengineered full thickness skin equivalents and models with a pigmentary phenotype were produced. These models are comparable to other research and are representative of native human skin.

4.2 Ageing Bioengineered *in vitro* Skin Models Show Changes in Pigmentation

We have presented evidence that changes in melanin synthesis, melanin distribution, and melanocyte density caused various pigmentary changes to arise in the ageing HSEs. This supports the hypothesis that skin ageing would affect pigmentation *in vitro.*

4.2.1 Ageing Reduces Overall Pigmentation

It is well documented that the number of melanocytes deplete by up to 20 % per decade with intrinsic skin ageing, which can lead to a reduction in overall skin pigmentation levels (Ho &

Dreesen, 2021; Rittie & Fisher, 2015). In addition, melanogenesis can be inhibited via the downregulation of MITF, TRP-1 and TRP-2 in senescent melanocytes, resulting in age-related hypopigmentation (Lee, 2021). In this study, an overall reduction in pigmentation could be observed in the ageing versus neonatal HSEs (**Figure 31**), which is supported by the colourimeter readings (**Figure 32b**; **Figure 32c**) and Fontana-Masson histological staining (**Figure 34**). These analyses showing changes in pigmentation are also a deviation from what was seen in the neonatal pigmented HSEs constructed by Goncalves *et al.* (2023) and De Los Santos Gomez *et al.* (2024). Therefore, the reduction in pigmentation in this study is likely due to the ageing cells used and the resultant alterations in crosstalk from the ageing keratinocytes and fibroblasts to the neonatal melanocytes in these models (**Figure 9**).

This change matches the results from a study using a collagen gel-based 3D *in vitro* skin model system, where a drastic decrease in pigmentation was observed in a model using adult fibroblasts from a photo-protected region compared with foetal fibroblasts (Duval *et al*., 2014). This indicates that the intrinsic differences between the populations of fibroblasts of different ages may be responsible for the variation in pigmentation seen in this study, and perhaps infers a mechanism of crosstalk causing disruption to normal pigmentary patterns. This disrupted crosstalk has previously been implicated in pigmentary changes (De Los Santos Gomez *et al*., 2024).

Duval *et al*. (2014) also found a decrease in the number of melanocytes in the ageing pigmented HSEs, which can also be observed in this research (**Figure 35a**); this could account for the reduction in pigmentation. However, despite the clear visual difference in melanocyte density, the difference is ultimately not significant (**Figure 35b**). In order to gain a more conclusive answer, further repeats and analyses of this experiment would need to be carried out. Additionally, a study involving a co-culture between keratinocytes and melanocytes could be set up to determine whether the proliferation of keratinocytes is affected, which would potentially infer a crosstalk between the cell types.

The decrease in melanocyte numbers observed in Duval *et al.*'s 2014 study was hypothesised to result from reduced levels of HGF in the supernatant of adult fibroblasts, as HGF is commonly described as a melanocyte mitogenic factor, potentially contributing to the increased melanocyte numbers in their HSE with foetal fibroblasts. However, it is important to note that foetal fibroblasts may behave differently from the neonatal fibroblasts used in this study.

Nonetheless, the reduction in pigmentation and the visual difference in melanocyte density (**Figure 35a**) in the ageing pigmented HSEs are still quite notable, considering that the melanocytes were seeded into the models at the same 1:10 ratio, which has been shown to produce optimal pigmentation *in vitro* (De Los Santos Gomez *et al*., 2024). In addition, darkly pigmented neonatal melanocytes were used, even in the ageing skin equivalents. These pigmentary changes have been observed in other *in vitro* studies of intrinsic ageing (Duval *et al*., 2014) and could suggest a mechanism of melanocyte inhibition resultant from potential differences in the secretome of the ageing fibroblasts (Waldera, Lupa *et al*., 2015).

4.2.2 Pigmentation Abnormalities Arise in Old Aged Models

Hyperpigmented lesions can arise in ageing human skin due to the excessive synthesis and deposition of melanin (Jdid *et al*., 2024). There is evidence that the disruption of such processes involved in melanogenesis and melanin localisation can be caused by fibroblasts with a SASP, indicating that altered crosstalk between fibroblasts and melanocytes can contribute to pigmentation abnormalities (Kim *et al*., 2022). In **Figure 31**, the appearance of dark spots in the old aged models can clearly be observed, which bear a remarkable resemblance to those seen in ageing human skin. It is important to note that neonatal melanocytes were cocultured with ageing keratinocytes and fibroblasts in these HSEs, which provides further evidence for the mechanism of dysregulated cross talk between these cell types.

The appearance of hyperpigmented lesions could also be observed in a 2014 study by Duval *et al*., in a 3D *in vitro* skin model with the incorporation of naturally photo-aged fibroblasts with a confirmed SASP. These pigmentary abnormalities cannot be visualised as clearly as the dark spots on the ageing pigmented HSEs in this study on a macroscopic level, which could be due to the differences in culture method. The Alvetex® scaffold more closely mimics the nuances and microanatomy of human skin (Roger *et al*., 2019), whereas the bovine collagen hydrogel used in their study is a simpler model system which may have additional effects as it is exogenous. Furthermore, the melanocytes used in their models derived from a moderately pigmented Caucasian donor, the ratio of keratinocytes: melanocytes was not specified or optimised, and they used foetal fibroblasts, may behave differently to neonatal fibroblasts since they are at an earlier stage of development. Additionally, the fibroblasts and keratinocytes used in this study were age matched, further increasing the complexity of this novel ageing pigmented skin equivalent.

Nevertheless, their results and analyses demonstrate that photo-aged fibroblasts with a SASP can contribute to hyperpigmentation associated with extrinsic skin ageing. It can be hypothesised that in the ageing pigmented HSEs in both studies, the physiological state associated with the dark spots could be linked to modifications that the fibroblasts accumulate over time (Duval *et al*., 2014), thereby altering the intercellular communication. This is, indeed, consistent with previous evidence, as increased levels of SASP have been detected in hyperpigmented lesions, (Yoon *et al*., 2018) indicating a strong link between ageing and pigmentary changes.

Dark spots are typically associated with UV-induced photo-ageing (Porcheron *et al*., 2014), rather than chronological ageing; however, in this study, the lesions of hyperpigmentation in the old aged models arose without being exposed to UVR. Perhaps this is due to photodamage in the donor from which the cells originated; however, it is important to note that the cells were harvested from a photo-protected area. To understand why this might be, a repeat of full thickness models using cells from photo-protected vs photo-exposed regions of the same donor could be conducted. Additionally, analysis of the dark spots on the images in **Figure 31** could be completed using an image analysis software to quantify the intensity and distribution of dark spots. This could then be compared with a macroscopic image of human skin with solar lentigines to determine whether the pigmentation abnormalities in the skin models are consistent with native human skin.

Some evidence has suggested that melanocytes become increasingly unevenly distributed with age (Yaar *et al*., 2002). Therefore, the non-significant difference in melanocyte density in the ageing pigmented HSEs could be explained by the distribution of melanocytes across the epidermis becoming more uneven; the melanocytes in the ageing pigmented skin models appear to be unevenly distributed and clumped in areas (**Figure 35**). Duval *et al.* (2014) also found no significant difference in the number of melanocytes, despite the appearance of hyperpigmented lesions in their photo-aged pigmented skin equivalents. Although this study did not confirm whether the dark spots accumulated in regions with higher melanocyte numbers or melanin density, the non-uniform localisation of melanin may have been caused by the underlying uneven distribution of melanocytes. To investigate a potential link, a follow-up study could be conducted, where immunostained epidermal punch biopsies are visualised under a light microscope to examine the regions with dark spots, comparing these areas to the immunofluorescence images.

Overall, it appears that the changes in pigmentation observed in the skin equivalents in this study are strongly linked to the age of the primary cells incorporated into the model. Like other ageing pigmented *in vitro* studies (Duval *et al*., 2014), and in contrast to the neonatal controls in this study and the neonatal pigmented HSEs generated by Hall *et al*. (2022), Goncalves *et al*. (2023), and De Los Santos Gomez *et al*. (2024), the ageing pigmented models exhibit altered pigmentation. These changes are comparable to some of the pigmentary alterations observed in ageing human skin, as discussed in Section 1.3.2.

4.3 Age-Related Dermal Changes Arise in the Ageing Pigmented Skin Equivalents

It is well understood that various dermal changes occur with skin ageing; as outlined in Section 1.2.2, the activity of the fibroblasts decline, and synthesis of the ECM becomes reduced (Reilly & Lozano, 2021). Sirius red staining (**Figure 37**) and immunofluorescence analysis (**Figure 38a**) confirm that fibroblasts in the ageing pigmented HSEs can successfully construct a collagen-rich ECM, and that overall collagen density appears to be reduced with age. This is consistent with other *in vitro* ageing skin studies where a decline in collagen content is observed with senescent fibroblasts (Low *et al*., 2024; Diekmann et al., 2016) and intrinsically aged fibroblasts (Costello *et al*., 2024). However, for a more reliable quantification of collagen, the experiment would need to be repeated, and a collagen assay would be carried out.

Fibronectin is a glycoprotein involved in the formation of the ECM in tissue development and wound healing (Dalton & Lemmon, 2021) and plays a regulatory role in proliferation and reepithelialisation (Lenselink, 2015), as discussed in Section 1.1.3. Fibronectin is successfully synthesised by fibroblasts in the ageing pigmented HSEs (**Figure 38a**), and the fluorescence intensity of fibronectin in the ageing pigmented HSEs across both age groups significantly decreased compared with the neonatal pigmented models (**Figure 38c**). These results are to be expected, since it is understood that the expression of fibronectin is downregulated with age, especially by senescent fibroblasts (Cho *et al.,* 2022). Since the tissue in the skin models is newly developed, it could be hypothesised that this influences the fibronectin levels in this bioengineered skin model platform compared with native human skin. However, this would have to be confirmed by completing immunofluorescence analysis of the fibronectin marker in the ageing pigmented models compared to *ex vivo* human skin.

In both intrinsic and extrinsic skin ageing, ECM remodelling occurs, resulting in a more disorganised ECM with an uneven distribution of proteins (Naylor *et al*., 2011). In the ageing

pigmented HSEs, the ECM appears to become more clumped and unevenly distributed in the ageing pigmented skin models (**Figure 38a**), although these results are not conclusive and would need to be confirmed using an image analysis software. This age-related ECM remodelling was also observed in *in vitro* HSEs with an intrinsically aged dermal compartment constructed by Costello *et al*. (2024).

Overall, the ageing pigmented HSEs show a decline in the density of the ECM, indicating a decrease in the synthesis of its components such as extracellular collagens by fibroblasts. Age-related ECM remodelling can also be observed, a characteristic of intrinsic and extrinsic ageing (Naylor *et al*., 2011). Several additional analyses could be carried out to provide us with a more detailed understanding of the dermal changes that can be observed on the ageing pigmented HSEs. For example, further immunostaining analysis could be carried out to determine the expression of a fibroblast marker such as vimentin and determine whether there is a change in number of fibroblasts in the ageing pigmented models. In addition, cytokine analysis could be carried out to determine whether the fibroblasts have a SASP. Furthermore, expression of collagenases such as MMP1 could be investigated using immunofluorescence analysis to identify whether it is upregulated and therefore collagen degradation is increased with age, as with in human skin.

4.4 Age-Related Epidermal Changes Occur in the Ageing Pigmented Skin Models

There are various age-related epidermal changes that will be discussed in this section, such as differences in the morphology of the epidermis and keratinocytes, proliferation, differentiation, and expression of epidermal senescence-associated markers. Combining the two ageing cell populations in the ageing pigmented 3D *in vitro* full thickness skin models confirms several of these aspects.

It is broadly understood that the epidermis thins with chronological ageing (Fenske and Lober, 1986; Waller and Maibach, 2005), and the skin cells used in the ageing pigmented models originate in a photo-protected region. Therefore, a decreased epidermal thickness in the ageing compared to neonatal pigmented models is to be expected. The results for the middle-aged skin equivalents are unexpected (**Figure 33b**), as the epidermal thickness is significantly higher than in both the neonatal and old-aged pigmented skin models. This is likely an anomaly caused by variations between the donor cells, or it may indicate that the neonatal keratinocytes are not as proliferative as anticipated, resulting in a thinner epidermis than

expected for the neonatal control. However, if the focus is shifted to the decrease in epidermal thickness in the old aged pigmented models compared with the neonatal control, these findings are similar to those in other 3D *in vitro* ageing skin equivalents (Low *et al*., 2024; Dos Santos *et al*., 2016; Costello *et al*., 2024; Weinmüllner *et al,* 2020; Costello *et al*., 2023).

There are several factors that may be involved in this age-related epidermal thinning, such as changes to the dermal epidermal junction. Some ageing studies have provided evidence that changes in the DEJ cause a decrease in epidermal thickness in *in vitro* models of chronological skin ageing (Costello *et al*., 2024), *in vitro* senescence models (Low *et al*., 2024), and *ex vivo* chronologically and photo-aged skin (Costello *et al*., 2023). Mimicking the dermal-epidermal junction and epithelial-mesenchymal cross talk when studying the skin is highly significant, particularly when developing methods of tissue engineering such as 3D *in vitro* full thickness skin models (Aleemardani *et al.,* 2021). When generating skin equivalents using this protocol, a basement membrane forms when keratinocytes are seeded upon the dermal component. The fact that there is no infiltration in the ageing pigmented HSEs (data not shown) suggests that there is the presence of a basement membrane. Costello *et al.* (2024) highlights this with integrin a6 immunostaining, where the basal lamina can be detected in 3D *in vitro* full thickness skin models with both a neonatal and ageing dermis, therefore basement membrane formation occurs even in ageing skin models. In future, the ageing pigmented HSEs should be stained for the integrin a6 biomarker so that the dermal-epidermal junction can be visualised.

In the ageing pigmented skin models, the number of layers of viable cells is reduced compared with in the neonatal models, even though the same number of keratinocytes were counted and seeded in all models. This could contribute to the overall decrease in the epidermal thickness of the ageing pigmented models. Other ageing studies with senescent fibroblasts have shown a reduction of epidermal thickness accompanied by a significant reduction in the number of layers of the viable epidermis (Costello *et al*., 2024; Dos Santos *et al*., 2016); these results are highly reflective of the results displayed in **Figures 33b** and **39a**. However, *in vivo* studies have shown the number of viable cell layers does not differ between young and ageing subjects (Waller and Maibach, 2005), therefore the opposite results seen *in vitro* and in the ageing pigmented HSEs could be due to altered keratinocyte behaviour due to the *de novo* synthesis of the tissue.

Nevertheless, the *in vitro* results across multiple studies suggest that the mechanism underlying the observed epidermal thinning may be due to reduced proliferation. A thinning epidermis is often accompanied by a reduced epidermal turnover (Farage *et al*., 2013) and

impaired proliferation of keratinocytes (Ding *et al*., 2021). Upon performing analyses of proliferation biomarkers p63 and Ki67 in the 2D keratinocytes and HSEs (**Figure 30**; **Figure 42**; **Figure 43**), no noteworthy significant differences in expression were observed, indicating no significant changes in proliferation with different ages in human skin. There exists evidence for increases (Giangreco *et al*., 2010; Low *et al*., 2024), decreases (Rübe *et al*., 2021, Shamitova *et al*., 2018; Low *et al*., 2024; Weinmüllner *et al.,* 2020), and no significant changes (Costello *et al*., 2023; Ressler *et al*., 2006; Costello *et al*., 2024) in markers Ki67 and p63 in ageing human skin. The variability using *in vitro* methods may be attributed to the heterogeneity as the keratinocytes originate from a single donor, or the lower proliferative capacity of ageing keratinocytes that must construct an entire *in vitro* full thickness model from scratch. Overall, the evidence around proliferation markers in ageing 3D *in vitro* full thickness skin models in the literature is conflicting. However, a decrease in proliferation is most likely to occur and contribute to the age-related epidermal thinning. Epidermal thinning has been observed alongside proliferative changes in senescent *in vitro* HSEs (Weinmüllner *et al*., 2020; Low *et al*., 2024), indicating that the two attributes may influence one another. However, the senescent fibroblasts in these studies are cocultured with neonatal keratinocytes, or do not specify the age of donors. Although the proliferation data from the ageing pigmented models is not significant or highly compelling, the Ki67 expression is somewhat indicative of a general decline in cellular proliferation with age (**Figure 42**). However, further repeats would need to be conducted to provide stronger evidence to support this.

Alterations in the morphology of basal cells are recognised as a key feature of ageing in human skin (Farage *et al*., 2013; Lin *et al*., 2020; Ding *et al*., 2021). In fact, even simpler epidermal models display a similar phenotype, including atypical basal cell morphology in ageing models (Waller and Maibach, 2005). Senescent cells have been previously observed to display a flattened morphology and enlarged nuclei *in vitro* (Chin *et al*., 2023). The thinning of the epidermis in the ageing pigmented HSEs may partially be caused by the flattening cellular morphology with age (**Figure 39a**), which is consistent with data from other *in vitro* (Costello *et al*., 2024) and *ex vivo* (Costello *et al*., 2023) studies of intrinsic skin ageing. Overall, these changes in cellular morphology provide evidence for altered intercellular communication and disrupted crosstalk between fibroblasts and keratinocytes. In Costello *et al*.'s 2024 study, these morphological changes were hypothesised to be caused via proinflammatory mediators from the senescent fibroblasts. Although senescent fibroblasts were not directly seeded into the ageing pigmented HSEs, the ageing fibroblasts may have displayed a SASP phenotype, resulting in a similar disruption to fibroblast-keratinocyte communication.

Senescence associated marker HMGB1 significantly increased in the old aged pigmented HSEs (**Figure 44**) and lamin-B1 appears to have increased in the ageing pigmented skin models (**Figure 45**), although its expression levels were not quantified. These results are not indicative of senescence, since other studies have seen conflicting results with expression of these senescence associated markers: *in vitro* senescent fibroblasts and *in vivo* intrinsically aged human skin showed a decrease in HMGB1 and lamin-B1 (Wang *et al*., 2022), and *in vitro* HSEs with senescent fibroblasts cocultured with neonatal keratinocytes saw no significant changes in expression of these markers (Costello *et al*., 2024; Low *et al*., 2024). Therefore, it cannot be confirmed from this study whether the cells in the intrinsically aged pigmented HSEs display a SASP. Conducting further repeats and analyses may provide us with a deeper insight into age-related senescence in the pigmented HSEs. For example, cytokine assays could be performed using the media that the ageing pigmented models are grown in, such as an ELISA to detect changes in IL-1a. Additionally, there were several staining issues and inconsistencies with Lamin-B1 and HMGB1. Therefore, in future studies, other markers of cellular senescence, for example pro-inflammatory cytokines like IL-8, could be investigated.

5 Conclusions and Future Directions

This research has utilised bioengineered ageing pigmented 3D *in vitro* full thickness skin models as a platform to investigate how skin ageing affects pigmentation. The findings of this study demonstrate that melanocytes can be successfully incorporated into ageing 3D full thickness skin equivalents with age-related pigmentary changes being observed *in vitro*. In the ageing pigmented models, the fibroblasts were able to produce an ECM-rich dermis, and the keratinocytes successfully differentiated to form a stratified, multi-layered epidermis with a normal barrier function. An overall reduction in pigmentation was seen in the ageing pigmented skin models, as well as the appearance of hyperpigmented lesions in the old aged equivalents. Furthermore, the analyses in this study provide evidence for the underlying mechanisms of these pigmentary alterations, for example changes in distribution of melanocytes and disrupted intercellular communication. Additionally, this research highlights the notion that the dermis is required for correct melanin localisation and supranuclear cap formation, emphasising the importance of developing more complex full thickness skin models representative of native human skin. The ageing pigmented skin equivalents generated in this research are the most complex of its kind, with its novel aspects including the age-matched dermal and epidermal components and the use of the Alvetex® platform.

Although extremely useful for research, the 3D full thickness skin models currently have several limitations. For instance, current models lack appendages that are present in human skin such as cells of the immune system and mechanical stress (Goncalves *et al.*, 2023), as well as the influence of hormones. However, these factors are now being accounted for within the 3D skin equivalents. For example, an immune competent *in vitro* 3D full thickness model has been developed with the incorporation of Langerhans cells, to facilitate the study of inflammatory responses in the skin (Simpson, 2022; Simpson *et al*., 2024). However, this protocol used neonatal cells and did not incorporate melanocytes. Inflammation is a feature of the processes of both ageing and pigmentation; therefore, it could be useful to develop immune competent ageing and pigmented models in the future.

In addition, the ageing pigmented skin models have their own limitations and need further optimisation. For example, the models can be sensitive and liable to processing errors. Disorganisation and staining anomalies for differentiation markers occurred in the ageing pigmented HSEs and has also been observed in other *in vitro* skin ageing studies (Dos Santos *et al*., 2016) Although this may reflect the disorganisation and abnormalities in the differentiation process in ageing skin, it is a key limitation of constructing *in vitro* models using

ageing cells. Given the long time period needed to culture the 3D *in vitro* full thickness skin models, the generation of data is relatively time-consuming compared with more simple model systems. Additionally, the ageing cells can be more vulnerable and difficult to work with at times and show variability and heterogeneity between populations, as well as the increased amount of time that is required to construct the ageing models.

Additionally, it must be considered that the ethnicity of the donors may have affected the thickness and structure of the epidermis, which was highlighted in Section 1.3.3. Although the melanocytes are derived from a darkly pigmented donor, the keratinocytes and fibroblasts were derived from Caucasian donors, which may also have affected the pigmentation levels in these models due to existing melanin in the keratinocytes. Therefore, it should be noted that the results of this experiment may be variable depending on the ethnic group from the donors of the skin cells.

Given that this research is the first of its kind and a pilot study, a triplicate repeat is required to ensure that the results are reproducible and generalisable. Intrinsically aged cells have been shown to display phenotypic and behavioural differences compared to senescent cells (Waldera Lupa et al., 2015). Therefore, it is important to design experiments that combine both intrinsically aged and senescent cells to better understand the complex mechanisms underlying physiological age-related changes in the skin. In future, the skin equivalents should be constructed incorporating skin cells from more donors, senescent cells, and ageing melanocytes, to increase the complexity of the model platform. Further analyses could also be carried out on these repeats such as qPCR to quantify gene expression of Western blotting to measure protein expression. In addition, the platform could be utilised as a testing platform for cosmetic actives such as retinoids. The models could also be used to test other skin-ageing pigmentation approaches such as senolytic compounds, to evaluate their efficacy in regulating or disrupting cellular senescence and the process of ageing.

6 References

1. Aleemardani, M., Trikić, M. Z., Green, N. H. & Claeyssens, F. (2021) The Importance of Mimicking Dermal-Epidermal Junction for Skin Tissue Engineering: A Review. *Bioengineering*. 8(11):148.

2. Amiri, N., Golin, A. P., Jalili, R. B. & Ghahary, A. (2021) Roles of cutaneous cell-cell communication in wound healing outcome: An emphasis on keratinocyte-fibroblast crosstalk. *Exp Dermatol*. 31: 475–484.

3. Arda, O., Göksügür, N. & Tüzün, Y. (2014) Basic histological structure and functions of facial skin. *Clinics in Dermatology*, 32(1): 3-13.

4. Arnal-Forné, M., Molina-García, T., Ortega, M., Marcos-Garcés, V., Molina, P., Ferrández-Izquierdo, A., Sepulveda, P., Bodí, V., Ríos-Navarro, C. & Ruiz-Saurí, A. (2024) Changes in human skin composition due to intrinsic aging: a histologic and morphometric study. *Histochem Cell Biol.* 162: 259–271.

5. Baker, B. M. & Chen, C. S. (2012) Deconstructing the third dimension: how 3D culture microenvironments alter cellular cues. *Journal of cell science*. 125(13): 3015–3024.

6. Baker, D. J., Childs, B. G., Durik, M., Wijers, M. E., Sieben, C. J., Zhong, J., A. Saltness, R., Jeganathan, K. B., Verzosa, G. C., Pezeshki, A., Khazaie, K., Miller, J. D. & van Deursen, J. M. (2016) Naturally occurring p16 Ink4a-positive cells shorten healthy lifespan. *Nature*. 530(7589): 184–189.

7. Bastonini, E., Kovacs, D., & Picardo, M. (2016). Skin pigmentation and pigmentary disorders: focus on epidermal/dermal cross-talk. *Annals of dermatology*. *28*(3): 279-289.

8. Barnard, I.R.M., Tierney, P., Campbell, C.L., McMillan, L., Moseley, H., Eadie, E., Brown, C.T.A. and Wood, K. (2018), Quantifying Direct DNA Damage in the Basal Layer of Skin Exposed to UV Radiation from Sunbeds. Photochem Photobiol, 94: 1017-1025.

9. Bouameur, J-E., Favre, B. & Borradori, L. (2014) Plakins, a Versatile Family of Cytolinkers: Roles in Skin Integrity and in Human Diseases, *Journal of Investigative Dermatology*. 134(4): 885-894.

10. Branquinho, M. S., Silva, M. B., Silva, J. C., Sales, M. C., Barros, S. B., Maria-Engler, S. S. & Campa, A. (2020) A 2D and 3D melanogenesis model with human primary cells induced by tyrosine. *J Biol Methods*. 7(3): e134.

11. Breitkreutz, D., Koxholt, I., Thiemann, K. & Nischt, R. (2013) Skin Basement Membrane: The Foundation of Epidermal Integrity—BM Functions and Diverse Roles of Bridging Molecules Nidogen and Perlecan. *BioMed Research International*. 2013(1): 179784.

12. Brenner, M., & Hearing, V. J. (2008). The protective role of melanin against UV damage in human skin. *Photochemistry and photobiology*. 84(3): 539-549.

13. Brown, T. M. & Krishnamurthy, K. (2023) Histology, Dermis. In: StatPearls. StatPearls Publishing, Treasure Island (FL): PMID: 30570967.

14. Cario, M. (2019) How hormones may modulate human skin pigmentation in melasma: an in vitro perspective. *Exp Dermatol*. 28: 709-718.

15. Chambers, E. S. & Vukmanovic-Stejic, M. (2020), Skin barrier immunity and ageing. *Immunology*. 160: 116-125.

16. Chan, J. K. L., Yuen, D., Too, P. H-M., Sun, Y., Willard, B., Man, D. & Tam, C. (2018) Keratin 6a reorganization for ubiquitin–proteasomal processing is a direct antimicrobial response. *J Cell Biol*. 217(2): 731–744.

17. Chen, W., Kang, J., Xia, J., Yang, B., Chen, B., Sun, W., ... & Bi, Z. (2008). p53-related apoptosis resistance and tumor suppression activity in UVB-induced premature senescent human skin fibroblasts. *International journal of molecular medicine*, *21*(5), 645-653.

18. Chin, T., Lee, X. E., Ng, P. Y., Lee, Y. & Dreesen, O. (2023) The role of cellular senescence in skin aging and age-related skin pathologies. *Frontiers in Physiology.* 14.

19. Cho, K., Yang, K.E., Nam, SB. *et al. (*2022*)* Shotgun proteomics of extracellular matrix in late senescent human dermal fibroblasts reveals a down-regulated fibronectin-centered network. *J Anal Sci Technol* **13**, 20.

20. Choi, H. R., Cho, K. A., Kang, H. T., Lee, J. B., Kaeberlein, M., Suh, Y., Chung, I. K. & Park, S. C. (2011) Restoration of senescent human diploid fibroblasts by modulation of the extracellular matrix. *Aging Cell*. 10: 148-157.

21. Corcuff, P., Lotte, C., Rougier, A. & Maibach, H.I. (1991) Racial differences in corneocytes. *Acta Derm. Venereol. (Stockh).* 71: 146–148.

22. Costello, L. (2019) Bioengineering Novel Ageing Skin Equivalents and their Application to Study the Importance of Dermal-Epidermal Interactions during Skin Ageing. Thesis.

23. Costello, L., Dicolandrea, T., Tasseff, R., Isfort, R., Bascom, C., von Zglinicki, T., & Przyborski, S. (2022). Tissue engineering strategies to bioengineer the ageing skin phenotype in vitro. *Aging cell*. 21(2): e13550.

24. Costello, L., Goncalves, K., De Los Santos Gomez, P., Simpson, A., Maltman, V., Ritchie, P., Tasseff, R., Isfort, R., Dicolandrea, T., Wei, X., Määttä, A., Karakesisoglou, I., Markiewicz, E., Bascom, C. C. & Przyborski, S. (2023) Quantitative morphometric analysis of intrinsic and extrinsic skin ageing in individuals with Fitzpatrick skin types II–III. *Exp Dermatol*. 32: 620-631.

25. Costello, L., Goncalves, K., De Los Santos Gomez, P., Hulette, B., Dicolandrea, T., Flagler, M. J., Isfort, R., Oblong, J., Bascom, C., & Przyborski, S. (2024). Investigation into the significant role of dermal-epidermal interactions in skin ageing utilising a bioengineered skin construct. *Journal of Cellular Physiology*. e31463.

26. Dalton, C. J., & Lemmon, C. A. (2021). Fibronectin: Molecular Structure, Fibrillar Structure and Mechanochemical Signaling. *Cells*. 10(9): 2443.

27. De Los Santos Gomez, P. (2023) Development of *in vitro* Human Pigmented Skin Equivalents to Study Skin Pigmentation, Photodamage and Photoprotection. Thesis.

28. De Los Santos Gomez, P., Costello, L., Goncalves, K., & Przyborski, S. (2024). Comparison of photodamage in non-pigmented and pigmented human skin equivalents exposed to repeated ultraviolet radiation to investigate the role of melanocytes in skin photoprotection. *Frontiers in Medicine*. *11*: 1355799.\

29. Diekmann, J., Alili, L., Scholz, O., Giesen, M., Holtkötter, O. & Brenneisen, P. (2016) A three-dimensional skin equivalent reflecting some aspects of *in vivo* aged skin. *Exp Dermatol*. 25: 56-61.

30. Ding, X., Kakanj, P., Leptin, M., Eming, S.A., 2021. Regulation of the Wound Healing Response during Aging. *J. Invest. Dermatol*. 141: 1063–1070.

31. Dos Santos, M., Michopoulou, A., André-Frei, V., Boulesteix, S., Guicher, C., Dayan, G., Whitelock, J., Damour, O. & Rousselle, P. (2016) Perlecan expression influences the keratin 15-positive cell population fate in the epidermis of aging skin. *Aging (Albany NY).* 8(4): 751-68.

32. Duval, C., Cohen, C., Chagnoleau, C., Flouret, V., Bourreau, E. & Bernerd, F. (2014) Key regulatory role of dermal fibroblasts in pigmentation as demonstrated using a reconstructed skin model: impact of photo-aging. *PLoS One*. 9(12): e114182.

33. Egles, C., Shamis, Y., Mauney, J. R., Volloch, V., Kaplan, D. L. & Garlick, J. A. (2008) Denatured Collagen Modulates the Phenotype of Normal and Wounded Human Skin Equivalents. *Journal of Investigative Dermatology*. 128(7): 1830-1837.

34. European Union (2009) Regulation (EC) No 1223/2009 of the european parliament and of the council. *Official Journal of the European Union L*. 342: 59.

35. Farage, M. A., Miller, K. W., Elsner, P., & Maibach, H. I. (2008). Intrinsic and extrinsic factors in skin ageing: a review. *International journal of cosmetic science*, *30*(2), 87-95.

36. Farage, M.A., Miller, K.W., Elsner, P., Maibach, H.I., 2013. Characteristics of the Aging Skin. *Adv. Wound Care*. 2: 5–10.

37. Fenske, N.A., Lober, C.W., 1986. Structural and functional changes of normal aging skin. *J. Am. Acad. Dermatol*. 15: 571–585.

38. Fernandes, B., Matamá, T., Guimarães, D., Gomes, A. and Cavaco-Paulo, A. (2016), Fluorescent quantification of melanin. *Pigment Cell Melanoma Res*. 29: 707-712.

39. Ganier, C., Rognoni, E., Goss, G., Lynch, M. & Watt, F. (2022) Fibroblast Heterogeneity in Healthy and Wounded Skin. *Cold Spring Harb Perspect Biol*. 14: a041238.

40. García-Borrón, J.C., Sánchez-Laorden, B.L. & Jiménez-Cervantes, C. (2005), Melanocortin-1 receptor structure and functional regulation. *Pigment Cell Research.* 18: 393-410.

41. Giangreco, A., Goldie, S.J., Failla, V., Saintigny, G., Watt, F.M., 2010. Human Skin Aging Is Associated with Reduced Expression of the Stem Cell Markers β1 Integrin and MCSP. *J. Invest. Dermatol*. 130: 604–608.

42. Goncalves, K., De Los Santos Gomez, P., Costello, L., Smith, L., Mead, H., Simpson, A., & Przyborski, S. (2022). Investigation into the effect of skin tone modulators and exogenous stress on skin pigmentation utilizing a novel bioengineered skin equivalent. *Bioengineering & translational medicine*. 8(2): e10415.

43. Groot, K. R., Sevilla, L. M., Nishi, K., DiColandrea, T. & Watt, F. M. (2004) Kazrin, a novel periplakin-interacting protein associated with desmosomes and the keratinocyte plasma membrane. *J Cell Biol.* 166(5): 653–659.

44. Hall, M. J., Lopes-Ventura, S., Neto, M. V., Charneca, J., Zoio, P., Seabra, M. C., Oliva, A., & Barral, D. C. (2022). Reconstructed human pigmented skin/epidermis models achieve epidermal pigmentation through melanocore transfer. *Pigment Cell & Melanoma Research*. 35: 425–435.

45. Ho, C. Y. & Dreesen, O. (2021) Faces of cellular senescence in skin aging, *Mechanisms of Ageing and Development.* 198: 111525.

46. Jarrold, B. B., Tan, C. Y. R., Ho, C. Y., Soon, A. L., Lam, T. T., Yang, X., Nguyen, C., Guo, W., Chew, Y. C., DeAngelis, Y. M., Costello, L., De Los Santos Gomez, P., Przyborski, S., Bellanger, S., Dreesen, O., Kimball, A. B. & Oblong, J. E. (2022). Early onset of senescence and imbalanced epidermal homeostasis across the decades in photoexposed human skin: Fingerprints of inflammaging. *Experimental dermatology*. 31(11): 1748–1760.

47. Jdid, R., Pedrazzani, M., Lejeune, F., Fischman, S.., Cazorla, G., Forestier, S. & Khalifa, Y. B. (2024) Skin dark spot mapping and evaluation of brightening product efficacy using Line-field Confocal Optical Coherence Tomography (LC-OCT). *Skin Res Technol*. 30: e13623.

48. Jenkins, N. C., & Grossman, D. (2013). Role of melanin in melanocyte dysregulation of reactive oxygen species. *BioMed research international*. 908797.

49. Jevtić, M., Löwa, A., Nováčková, A., Kováčik, A., Kaessmeyer, S., Erdmann, G., Vávrová, K. & Hedtrich, S. (2020) Impact of intercellular crosstalk between epidermal keratinocytes and dermal fibroblasts on skin homeostasis. *Biochimica et Biophysica Acta (BBA) - Molecular Cell Research*. 1867(8): 118722.

50. Keyes, W. M. & Mills, A. A. (2006) p63: a new link between senescence and aging. *Cell cycle (Georgetown, Tex.)*, *5*(3), 260–265.

51. Keyes, W. M., Wu, Y., Vogel, H., Guo, X., Lowe, S. W., & Mills, A. A. (2005). p63 deficiency activates a program of cellular senescence and leads to accelerated aging. *Genes & development*, *19*(17), 1986–1999.

52. Kim, J. C., Park, T. J. & Kang, H. Y. (2022) Skin-Aging Pigmentation: Who Is the Real Enemy? *Cells*. 11: 2541.

53. Knaggs, H. E., Holland, D. B., Morris, C., Wood, E. J., & Cunliffe, W. J. (1994). Quantification of cellular proliferation in acne using the monoclonal antibody Ki-67. *The Journal of investigative dermatology*. 102(1), 89–92.

54. Kolarsick, P.A.J. BS., Kolarsick, M. A. MSN. ARHP-C. & Goodwin, C. APRN-BC. FNP. (2011) Anatomy and Physiology of the Skin. *Journal of the Dermatology Nurses' Association.* 3(4): 203-213.

55. Kunisada, T., Yoshida, H., Yamazaki, H., Miyamoto, A., Hemmi, H., Nishimura, E., … Hayashi, S. (1998). Transgene expression of steel factor in the basal layer of epidermis promotes survival, proliferation, differentiation and migration of melanocyte precursors. *Development*. 125(15): 2915–2923.

56. Lagarrigue, S. G., George, J., Questel, E., Lauze, C., Meyer, N., Lagarde, J.-M., Simon, M., Schmitt, A.-M., Serre, G. and Paul, C. (2012) *In vivo* quantification of epidermis pigmentation and dermis papilla density with reflectance confocal microscopy: variations with age and skin phototype. *Experimental Dermatology*. 21: 281-286.

57. Langton, A.K., Halai, P., Griffiths, C.E.M., Sherratt, M.J. & Watson, R.E.B. (2016) The impact of intrinsic ageing on the protein composition of the dermal-epidermal junction. *Mechanisms of Ageing and Development*. 156: 14-16.

58. Langton, A. K., Alessi, S., Hann, M., Chien, A. L., Kang, S., Griffiths, C. E. M., & Watson, R. E. B. (2019). Aging in Skin of Color: Disruption to Elastic Fiber Organization Is Detrimental to Skin's Biomechanical Function. *The Journal of investigative dermatology*. 139(4): 779–788.

59. Lee, A.Y. (2021) Skin Pigmentation Abnormalities and Their Possible Relationship with Skin Aging. *Int. J. Mol. Sci.* 22: 3727.

60. Lenselink, E.A. (2015) Role of fibronectin in normal wound healing. *Int Wound J*. 12: 313-316.

61. Li, Y., Giovannini, S., Wang, T., Fang, J., Li, P., Shao, C., Wang, Y., TOR centre, Shi, Y., Candi, E., Melino, G. & Bernassola, F. (2023) p63: a crucial player in epithelial stemness regulation. *Oncogene.* 42: 3371–3384.

62. Lin, K., Liao, Y., Wei, M., Sun, C., 2020. Comparative analysis of intrinsic skin aging between Caucasian and Asian subjects by slide-free in vivo harmonic generation microscopy. *J. Biophotonics*. 13: e201960063.

63. López-Otín, C., Blasco, M.A., Partridge, L., Serrano, M. & Kroemer, G. (2023) Hallmarks of aging: An expanding universe. *Cell.* 186(2): 243-278.

64. Low, E., Alimohammadiha, G., Smith, L. A., Costello, L. F., Przyborski, S. A., von Zglinicki, T. & Miwa, S. (2021) How good is the evidence that cellular senescence causes skin ageing? *Ageing Research Reviews*. 71: 101456.

65. Low, E., Smith, L.A., Miwa, S., Fielder, E. Przyborski, S. & von Zglinicki, T. (2024) Senescent dermal fibroblasts decrease stemness in basal keratinocytes in a bioengineered model of human full thickness skin. *Journal of Investigative Dermatology.* https://doi.org/10.1016/j.jid.2024.07.004

66. Makrantonaki, E., Schönknecht, P., Hossini, A. M., Kaiser, E., Katsouli, M. M., Adjaye, J., Schröder, J., & Zouboulis, C. C. (2010). Skin and brain age together: The role of hormones in the ageing process. *Experimental gerontology*, *45*(10), 801–813.

67. Manuskiatti, W., Schwindt, D.A. & Maibach, H.I. (1998) Influence of age, anatomic site and race on skin roughness and scaliness. *Dermatology.* 196: 401–407.

68. Markiewicz, E., Karaman-Jurukovska, N., Mammone, T., & Idowu, O. C. (2022). Post-Inflammatory Hyperpigmentation in Dark Skin: Molecular Mechanism and Skincare Implications. *Clinical, Cosmetic and Investigational Dermatology*. 15: 2555–2565.

69. McLafferty, E., Hendry, C., & Farley, A. (2012). The integumentary system: anatomy, physiology and function of skin. *Nursing Standard (through 2013)*. 27(3): 35.

70. Menon, G. K., Cleary, G. W. & Lane, M. E. (2012) The structure and function of the stratum corneum. *International Journal of Pharmaceutics*. 435(1): 3-9.

71. Michaels, A.S., Chandrasekaran, S.K. and Shaw, J.E. (1975) Drug permeation through human skin: Theory and invitro experimental measurement. *AIChE J.* 21: 985-996.

72. Milstone, L. M. (2004) Epidermal desquamation. *Journal of Dermatological Science*. 36(3): 131-140.

73. Mohamed & Hargest (2022) Surgical anatomy of the skin. *Surgery*. 40(1): 1-7.

74. Montagna, W., & Carlisle, K. (1991) The architecture of black and white facial skin. *Journal of the American Academy of Dermatology*. 24(6): 929-937.

75. Montagna, W., Prota, G., & Kenney, J. A. (1993) *Black skin: structure and function*. Gulf Professional Publishing.

76. Moreiras, H., Seabra, M.C., & Barral, D.C. (2021) Melanin Transfer in the Epidermis: The Pursuit of Skin Pigmentation Control Mechanisms. *International journal of molecular sciences*. *22*(9): 4466.

77. Mykhaliuk, V. V., Havryliak, V. V. & Salyha, Y. T. (2022) The Role of Cytokeratins in Ensuring the Basic Cellular Functions and in Dignosis of Disorders. *Cytol. Genet.* 56: 530–540.

78. Naidoo. K. & Birch-Machin, M.A. (2017) Oxidative Stress and Ageing: The Influence of Environmental Pollution, Sunlight and Diet on Skin. *Cosmetics.* 4(1): 4.

79. Nakano, S., Abe, Y., Nakajima, K., Sano, S., Yamamoto, O., Wakamatsu, K., Ito, S., Hayashi, M. & Suzuki, T. (2021) Establishment of a mouse model for post-inflammatory hyperpigmentation. *Pigment Cell Melanoma Res*. 34: 101–110.

80. National Council for Voluntary Organisations (2023) https://www.ncvo.org.uk/news-and-insights/news-index/why-language-matters-in-building-belonging/

81. National Health Service (2022) https://service-manual.nhs.uk/content/inclusive-content/skin-symptoms

82. Naylor, E. C., Watson, R. E. B., Sherratt, M. J. (2011) Molecular aspects of skin ageing. *Maturitas.* 69(3): 249-256.

83. Nouveau-Richard, S., Yang, Z., Mac-Mary, S., Li, L., Bastien, P., Tardy, I., Bouillon, C., Humbert, P. & De Lacharrière, O. (2005) Skin ageing: a comparison between Chinese and European populations: a pilot study. *Journal of dermatological science*. 40(3): 187-193.

84. Oender, K., Trost, A., Lanschuetzer, C., Laimer, M., Emberger, M., Breitenbach, M., Richter, K., Hintner, H. & Bauer, J. W. (2008) Cytokeratin-related loss of cellular integrity is not a major driving force of human intrinsic skin aging. *Mechanisms of Ageing and Development*. 129(10): 563-571.

85. Porcheron, A., Latreille, J., Jdid, R., Tschachler, E. & Morizot, F. (2014), Influence of skin ageing features on Chinese women's perception of facial age and attractiveness. *Int J Cosmet Sci*. 36: 312-320.

86. Rawlings, A.V. (2006), Ethnic skin types: are there differences in skin structure and function? *International Journal of Cosmetic Science*. 28: 79-93.

87. Rittié, L. & Fisher, G.J. (2015) Natural and sun-induced aging of human skin. *Cold Spring Harb Perspect Med.* 5;5(1): a015370.

88. Reilly, D. M. & Lozano, J. (2021) Skin collagen through the lifestages: importance for skin health and beauty. *Plast Aesthet Res*. 8: 2.

89. Ren, M., Hao, S., Yang, C., Zhu, P., Chen, L., Lin, D., Li, N. & Yan, L. (2013). Angiotensin II regulates collagen metabolism through modulating tissue inhibitor of metalloproteinase-1 in diabetic skin tissues. Diabetes & vascular disease research. *Official Journal of the International Society of Diabetes and Vascular Disease.* 10(5).

90. Ressler, S., Bartkova, J., Niederegger, H., Bartek, J., Scharffetter-Kochanek, K., Jansen-Dürr, P. & Wlaschek, M. (2006). p16INK4A is a robust in vivo biomarker of cellular aging in human skin. *Aging Cell*. 5: 379–389.

91. Rinnerthaler, M., Duschl, J., Steinbacher, P., Salzmann, M., Bischof, J., Schuller, M., Wimmer, H., Peer, T., Bauer, J.W. and Richter, K. (2013) Age-related changes in the composition of the cornified envelope in human skin. *Exp Dermatol*. 22: 329-335.

92. Rinnerthaler M, Bischof J, Streubel MK, Trost A, Richter K. Oxidative Stress in Aging Human Skin. *Biomolecules*. 2015; 5(2):545-589.

93. Roger, M., Fullard, N., Costello, L., Bradbury, S., Markiewicz, E., O'Reilly, S., Darling, N., Ritchie, P., Määttä, A., Karakesisoglou, I., Nelson, G., von Zglinicki, T., Dicolandrea, T., Isfort, R., Bascom, C. & Przyborski, S. (2019), Bioengineering the microanatomy of human skin. *J. Anat.* 234: 438-455.

94. Roth-Carter, Q.R., Koetsier, J.L., Broussard, J.A. & Green, K.J. (2022) Organotypic Human Skin Cultures Incorporating Primary Melanocytes. *Curr Protoc*. 2(9): e536.

95. Rousselle, P., Gentilhomme, E., & Neveux, Y. (2017). Markers of epidermal proliferation and differentiation. *Agache's Meas Ski Non-invasive Investig Physiol Norm Constants*. 407-15.

96. Rübe, C.E., Bäumert, C., Schuler, N., Isermann, A., Schmal, Z., Glanemann, M., Mann, C. & Scherthan, H., (2021). Human skin aging is associated with increased expression of the histone variant H2A.J in the epidermis. *NPJ Aging Mech. Dis*. 7: 7.

97. Russo, B., Brembilla, N. C. & Chizzolini, C. (2020) Interplay Between Keratinocytes and Fibroblasts: A Systematic Review Providing a New Angle for Understanding Skin Fibrotic Disorders. *Frontiers in Immunology*. 11, ISSN=1664-3224.

98. Sandilands, A., Sutherland, C., Irvine, A.D. & Irwin McLean, W.H. (2009) Filaggrin in the frontline: role in skin barrier function and disease. *J Cell Sci.* 122(9):1285-1294.

99. Schallreuter, K.U., Kothari, S., Chavan, B. and Spencer, J.D. (2008) Regulation of melanogenesis – controversies and new concepts. *Experimental Dermatology*. 17: 395-404.

100. Schumacher, B., Pothof, J., Vijg, J. & Hoeijmakers, J.H.J. (2021) The central role of DNA damage in the ageing process. *Nature.* 592: 695–703.

101. Seo, J.Y. & Chung, J.H. (2006) Thermal aging: A new concept of skin aging. *Journal of Dermatological Science Supplement.* 2(1): 13-22.

102. Serre, C., Busuttil, V. and Botto, J.-.-M. (2018), Intrinsic and extrinsic regulation of human skin melanogenesis and pigmentation. *Int J Cosmet Sci.* 40: 328-347.

103. Shamitova, E. N., Pikushkin, V. V. & Myasnikova, I. A. (2018) Biochemical markers of skin ageing. *European Journal of Natural History* 3. 13-16.

104. Sibilla, S. & Borumand, M. (2014) Current understanding of the effects of diet on skin health. In: Godfrey M, editor. Losing weight simply and safely. Florence: Officina Editorale Oltrarno; 241-68.

105. Simpson, A. (2022) Development of an Immune Competent *In Vitro* Skin Equivalent to Investigate the Impact of Air Pollution on Skin Health. Thesis.

106. Simpson, A., DiColandrea, T. & Przyborski, S. (2024) Assessing the impact of airborne particulate pollution on human skin utilizing a novel human skin equivalent containing MUTZ-3-derived Langerhans cells. *Bioeng Transl Med*. e10738.

107. Sommer, M., Poliak, N., Upadhyay, S., Ratovitski, E. A., Nelkin, B. D., Donehower, L. A., & Sidransky, D. (2006). ΔNp63&alpha Overexpression Induces Downregulation of Sirt1 and an Accelerated Aging Phenotype in the Mouse. *Cell Cycle*. 5(17): 2005–2011.

108. Song, S., Li, F., Zhao, B., Zhou, M., & Wang, X. (2024). Ultraviolet Light Causes Skin Cell Senescence: From Mechanism to Prevention Principle. *Advanced biology*. e2400090. Advance online publication.

109. Sreedhar, A., Aguilera-Aguirre, L., & Singh, K. K. (2020). Mitochondria in skin health, aging, and disease. *Cell death & disease*. 11(6), 444.

110. Fülöp, T., Larbi, A. & Witkowski, J. M. (2019) Human Inflammaging. *Gerontology*. 65(5): 495–504.

111. Tharakan, S., Pontiggia, L., Biedermann, T., Böttcher-Haberzeth, S., Schiestl, C., Reichmann, E. & Meuli, M. (2010) Transglutaminases, involucrin, and loricrin as markers of epidermal differentiation in skin substitutes derived from human sweat gland cells. *Pediatr Surg Int.* 26: 71–77.

112. Tomitaka, A., Akamatsu, H., Matsunaga, K. & Denda, M. (2003) Altered Distribution of Calcium in Facial Epidermis of Aged Adults. *Journal of Investigative Dermatology*. 121(6): 1557-1558.

113. Tsujita-Kyutoku, M., Kiuchi, K., Danbara, N., Yuri, T., Senzaki, H. and Tsubura, A. (2003), p63 expression in normal human epidermis and epidermal appendages and their tumors. *Journal of Cutaneous Pathology*. 30: 11-17.

114. Tsukahara, K., Kakuo, S., Moriwaki, S., Hotta, M., Ohuchi, A., Kitahara, T., & Harada, N. (2008). The characteristics of aromatase deficient hairless mice indicate important roles of extragonadal estrogen in the skin. *The Journal of steroid biochemistry and molecular biology*. 108(1-2): 82–90.

115. Uche, L. E., Gooris, G. S., Bouwstra, J. A. & Beddoes, C. M. (2019) Barrier Capability of Skin Lipid Models: Effect of Ceramides and Free Fatty Acid Composition. *Langmuir.* 35(47): 15376-15388.

116. United Nations (2010) World Population Prospects: The 2010 Revision. Available at https://www.un.org/en/development/desa/population/publications/pdf/trends/WPP2010/WPP2010_Volume-I_Comprehensive-Tables.pdf

117. Vashi, N.A., de Castro Maymone, M. B. & Kundu, R. V. (2016) Aging Differences in Ethnic Skin. *J Clin Aesthet Dermatol*. 9(1): 31-8.

118. Waldera Lupa, D. M., Kalfalah, F., Safferling, K., Boukamp, P., Poschmann, G., Volpi, E., Götz-Rösch, C., Bernerd, F., Haag, L., Huebenthal, U., Fritsche, E., Boege, F., Grabe, N., Tigges, J., Stühler, K. & Krutmann, J. (2015) Characterization of Skin Aging–Associated Secreted Proteins (SAASP) Produced by Dermal Fibroblasts Isolated from Intrinsically Aged Human Skin. *Journal of Investigative Dermatology.* 135(8): 1954-1968.

119. Waller, J.M., Maibach, H.I., 2005. Age and skin structure and function, a quantitative approach (I): blood flow, pH, thickness, and ultrasound echogenicity. *Skin Res. Technol.* 11: 221–235.

120. Wang, A. S., Ong, P. F., Chojnowski, A., Clavel, C., & Dreesen, O. (2017). Loss of lamin B1 is a biomarker to quantify cellular senescence in photoaged skin. *Scientific Reports*. 7(1): 15678.

121. Wang, A. S., Nakamizo, S., Ishida, Y., Klassen, G., Chong, P., Wada, A., Lim, J. S. Y., Wright, G. D., Kabashima, K. & Dreesen,O. (2022) Identification and quantification of senescent cell types by lamin B1 and HMGB1 in Actinic keratosis lesions. *Journal of Dermatological Science*. 105(1): 61-64.

122. Warrier, A.G., Kligmn, A.M., Harper, R.A., Bowman, J. & Wickett, R.R. (1996) A comparison of black and white skin using non-invasive methods. *J. Soc. Cosmet. Chem.* 47: 229–240.

123. Watt, F.M. & Fujiwara, H. (2011) Cell-extracellular matrix interactions in normal and diseased skin. *Cold Spring Harb Perspect Biol.* 3(4): a005124.

124. Weinmüllner, R., Zbiral, B., Becirovic, A. *et al.* (2020) Organotypic human skin culture models constructed with senescent fibroblasts show hallmarks of skin aging. *npj Aging Mech Dis.* 6: 4.

125. Wong, V. W., Sorkin, M., Glotzbach, J. P., Longaker, M. T. & Gurtner, G. C. (2011). Surgical approaches to create murine models of human wound healing. *Journal of Biomedicine and Biotechnology*. 1–8.

126. World Health Organisation (2023), https://www.who.int/news-room/fact-sheets/detail/ageing-and-health.

127. Wurbs, A., Karner, C., Vejzovic, D., Singer, G., Pichler, M., Liegl-Atzwanger, B. & Rinner, B. (2024) A human ex vivo skin model breaking boundaries. *Sci Rep.* 14: 24054.

128. Yaar, M., Eller, M. S. & Gilchrest, B. A. (2002) Fifty Years of Skin Aging. *Journal of Investigative Dermatology Symposium Proceedings*. 7(1): 51-58.

129. Yamada, K. M. & Cukierman, E. (2007) Modeling Tissue Morphogenesis and Cancer in 3D. *Cell.* 130(4): 601-610.

130. Yoon, J.E., Kim, Y., Kwon, S., Kim, M., Kim, Y.H., Kim, J.H., Park, T.J., Kang, H.Y. (2018). Senescent fibroblasts drive ageing pigmentation: A potential therapeutic target for senile lentigo. *Theranostics.* 8(17): 4620-4632.

131. Yousef, H., Alhajj, M., Fakoya, A. O. & Sharma, S. (2023) Anatomy, Skin (Integument), Epidermis. In: StatPearls. StatPearls Publishing, Treasure Island (FL); PMID: 29262154.

132. Zhou, L., Ji, W., Dicolandrea, T., Finlay, D., Supp, D., Boyce, S., Wei, K., Kadekaro, A. L. & Zhang, Y. (2023) An improved human skin explant culture method for testing and assessing personal care products. *J Cosmet Dermatol*. 22: 1585-1594.

133. Zhou, S., Zeng, H., Huang, J., Lei, L., Tong, X., Li, S., Zhou, Y., Guo, H., Khan, M., Luo, L., Xiao, R., Chen, J. & Zeng, Q. (2021) Epigenetic regulation of melanogenesis. *Ageing Research Reviews*. 69: 101349.

134. Zhou, X., Li, G., Wang, D., Sun, X., & Li, X. (2019). Cytokeratin expression in epidermal stem cells in skin adnexal tumors. *Oncology Letters*. 17: 927-932.